Development and Validation of a Microfluidic Brain-On-A-Chip Model for Examining Cerebral Microvascular Barrier Response to the Tumor Microenvironment

By

Stacey Line

A thesis submitted to the Faculty of Graduate Studies of the University of Manitoba

In partial fulfilment of the requirements of the degree of

MASTER OF SCIENCE

Department of Pharmacology and Therapeutics

University of Manitoba

Winnipeg

Abstract:

Introduction: The BBB is composed of specialized endothelial cells that limit permeability of solutes across the BBB. Microfluidic technology that allows formation of 3D tubular microvessels has been applied to in vitro BBB models, having advantages of fluid flow, cell-cell contact, and can provide a more robust and predictive model for assessing vascular permeability.

Methods: Human brain microvessel endothelial cells (hCMEC/d3) were seeded (10,000 cells/µL) into the vascular channel and various human brain tumor cell lines (SF8628, U87, and U251) were seeded in the adjacent brain channel of the microfluidic unit. Additionally, endothelial cells were seeded in 0.4um Transwell inserts (40,000cells/cm^2). Tumor-induced alterations in barrier function were examined using paracellular and transcellularly transported dyes and correlated to changes of expression of selected BBB specific genes and secretome. Modulation of permeability using cadherin peptides was examined to determine potential for improving drug delivery across the BBB.

Results: The microfluidic BBB culture model showed reduced permeability compared to Transwell™ inserts and comparable values to *in vivo* studies. Compared to monoculture, no significant changes in permeability were observed with U251 co-culture model. However, SF8628 enhanced barrier properties, while U87 increased paracellular leakiness. Examination of the barrier enhancing microenvironment observed with the SF8628 co-culture model indicated a Sonic Hedgehog dependent process. Increased levels of fatty acids seemed responsible at least in part, for the barrier diminishing effects in U87 co-culturing. Cadherin peptides increases permeability and were BBB endothelial cell selective.

Conclusion: DMF model can be used to identify tumor-driven changes in brain endothelial cells.

Acknowledgements:

I am extremely grateful to Dr. Donald Miller for all his support, supervision, encouragement, patients, and dedication throughout my time working in his laboratory. This project would not have been possible without all of his knowledge and guidance. I would also like to thank my committee members, Dr. Ted Lakowski and Dr. Grant Hatch for their time, flexibility, and thoughtful suggestions throughout the course of my thesis. Additionally, I would like to thank Dr. Migimirajan Vanan, Dr. Siahaan Teruna, and Dr. Lang Li and lab members for all their collaboration and support throughout my project. To my valued lab members, thank you for making the lab a positive, inclusive, and enjoyable space! It was a pleasure working with all of you, special thanks to Wei Xiong for being extremely patient and supportive of my work while help me learn new techniques. Lastly, I would like to thank the Canadian Institute for Health Research, Research Manitoba and the University of Manitoba Graduate studies for their financial support and allowing me to achieve my goal.

Table of Contents:

List of Tables:

List of Figures:

Abbreviations:

2-D	Two-dimensional
3-D	Three-dimensional
ADME	Absorption, Distribution, Metabolism, and Excretion
ADT5, TPP, HAVN1, and HAV6	Cadherin Peptides
ATP	Adenosine triphosphate
ATP –ABC efflux transporters	adenosine triphosphate (ATP) – binding cassette (ABC) efflux transporters

BBB	Blood brain barrier
BCRP	Breast Cancer Resistance protein
BM	Basement membrane
BMEC	Brain microvessel endothelial cells
BOILED-Egg model	Brain Or IntestinaL EstimateD permeation predictive model
BSA	Bovine Serum Albumin
BTM	Brain-tumor barrier
CBF	Cerebral blood flow
CNS	Central Nervous System
DIPG	Diffuse Intrinsic Pontine Glioma
DMEM	Dulbecco's Modified Eagle Medium
DMF	Dynamic microfluidic model
EBM-2	Endothelial Basal Media
ECM	Extracellular matrix
ECS	Extracellular space
FBS	Fetal Bovine Serum
FDX	Fluorescein Dextran Dye
GBM	Glioblastoma Multiforme

GF	Elacradir
$GLUT_1$	Glucose transporter 1
GSC	Glioblastoma Stem Cells
HA	Primary Human Astrocyte Cells
hCMEC/d3	Human Cerebral Microvascular Endothelial Cell
IL	Interleukin
JAMs	Junctional adhesion Molecules
LC-MS	Liquid Chromatography-Mass Spectrometry
Log-P	n-octanol/water Partition Coefficient
mAb	Monoclonal Antibody
MCP-1	Monocyte Chemoattractant Protein-1
MDCK-MDR	Madin-Darby Canine Kidney-Multi Drug Resistance Epithelial Cell Line
Mfsd2a	Sodium-dependent lysophosphatidylcholine symporter
MMP's	Metalloproteinases
MRPs	Multidrug resistance-associated Proteins
MRI	Magnetic Resonance Imagine
MSD	Mesoscale discovery
Na-F	Sodium Fluorescein

N-Cadherin	Neural Cadherin
NVC	Neurovascular Coupling
NVU	Neurovascular Unit
PC	Pericyte Cells
PCR	Polymerase Chain Reaction
PDGFRβ	Platelet Derived Growth Factor β, PDGF receptor β
PDGF-β	Platelet Derived Growth Factor β
PDX	Patient derived xenograft
P-gp	P-glycoprotein
PIP	Peripheral inflammatory pain
rhSHH	Recombinant human sonic hedge hog
RMT	Receptor Mediated Transcytosis
RT-PCR	Reverse Transcriptase Polymerase Chain Reaction
SAT1	spermidine/spermine N(1)-acetyltransferase
SHH	Sonic hedge Hog
SLC	Solute carriers
TCM	Tumor conditioned media
TEER	Trans-endothelial electrical resistance

TJP	TJ tight junction proteins
Ve-Cadherin	Vascular Endothelial cadherin
VEGF	Vascular endothelial growth factor
VEGF-A	Vascular Endothelial Growth Factor Alpha
ZO	Zonula Occludens

1.0 Introduction:

1.1 Overview of the Neurovascular Unit Structure and Physiological Properties.

The brain is the control center of the body with complex neuronal networks that carry out a wide array of daily bodily functions including memory, perception, emotions, movement as well as autonomic functions. Functionally, the brain is made up of the neurovascular unit (NVU) which consists of specialized vascular endothelial cells (EC), neurons, astrocytes (AC), pericytes (PC), and other support cells (Luissint et al., 2012) (refer to Figure 1).

The BBB component of the NVU is formed from a single continuous layer of non-fenestrated endothelial cells which aids in the restrictiveness of the barrier (Luo & Shusta, 2020). Characteristics that differentiate and make endothelial cells lining the BBB distinct from peripheral vascular endothelial cells include (1) expression of tight junction proteins (TJ) that effectively prevent paracellular transport of polar molecules between adjacent endothelial cells (2) absence of fenestrations which limits solute transfer through channels or pores in the cells (3) reduced vesicular transport activity and (4) expression of carriers and active transporters that aid in the passage of essential molecules into the brain and the selective removal of metabolites and solutes from the brain (Kadry et al., 2020). Structurally, endothelial cells composing the BBB are highly polarized consisting of a basolateral (abluminal) and apical (luminal) side (Chow & Gu, 2015). The apical side of the endothelial cell is in contact with the blood while the basolateral side faces the brain. The polarized nature of the~~se~~ BBB endothelial cells helps establish paracellular restrictiveness while allowing important nutrients and metabolite molecules to selectively gain entry into, or be removed from, the brain (Chow & Gu, 2015).

Pericyte cells within the NVU share a basement membrane with endothelial cells and form direct membrane connections with the endothelium through connexins and N-cadherin proteins (Kadry et al., 2020). The cell-to-cell contact between endothelial cells and pericytes allows for the free exchange of ions, second messengers and metabolites that helps to maintain BBB integrity (Kadry et al., 2020). Cerebral blood flow (CBF) regulation is critical to meet the energy demands of active cellular structures within the brain (Brown et al., 2019). Pericytes are one of several cell types within the NVU that plays an essential role in neurovascular coupling (NVC) leading to cerebral blood flow modulation (Brown et al., 2019). Neurovascular coupling describes the linking of signaling pathways between neuronal, cerebral support cells and vascular endothelial cells to ensure adequate blood flow through the BBB to fulfill cellular energy requirements (Brown et al., 2019). Pericytes express key regulator receptors such as catecholamines, angiotensin 1, vascular mediators, endothelin-1, and vasopressin (Kadry et al., 2020). Ligands that bind these receptors promote pericyte contraction or relaxation which can trigger molecular and functional responses in endothelial cells leading to blood vessel vasodilation or vasoconstriction which ultimately generate changes in CBF (Brown et al., 2019).

In addition, the contact with the brain endothelium makes pericytes anatomically well-positioned to help promote and regulate BBB integrity. (Sengillo et al., 2013). Studies have shown pericytes promote and induce endothelial cell tight junction protein expression which support the barrier properties of brain endothelial cells, while pericyte deficiency has been mechanistically linked with endothelial cell apoptosis and BBB breakdown (Sengillo et al., 2013). Normal brain microvessel development relies on hormonal signals such as platelet derived growth factor β (PDGF-β) which is imperative in PCs recruitment (Quaegebeur et al., 2010). Pericyte cells express receptors that bind platelet derived growth factor β, PDGF receptor

β (PDGFRβ) and studies have shown mice embryos lacking these receptors fail to develop (Hellström et al., 2001). Lack of pericyte recruitment results in irregular vessels that become fragile and result in leakage of solutes across the BBB (Hellström et al., 2001). Abnormal pericyte function, deficiency or both has been document in many CNS disorders including diabetic retinopathy and neurodegenerative disorders (Bergers & Song, 2005). Taken together these results suggest PCs play an essential role in neuroprotection and BBB maintenance and integrity.

Astrocyte cells are the most abundant cell type within the CNS and contribute to a variety of different functions within the brain including but not limited to maintaining the ionic homeostasis of the extracellular space, regulating pH, and processing and regulating signals from neurons to the vasculature (Kadry et al., 2020). Astrocyte cells are also critical in maintaining BBB properties under both normal and pathological conditions and secrete molecules that are essential for regulating interactions between the endothelium and pericytes (Cabezas et al., 2014). *In vitro* studies have shown astrocyte, neuron and endothelial cell tri-culture models induced barrier properties in brain microvessel endothelial cells, increased trans-endothelial electrical resistance (TEER), and reduced passive permeability (Canfield et al., 2017). The close anatomical relationship between endothelial cells and the astrocytic end-feet allow various lipid mediators released by astrocyte cells such as prostaglandins and epoxyeicosatrienoic acids to influence vasodilation and therefore, helps to regulate cerebral blood flow and BBB permeability (Liu et al., 2018). Furthermore, in animal models of brain injury, such as ischemic stroke, there is evidence to suggest an important role of astrocytes in the disruption of the BBB by releasing factors like VEGF-A and metalloproteinase which have been shown to disrupt tight junction proteins and compromise the BBB (Michinaga & Koyama, 2019). These results suggest that

astrocyte cells within the NVU play an essential role in endothelial cell development, anatomical arrangement, and support functional and metabolic processes that help maintain the integrity of the BBB.

In addition to pericyte and astrocyte cells within the NVU, the basement membrane (BM) that forms the extracellular matrix (ECM) found underneath endothelial cells also helps maintain structural support for the brain microvasculature (L. Xu et al., 2018). Two major endothelial cell receptors in contact with the ECM are dystroglycan and integrins (Baeten & Akassoglou, 2011). These matrix receptors play essential roles in signal transduction by binding ligands within the ECM and activating cellular signaling pathways that regulate processes including survival, proliferation and differentiation (Baeten & Akassoglou, 2011). Additionally, the matrix proteins also provide a linkage point anchoring the cell, ECM and cytoskeleton (L. Xu et al., 2018). The BM consists of four major ECM proteins: collagen IV, laminin, perlecan and nidogen which are synthesized at the BBB by endothelial cells, PC and AC (L. Xu et al., 2018). Taken together, these results illustrate important interactions of PC, AC, BM, within the NVU to regulate endothelial cell function.

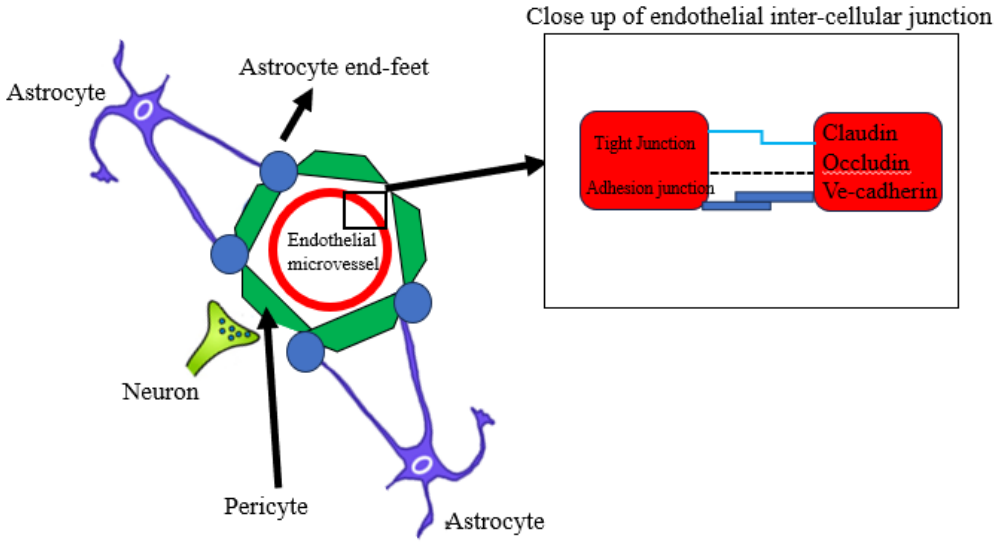

Figure 1: Schematic representation of the neurovascular unit

1.2. Structural and Biochemical Features Comprising BBB Endothelial Cells.

The paracellular and transcellular passage of solutes across the BBB is heavily influenced by tight junction proteins (TJP), adhesion molecules, adenosine triphosphate (ATP) – binding cassette (ABC) efflux transporters and solute carriers (SLC). Localized junctional proteins and adhesion molecules effectively limit paracellular diffusion/exchange of hydrophilic solutes between the blood and brain extracellular compartments (Chow & Gu, 2015). Regarding transcellular passage, efflux transporters and SLC work together to selectively limit uptake of solutes and macromolecules which prevent potential toxic agents from accumulating in the brain, and permit uptake of glucose, amino acids, and other molecules essential to normal brain function. (Kusuhara & Sugiyama, 2005).

Brain microvessel endothelial cells (BMEC) maintain a distinct barrier phenotype which is characterized by the presence of tight junction proteins and polarized transport systems (Luissint et al., 2012). Tight junction proteins form a restrictive paracellular barrier which effectively limits the passage of polar molecules from the blood into the brain (Kadry et al., 2020). Some important tight junction integral membrane proteins include occludin, claudin, junctional adhesion molecules (JAMs), cadherins and junction-associated proteins like zonula occludens (ZO) (Luissint et al., 2012). Mechanisms of transport including solute carriers and intracellular transport processes are discussed below.

BBB Junctional Complexes:

Morphologically, the claudins, specifically claudin 1-5 have a major contribution to the restricted paracellular diffusion of the BBB. Claudin proteins on adjacent endothelial cells bind to one another and help form the TJ seal while intracellular linkages are also formed with cytoplasmic proteins including ZO-1 (Kadry et al., 2020). Occludin is an additional TJ protein that is highly expressed in brain ECs compared to nonneural tissues and plays an important role in limiting paracellular permeability (Kadry et al., 2020). Furthermore, occludin proteins also play an important role in the maintenance of TJ functional integrity (Kadry et al., 2020)

Crucial to TJ protein assembly are ZO cytoplasmic accessory proteins. These intracellular proteins form a cytoplasmic bridge linking the TJ proteins to the cytoskeleton of the cell (Kadry et al., 2020). Within the brain microvasculature, ZO-1-3 are important intracellular proteins that link the actin cytoskeleton to the junctional molecules claudin and occludin via cingulin which plays a vital role in maintenance and integrity of the TJ complexes (Kadry et al., 2020). Research suggests that damage to the BBB is highly associated with changes in ZO-1 expression

levels and reduced ZO-1 expression results in compromised BBB integrity (Wang et al., 2016). Lastly, decreased levels of ZO-1 have been reported to decrease cerebral vascular permeability leading to restricted exchange of molecular compounds (Wang et al., 2016). Taken together, ZO cytoplasmic accessory proteins play critical roles in establishing leak tight vascular endothelial barriers.

Junction adhesion molecules (JAMs) are members of the immunoglobulin family (Jia et al., 2013). Expressed in epithelial and endothelial cells are JAM-1,2, and 3, however, studies conducted in the brain of rodents indicate JAM-1 and JAM-3 are localized within the cerebral microvasculature (Kadry et al., 2020). Studies suggest JAMs play a role in trafficking occludin proteins to the tight junction complexes and provide conclusive evidence that loss of JAM expression resulted in loss of BBB integrity (Kadry et al., 2020). Lastly, cadherin proteins act with the actin cytoskeleton of neighbouring cells via β-catenins, γ-catenins and p120 and are part of the adherens junctions (Li et al., 2018). Structurally, the proteins contributing to the adherens junctions differs from TJ proteins in the type of connections formed. For TJ proteins, interactions with neighbouring endothelial cells occur through the plasma membrane while adherens junctions connect neighbouring cells through the actin cytoskeleton (*The Different Types of Cell Junctions | Learn Science at Scitable*, n.d.). Two types of cadherin proteins are expressed in ECs, N-cadherin and VE-cadherin, however VE-cadherin is exclusive to EC while N-cadherin is also present in several other cell types (Li et al., 2018). Vascular endothelial-cadherin adhesion proteins create zipper-like structures which help endothelial cells communicate with one another and maintain cell integrity (Li et al., 2018). Figure 2 represents the major junctional interactions between adjacent endothelial cells in the BBB.

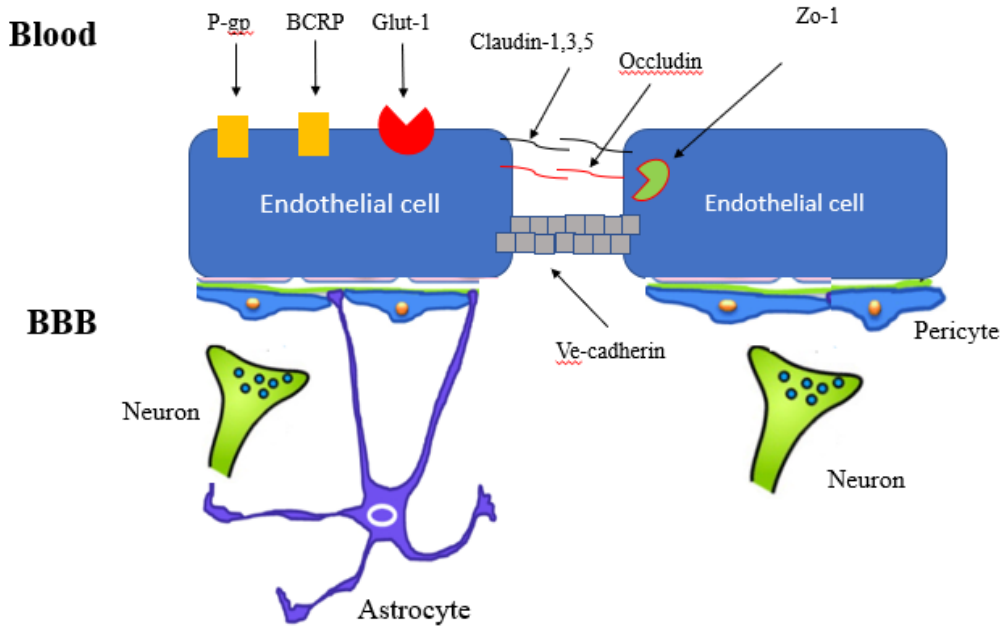

Figure 2: Anatomical arrangement of major junctional molecules connecting neighbouring endothelial cells

BBB Transporters:

Solute carriers are a family of proteins involved in facilitating the exchange of cationic/anionic substrates, nutrients, drugs, and signaling molecules across biological membranes including the endothelial cells of the BBB (Hu et al., 2020). Solute carriers expressed in endothelial cells of the BBB are essential for maintaining the metabolic needs of the brain by taking up essential molecules from the blood while excluding toxic substances (Hu et al., 2020). Glucose is the primary metabolic molecule used for energy by the brain, taking in about 100-150 grams of glucose per day and consuming 20% of glucose in the body (Patching, 2017). One of the important transporters for delivering the highly hydrophilic glucose molecule

from the blood across the BBB to the brain is glucose transporter 1 (GLUT1) (Patching, 2017). Glucose transporter 1 is a sodium-independent facilitative transporter located on both the luminal and abluminal sides of the endothelial cells composing the BBB (Patching, 2017). The driving force behind this transporter is the concentration gradient that exists between the blood and brain extracellular fluid (Patching, 2017). Glucose transporter 1 therefore plays an essential role in maintaining the metabolic needs of the brain.

The BBB also has a wide array of active drug efflux transporters, belonging to the ATP-binding cassette (ABC) superfamily of proteins (Löscher & Potschka, 2005) The ABC transporters are integral membrane proteins located predominantly on the luminal (apical) side of polarized brain endothelial cells and function to remove solutes from the cell through an active ATP-driven process (D. W. Miller et al., 2021). The ABC transporters expressed in brain endothelial cells forming the BBB play a critical role in neuroprotection, drug penetration into the brain and pharmacoresistance (D. W. Miller et al., 2021). Efflux transporters act as a general defense mechanism at the BBB, protecting the brain from toxins and potentially harmful agents that would otherwise readily enter the brain by simple diffusion without limitations (D. W. Miller et al., 2021). P-glycoprotein (P-gp), Multidrug Resistance-Associated Proteins (MRPs) and Breast Cancer Resistance Protein (BCRP) are some of the primary efflux transporters expressed on BBB endothelial cells. P-glycoprotein and BCRP are highly expressed on the luminal membrane of the BBB, with their primary role involving transportation of molecules that enter the endothelium from the blood out the cell and back into the blood, preventing substances from passing through the endothelial cells and reaching the brain (Kadry et al., 2020). Studies have shown considerable substrate overlap and cooperativity between P-gp and BCRP, indicating redundancy of efflux transporters within the brain (Kadry et al., 2020). While most of

the research has focused on P-gp expression in endothelial cells, pericyte and astrocyte cells can also express P-gp (Kadry et al., 2020). Under normal physiological conditions, P-gp in astrocyte and pericyte cells may not contribute greatly to barrier function, however, there is a possibility of upregulation of these transporters during pathological conditions such as brain tumors that may contribute to drug delivery to the brain (Kadry et al., 2020) Taken together, endothelial cell transporters play an essential role in maintaining the integrity of the BBB, maintaining the metabolic needs of the brain, and neuroprotection.

Table 1. Essential BBB genes contributing to physiological and morphological structure.

Gene name	Protein name	Type of protein	EC Localization	BBB function
SLC2A1	Glut-1	Solute carrier	Apical and basolateral sides	Facilitated transport of glucose from blood to meet energy demands of brain
CLDN1	Claudin -1	Integral membrane proteins and component of tight junction	Intercellular junction	Anchor EC through plasma membrane function in: Paracellular tightness
CLDN3	Claudin-3	Integral membrane proteins and component of tight junction	Intercellular Junction	Anchor EC through plasma membrane function in: Paracellular tightness
CLDN5	Claudin-5	Integral membrane proteins and component of tight junction	Intercellular junction	Anchor EC through plasma membrane function in: Paracellular tightness
ABCB1	P-glycoprotein	ABC efflux transporter	Apical	Active transport of ligands out of EC back into the blood
ABCG2	Breast Cancer Resistance Protein	ABC efflux transporter	Apical	Active transport of ligands out of EC back into the blood
TJP1	Zona Occludin-1	Cytoplasmic junctional associated protein	Intracellular	Forming cytoplasmic bridge, linking TJ proteins to the cytoskeleton
OCLN	Occludin	component of tight junction	Intercellular junction	Regulate integrity and permeability of BBB
CDH5	Ve-cadherin	Adherens junctional protein	Intercellular junction	Anchor neighbouring endothelial cells through actin filament
PVLAP	Plasmalemma vesicle Associated protein	Homodimer involved in transcytosis	Apical	Regulates the number of fenestrae and caveolae in cells in a VEGF dependent manner
Cav-1	Caveolin	Vesicle forming protein	Plasma membrane	Protein that allows for vesicle formation during endocytosis
Mfsd2a	Major facilitator super family domain containing 2a	a sodium-dependent lysophosphatidylcholine symporter	Apical	Endocytosis suppression- inhibits caveolae vesicle formation
Dyn-2	Dynamin 2	Protein that co-localizes with clathrin during transcytosis	Plasma membrane	Mediates clathrin dependent endocytosis

Intracellular Molecular Transport: Endocytosis

The final route of passage across the BBB to be discussed is through vesicular transport processes called endocytosis (Pulgar, 2019). In polarized endothelial cells this process can occur at both the basolateral and apical membranes and involves either charge dependent or receptor mediated internalization (Pulgar, 2019). Vascular endothelial cells, specifically ECs constituting the BBB are specialized cells that display unusually low levels of transcytosis and limited transcellular transport (Ayloo & Gu, 2019a). Decreased transcytosis in these cells provides an additional level of restrictiveness within the BBB. Transcytosis at the BBB can be regulated by endothelial cells (autonomous) or adjacent neurovascular cells and secreted factors (non autonomous). Cell non-autonomous regulation can result from the proximal location of EC and pericytes and their close interaction (Ayloo & Gu, 2019a). Studies have shown precise pericyte to endothelial cell ratios within the CNS to be crucial for maintenance of the BBB (Pulgar, 2019). In support, mice with deficiencies in signaling pathways that lead to pericyte recruitment or depletion of FoxF2, a pericyte transcription factor, contain phenotypically leaky barriers attributable to increased transcytosis through the brain endothelium (Pulgar, 2019). Therefore, pericytes are key cellular players in inducing endothelial cell properties and regulating EC transcytosis activity.

Cell-autonomous regulation of transcytosis involves an endothelial-driven process. One particularly important protein for vesicular transport in the BBB is Mfsd2a (a sodium-dependent lysophosphatidylcholine symporter) (Ayloo & Gu, 2019a). Studies suggest Mfsd2a inhibits caveolae-mediated transcytosis by modulating the composition of plasma membrane lipids (Ayloo & Gu, 2019a). In the case of Mfsd2a, this particular protein, found predominantly in the CNS vascular endothelial cells, was found to be critical for the BBB (Ayloo & Gu, 2019a). Lastly, two subtypes of transcytosis exist in CNS endothelial cells. One of which includes

receptor mediated transcytosis (RMT) involving ligands such as insulin or transferrin that bind membrane receptors to mediate endocytosis (Pulgar, 2019). Other forms of RMT include clathrin coated pits, caveolae mediated endocytosis, in which extracellular molecules are absorbed inward from the plasma membrane and macropinocytotic vesicles (Pulgar, 2019). However, the predominant type of endocytosis occurring under normal conditions in BBB endothelial cells appears to occur through clathrin coated pits (Pulgar, 2019).

In summary, paracellular, transporter and endocytosis pathways are essential for endothelial cell function and work to maintain the structural and biochemical features of the BBB. During pathological conditions like stroke, transcytosis has been shown to be upregulated in BBB cells and is an early event in break down of the BBB (Ayloo & Gu, 2019a). Using multiple models of stroke, an accumulation of vesicles can be seen within BBB endothelial cells as early as 4-6 hours post CNS injury, while tight junction or basement membrane break down is usually not reported until days later (Zhou et al., 2021). Additionally, mouse models of stroke have shown an increase in number of endothelial caveolae 6-hours after ischemia (Zhou et al., 2021). In support, studies have suggested a step wise BBB breakdown beginning with impairment of transcellular endocytosis followed by paracellular leakiness resulting from break down or rearrangement of tight junction proteins (Zhou et al., 2021). Taken together these results indicate that upregulation of transcytosis is a primary event that drives BBB permeability and the importance of endocytic regulation in formation and maintenance of BBB integrity.

1.3 Challenges of BBB in Delivering Drugs to the Brain.

The anatomical characteristics of the BBB as well as expression of transporters severely limits and complicates treatment of CNS disorders as many pharmacotherapeutics are restricted from entering the brain in large enough quantities to elicit a therapeutic response (Löscher &

Potschka, 2005). Effective drug development must take into account a multitude of factors including efficacy, toxicity and pharmacokinetic parameters like absorption, distribution, metabolism, and excretion (ADME) (Daina & Zoete, 2016). Physiochemical profiles of drug candidates can be used to predict their ADME properties, particularly oral absorption, and BBB permeability. In this regard, a computational model called the BOILED-Egg (Brain Or IntestinaL EstimateD permeation predictive model) has proven useful for assessing oral absorption and brain penetration. This model separates poorly and well-absorbed molecules based on their lipophilicity and polarity described by the n-octanol/water partition coefficient (log P) and the polar surface area (PSA) respectively (Daina & Zoete, 2016). Applying this model to large data sets of molecules that are known to be brain permeable compounds with oral absorption, it was found that compounds with a polar surface area of approximately 140 A or less and a log P between -2.3 and 6.8 were likely orally absorbed through passive diffusion (Daina & Zoete, 2016). These drugs are represented by the white elliptical area in Figure 3**.** In contrast, drugs with more restricted parameters consisting of a polar surface area of 80 A or less and log P between 0.4 and 0.6, were likely to cross the BBB and are confined to the yellow region on Figure 3, resembling the boiled egg structure (Daina & Zoete, 2016). The confined requirements of the boiled egg model, EC paracellular tightness resulting from TJ complexes, and active efflux transporters that remove drugs from endothelial cells consequently result in almost 95% of drugs being exclude from reaching the brain (Daina & Zoete, 2016). As a consequence, limited effective pharmacotherapy exists for CNS disorders (Ahlawat et al., 2020). It is therefore an important avenue for research to discover strategies that allow for efficient CNS pharmaceutical drug delivery to the brain to better treat CNS disorders.

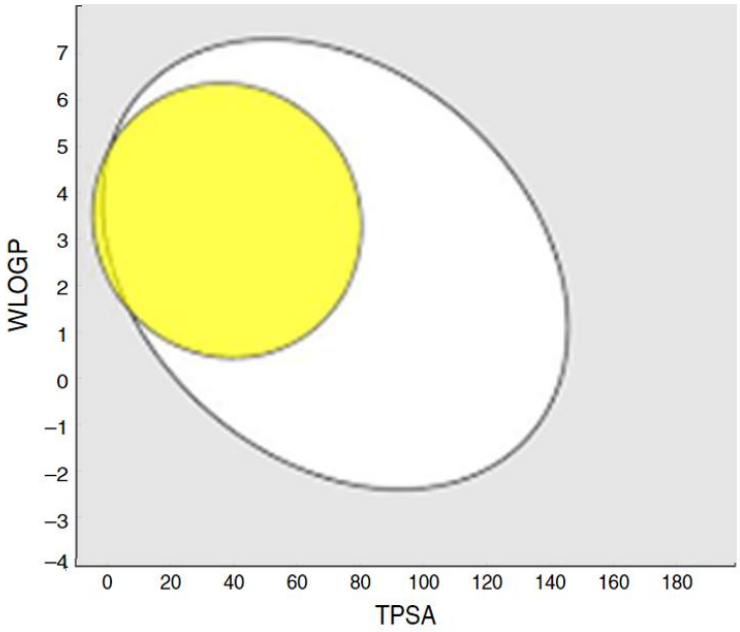

Figure 3: BOILED-egg model whereby intestinally orally dosed drugs are likely represented in the white elliptical area and drug likely to permeate the BBB are represented by the yellow region (Daina & Zoete, 2016).

Drug efficacy requires sufficient accumulation of active drug in the tissue compartment to produce the desired therapeutic response. Most drugs require the passage across at least one cellular barrier to reach their intended tissue target, however, for CNS therapeutics, the highly selective nature of the BBB presents a major obstacle for achieving therapeutic concentrations in the brain (Carpenter et al., 2014). Mechanisms for drug passage across the BBB include transporter processes and passive diffusion. Active transport involves a transport protein that uses hydrolysis of high energy phosphate bonds from ATP forming inorganic phosphate and ADP (Bellettato & Scarpa, 2018). The hydrolysis results in a sufficient amount of energy to shuttle the desired compound against its concentration gradient and through the membrane. On the other hand, passive diffusion is the most common mode of passage and involves the diffusion of compounds

down their concentration gradients through the membrane without the assistance of an energy source. The BBB penetration of drugs are based on it's physiochemical properties such as lipophilicity, hydrogen bonding, and molecular mass that determine how well the drug partitions across the BBB, as well as processes like metabolism, clearance, protein binding and degradation that dictate the concentration of drug in the bloodstream (Warren, 2018). Physiochemical drug parameters that favor passive diffusion across endothelial cells include high lipophilicity, small size and molecular weight (less than 400 Daltons) and low hydrogen bonding potential (Warren, 2018). It should also be noted that there are instances where CNS drugs can reach the brain in sufficient amounts despite having physiochemical properties that would likely prohibit the drug from reaching the brain by passive diffusion (Hu et al., 2020). In these instances, solute carrier transporters expressed on brain endothelial cells can aide in achieving therapeutic drug concentration in the brain (Hu et al., 2020). In addition to restricted physicochemical parameters, drugs that target the CNS face additional barriers in comparison to other cellular barriers. These include tight junctions between endothelial cells of the BBB which significantly reduce permeability of ions and small hydrophilic solutes through the paracellular pathway (Carpenter et al., 2014). Additionally, endothelial cells forming the BBB lack fenestrations which also plays a role in limiting drug distribution to the brain (Carpenter et al., 2014).

Drug penetration in the BBB is also heavily influenced by ABC efflux transporters. In this regard, the human multidrug resistance proteins (MRPs), P-glycoprotein (P-gp) and Breast Cancer Resistance Protein (BCRP) are of clinical relevance (D. W. Miller et al., 2021). Efflux transporters play an essential role in drug distribution due to their high expression levels in human brain capillary endothelial cells, luminal distribution within the BBB, and broad range of drug substrates (D. W. Miller et al., 2021). Pre-clinical studies using knockout mice, pharmacological inhibitors

and ABC transporter over-expressing cell lines have all contributed to a greater understanding of the functional role of active efflux transporter processes for drug permeability in the BBB (Löscher & Potschka, 2005). P-glycoprotein is a transporter localized on the luminal plasma membrane in capillary endothelial cells, and is therefore, in contact with the blood (D. S. Miller et al., 2008). This ideal localization results in P-gp's ability to significantly decrease drug accumulation with the CNS by binding to and actively leading to drug efflux a from the endothelial cells to the blood compartment. (Sun et al., 2003).

For many lipophilic drugs, genetic knockout and chemical inhibition of P-gp can result in substantial (i.e., 10-50-fold) increases in the brain accumulation of drug (Miller et al. 2008). Despite high levels of P-gp expression in the intestines, liver and kidneys, pharmacokinetic studies in knockout mice showed only slight increases in plasma levels, despite large increases in drug concentration in the brain, reflecting the importance of ABC efflux transporters in controlling the CNS accumulation of drugs (D. S. Miller et al., 2008). P-glycoprotein is encoded by the *hMDR1* gene, and has several important promoter elements responsive to drugs and drug metabolites (D. S. Miller et al., 2008). Some of the promoter regions bind to transcription factors that are sensitive to environmental stressors such as oxidative, inflammatory and hypoxic conditions alluding to possible modulation mechanisms during pathological conditions (D. S. Miller et al., 2008). Lastly, intracellular signals were also found to affect P-gp transporter activity without changing transporter expression suggesting post-translational modulation mechanisms such as transporter trafficking, degradation, phosphorylation/dephosphorylation and ability to associate with other proteins (D. S. Miller et al., 2008). Taken together, these studies highlight the complexity of P-gp's role in limiting BBB penetration of drugs under normal and pathological conditions.

1.4 Tumor Microenvironment and BBB Modulation.

Glioblastoma multiforme (GBM) is a highly aggressive malignant brain tumor formed by abnormal development of glial cells, specifically astrocytes (Alphandéry, 2018). Glioblastoma multiforme is the most common brain tumor among adults, with a diagnosis average age of 64, a survival time of less than 15 months and 225,000 deaths per year (Alphandéry, 2018). Typical course of treatment includes surgery for tumor resection followed by radiation and chemotherapy (Alphandéry, 2018). However, GMB is known for its frequent relapse due to difficulty in removing tumor tissues and resistance to current therapeutics (Alphandéry, 2018). Glioblastoma show marked tumor heterogeneity that can result in differential activation/silencing of various signaling pathways (Yeung et al., 2013). This variability in cellular and molecular signaling is an added element that makes response to treatment options variable and unpredictable (Yeung et al., 2013). Additionally, glioblastoma stem cells (GSC) and quiescent endogenous GB cells have been identified which are resistant to standard pharmacotherapy, display sustained long-term tumor growth and are highly invasive and proliferative cells (Yeung et al., 2013) further complicating treatment options for patients.

Diffuse intrinsic pontine glioma (DIPG) represents the leading cause of brain tumor mortality in children (Chaves et al., 2020). Diffuse intrinsic pontine glioma occurs within the brainstem and is diagnosed in children between the ages of 5 and 10 (Chaves et al., 2020). Similar to GMB, DIPG is a highly aggressive grade IV tumor with rapid onset and a survival time of less than a year after diagnosis (Chaves et al., 2020). Treatment options for DIPG are limited as anatomical location makes surgery impossible, and radiotherapy and chemotherapeutics have not been proven to increase life expectancy in pediatric patients (Chaves et al., 2020; Harder et al., 2018). Similar to GBM, DIPG chemoresistance likely arises due to protection by the BBB which

restricts drugs from entering tumor locations in therapeutic concentrations (Chaves et al., 2020). Clinically, MRI scans with gadolinium based contrast agents are an effective way to confirm the diagnosis of brain tumors (Warren, 2018). Disruption of BBB integrity in and around the tumor mass is observed through increased leakage of the gadolinium agent out of the endothelial lumen and into extracellular space (ECS) and enhancement is readily visible on MRI images (Warren, 2018). A leaky blood-brain tumor barrier is often observed with GB, although it can be a very heterogenous blood-brain tumor barrier with some areas leaky and others in tact (Mo et al., 2021). However, clinically most all DIPG tumors are non-enhancing at the time of initial diagnosis, indicating preservation of an intact BBB (Warren, 2018).

Glioblastoma multiforme are highly vascularized tumors with extensive angiogenesis and potential for regional hyperdilation and leaky vessels (De Vleeschouwer & Bergers, 2017). However, several studies have shown this BBB disruption to be heterogenous in GBM patients, with tumor mediated changes in the BBB varying with tumor stage, volume, type and location (Luo & Shusta, 2020). A major factor resulting in BBB compromise is VEGF. Under physiological conditions, vascular endothelial growth factor (VEFG) is mainly secreted by astrocytes (Deng et al., 2020). However, in GBM, it has been well documented that tumor cells produce large levels of VEGF leading to angiogenesis and BBB breakdown (Belykh et al., 2020). Large concentrations of VEGF lead to abnormal vascular endothelial expression of transporters and receptors to meet the demands of the highly metabolic tumor cells (Belykh et al., 2020). Studies have shown decreased expression of tight junction proteins in the brain-tumor barrier (BTB) which may, at least in part, be attributed to the high levels of VEGF (Mo et al., 2021). The induction of vascular hyperpermeability within BBB endothelial cells can lead to compromised vascular function and leakage of fluid into tumor tissues (De Vleeschouwer & Bergers, 2017). In response, immune cells

are recruited which release proangiogenic factors that aid in expanding the tumor vasculature (De Vleeschouwer & Bergers, 2017). In addition, astrocytes play a significant role in metabolic homeostasis within the CNS and regulating cerebral blood flow, however, during GBM, astrocytoma cells displace normal astrocytes from vessels and disrupt the normal astrocyte-endothelial cell interaction thereby hindering regulation of vascular tone (De Vleeschouwer & Bergers, 2017).

The inflammatory response also plays a critical role in gliomagenesis by promoting blood vessel formation with abnormal vessel structure, tumor growth and invasion, and increased endothelial cell permeability (Couto et al., 2019). Cytokines released by tumor cells, immune cells and endothelial cells play a significant role in the GBM pathophysiology (Alghamri et al., 2021). High levels of interleukin-6 (IL) are commonly found within the microenvironment of tumors and are associated with poor prognosis in patients (Couto et al., 2019). In support, studies find inflammatory cytokines IL-1β, IL-6 and IL-8 were significantly increased in GBM cell lines and patient derived tumor samples (Yeung et al., 2013). Research suggests these cytokines contribute and play a role in GBM proliferation, invasiveness, drug resistance, angiogenesis, tumor heterogeneity, and tumor growth (Yeung et al., 2013). In addition, tumor necrosis factor-alpha produced by tumor associated macrophages (macrophages that participate in the formation of the tumor microenvironment) can induce expression of inflammatory molecules in other cell types (Alghamri et al., 2021). Glial cells such as astrocytes and microglial as well as endothelial cells can secrete mediators such as metalloproteinases (MMP's) which help to form the tumor microenvironment and support tumor growth (Alghamri et al., 2021). Lastly, lipid metabolism is altered in rapidly proliferating cells and can be considered a hallmark of cancer cells, whereby GMB tissue has been shown to have increased lipid synthesis (Taïb et al., 2019). In addition to

regulating tumor responses, alterations in fatty acids, triglycerides, prostaglandins, and phospholipids can play a role in signal transduction which can mediate rapid endothelial cell responses and BBB modulation during tumor cell progression (Taïb et al., 2019).

Optimization of clinical protocol and treatment options require representative and accurate pre-clinical experimental models which so far have had major draw backs (Alphandéry, 2018). Since tumor and host immune cell interaction allows for the immune system to detect and recognize surface specific antigens that arise from genetic and/or epigenetic modifications within tumor cells, development of *in vivo* models becomes complex (Choi et al., 2018). Additionally, since mice and humans express different surface antigens, injection of mice models with human tumors becomes complicated for risks of human cell rejection and attack by the mouse immune system (Choi et al., 2018). Therefore, to reduce rejection of human tumor cells by the mouse, immunodeficient mice have been employed for *in vivo* research studies (Choi et al., 2018). Mouse models have become invaluable to cancer research development, specifically patient derived xenograft (PDX) models. In PDX models, human tumor patient samples are directly transplanted into immunocompromised mice (Okada et al., 2019). These models are of critical importance since they retain important characteristics of the patients tumor, allowing for more personalized medicine development, representation of tumor heterogeneity and retaining specific gene expression profiles of the patient specific derived tumor (Okada et al., 2019). Patient derived xenograft models play significant roles in pre-clinical cancer research, however, mice models are not without disadvantages. Since mice models required for human tumor research must be immunodeficient, this hinders proper evaluation of tumor growth and clinical patient responses that occur in real time during patient tumor progression, making drug relatability screening difficult (Pompili et al., 2016). In GBM, immune cells play a critical role in interacting with tumor

tissues during patient tumor progression and personalized drug treatment has limited relatability in PDX models. Lastly, tumors in mice are a lot smaller than humans and may have variability in tumor responses due to species and scaling differences between mice and humans (Alphandéry, 2018). Therefore, there is increased interest in the development of *in vitro* models that accurately reflect BBB and blood-tumor barriers and allow high throughput drug screening. Furthermore, as both GBM and DIPG display tumor heterogeneity, certain therapeutics may be beneficial for some patients but not others, and the development and exploration of *in vitro* models that can allow for fast and accurate identification of patient centered effective drug therapies is of critical importance (Alphandéry, 2018). These pre-clinical *in vitro* techniques will provide value in understanding the molecular and functional differences between tumors and individual patients that could lead to a better understanding of molecular and functional changes occurring in endothelial cells during tumor cell progression and the general tumor microcellular environment.

1.5 Limitations of *in vitro* Models for Studying BBB.

Cell culture models are paramount to discovery and understanding of cellular biology, mechanisms of disease, tissue morphology, and drug action to list a few (Kapałczyńska et al., 2018). Establishment of reliable culture models are critically important in cancer research for pre-clinical drug discovery processes involving therapeutic target validation and drug candidate selection. In the case of brain cancer, additional *in vitro* models that accurately predict drug delivery to the tumor target are needed. Tight junctions and ABC efflux transporters located on polarized endothelial cells present a major obstacle to pharmacotherapeutics reaching brain tumors in sufficient concentrations to exert anti-tumor effects. Therefore, it is critically important for *in vitro* cell culture models to support co-culture conditions allowing endothelial cells to be grown in close proximity to tumor cells to model the tumor microenvironment. This can more

accurately determine drug permeability across the brain microvasculature and identify methods for optimizing anti-tumor effects. In addition, models that would support patient tumor sample growth would provide value in determining patient specific tumor responses to drug candidates.

Currently, two-dimensional (2-D) cellular models are extensively used for *in vitro* studies of both endothelial cell and tumor cell biology. Two-dimensional cell culture models include cells attached to tissue culture surfaces or scaffold or suspended in culture medium (Kapałczyńska et al., 2018). The advantages of 2-D cell culture models include reduced cost, simple design, and lower level of technical complexity (Augustine et al., 2021). These culture models are also associated with high reproducibility and long term culture (Augustine et al., 2021). Lastly, these culture methods have been used to study transporter kinetics and solute permeability monitoring and to predict drug performance and brain penetration *in vivo* (Augustine et al., 2021).

Traditional 2-D models have several disadvantages, one of which includes accurately representing the natural structures of tissues or tumours (Augustine et al., 2021). Specifically, *in vivo* capillary brain endothelial cells form tubular microvessel structures, however, when studied using 2-D models, they only have the ability to form simple single monolayers which can severely limit replication of *in vivo* conditions and likely cannot replicate the biological environment, making data less representative of those encountered in the clinic (Augustine et al., 2021). Additionally, many 2-D models of biological barriers require culturing of the cells on some type of semi-permeable membrane. This membrane, while useful for assessing permeability across cellular barriers, can also limit the direct cell-cell interactions necessary for the more complex co-culture models required to closely replicate *in vivo* conditions (Kapałczyńska et al., 2018). These interactions are crucial for expression of key genes and

proteins, cellular function, differentiation and proliferation which become compromised when cellular interactions are limited (Kapałczyńska et al., 2018). For example, within the various culture models of the BBB, *in vitro* data suggest that co-cultures of astrocytes, neurons, endothelial cells, and pericytes exhibited greater barrier properties with decreased permeability and improved transendothelial resistance compared to monoculture endothelial cell conditions (Miranda-Azpiazu et al., 2018).

An additional limitation for many 2D cell culture models is that they are grown under static "no-flow" conditions which fails to capture the *in vivo* environment, especially with vascular endothelial models where flow is important to cell polarity and cell signaling (Kapałczyńska et al., 2018). Cell polarity is crucial for proper endothelial cell function and development. Additionally, lack of flow decreases access to oxygen, availability of nutrients, metabolites and signaling molecules and likely leads to an endothelial cell stress response which changes the microcellular environment (Kapałczyńska et al., 2018). While useful in many aspects, these 2D culture models cannot adequately take into account the natural interactions and environment of cells and therefore as a result, may not replicate the conditions observed *in vivo* (Edmondson et al., 2014). For example, in Transwell^{TM} inserts containing a monolayer of brain endothelial cells, *in vitro* permeability values using a small molecular weight marker, sodium fluorescein (384Da) was found to be $1x10^{-5}$cm/s (Eigenmann et al., 2013). However, *in vivo* permeability values in brain microvessels were 10-fold or more lower (Eigenmann et al., 2013; Shi et al., 2014). It can be speculated that these observed increases in permeability values in 2-D culture models can be attributed to the lack of natural cellular interactions and blood flow conditions observed during physiological BBB conditions. These results support the importance of more predictive models to predict and guide *in vivo* studies.

Due to the many disadvantages of 2-D conditions, three-dimensional (3-D) culture systems were developed to better access and understand cellular growth and microenvironment. In fact, recent research suggests that cells in a 3-D culture environment differ morphologically and physiologically from the 2-D environment with 3-D cultured cells more accurately reflecting *in vivo* cellular responses (Edmondson et al., 2014). By allowing formation of 3-D cellular structures, these models allow the spatial and physical arrangements that influence signal transductions, gene expression, cellular patterns and behavior (Edmondson et al., 2014). Three-dimensional cell culture models can be used to assess cell-cell interactions, stimulate flow conditions, and monitor permeability of solutes while forming 3-D scaffold structures allowing a greater understanding of interactions and conditions that occur within the natural CNS environment (Chen et al., 2021). Three-dimensional systems can be divided into cell spheroid/aggregates concentrated in gel-like matrixes, cultures on a gel matrix scaffold or 3-D spheroids grown in suspension (Białkowska et al., 2020). However, 3-D spheroids can also offer their own sets of disadvantages such as difficulty forming multicellular interactions, shear stress stimulation, lack of nutrient/waste/gaseous exchange and limited uniformity and reproducibility (F. Yu et al., 2019). These three-dimensional scaffolds also lack the ability monitor transport of compounds (Edmondson et al., 2014).

1.6 Microfluidic Cell Culture Systems.

Recently microfluidic techniques for cell culture were established, which refers to technologies that manipulate small fluid volumes (Halldorsson et al., 2015). There are a variety of microfluidic systems available that can be adjusted and set to individual cell type requirements or co-culture conditions. The ability to set up multiple cell types for co-culture systems can allow for replication of the *in vivo* brain anatomy (Edmondson et al., 2014). Microfluidic cell culture

systems also offer continuous perfusion of cultures, creation of chemical gradients, and reduced consumption of reagents (Halldorsson et al., 2015). However, there are disadvantages to some microfluidic techniques, not the least of which includes, complex design and due to this complexity, they typically require skilled and trained users (Edmondson et al., 2014). This complexity in design in both experimental set up and cellular monitoring also makes it difficult to satisfy high throughput requirements leading to low throughput and data yields. (Augustine et al., 2021). These microfluidic platforms are relatively expensive and many still require the presence of an artificial membranes for cell supports that separates co-cultured cells (Augustine et al., 2021). Lastly, cellular compartments are difficult to visualize, and are not easily standardization for quantification of parameters (Augustine et al., 2021).

Mimetas^{TM} microfluidic organoplate is an organ-on-chip model that can be used to culture various cell types such as endothelial cells, epithelial cells, neurons, and immune cells to name a few. This dynamic microfluidic model (DMF) differs from other microfluidic techniques in that it has a relatively simple design which limits complex set up (Duinen et al., 2017). Additionally, the DMF system offers a membrane free system, whereby the cellular compartments are separated by a phase guide (Duinen et al., 2017). The phase guide is a meniscus pinning barrier which is only one quarter the height of the microfluidic channel, therefore, it does not block cell-cell or cell-ECM interactions (Duinen et al., 2017). Having cell-cell and cell-ECM interactions is of critical importance to allow correct patterning, signaling and expression of key proteins within cells and more accurately represents *in vivo* like conditions (Duinen et al., 2017). Additionally, this membrane free system also allows for free diffusion of chemical gradients, compounds and proteins due to its composition of low absorbing materials (*Our Technology,* n.d.). Lastly, the DMF system does not rely on pump mechanisms to stimulate

fluid flow, but rather utilizes a rocking platform to stimulate perfusion of media across cells at conditions set by the user (*Our Technology*, n.d.). This pump free system decreases experimental complexity and allows for metabolic homeostasis. Perfusion of media can occur within the apical compartment, basolateral or both depending on cell culture needs (*Our Technology*, n.d.). A final consideration for this particular DMF system is the use of glass-based material, as opposed to plastic, which allows for excellent imaging that pairs with common laboratory equipment such as fluorescent, confocal and standard light microscopy (*Our Technology*, n.d.). Immunostaining, barrier integrity, permeability assays, TEER measurements, viability, sampling from apical and basolateral conditions for LC-MS, and RNA expression studies are some of the broad assays that are compatible with the DMF system. The broad assay compatibility makes this device easily suitable for multiple complex needs. To summarize, the DMF Mimetas^{TM} technique seems to support pre-clinical experimentation which can be used to model complex co-culture systems such as the neurovascular unit where multiple cell types can be cultured to create a complex microcellular environment. This model can also be used to study molecular and functional changes occurring at the BBB during normal and pathological conditions such as tumor progression.

1.7 Two Lane Microfluidic Plate.

The two lane organoplate is composed of 384 wells consisting of 96 individual microfluidic units (refer to Figure 4.) (*OrganoPlate® 2-Lane 96*, n.d.). Each of the 96 testing units can form independent tissue culture chips. Each unit contains a gel channel where ECM is added. Additionally, directly above the ECM channel, is the perfusion lane and is the site where cells to be perfused are seeded (*OrganoPlate® 2-Lane 96*, n.d.). Located in a position that captures both the gel and perfusion lane, the observation window is where cells can be visualized

and monitored. This set up is ideal for visualization experiments and flexible tissue culture configuration which include in gel cell cultures, cells seeded against ECM, tubular cultures or a combination to create co-culture settings (*OrganoPlate® 2-Lane 96*, n.d.). The two lane organoplate enables access to the apical compartment to allow for addition of compounds and/or stimuli. However, the two lane plate lacks a basolateral chamber, therefore experiments requiring basolateral sampling cannot be performed (*OrganoPlate® 2-Lane 96*, n.d.).

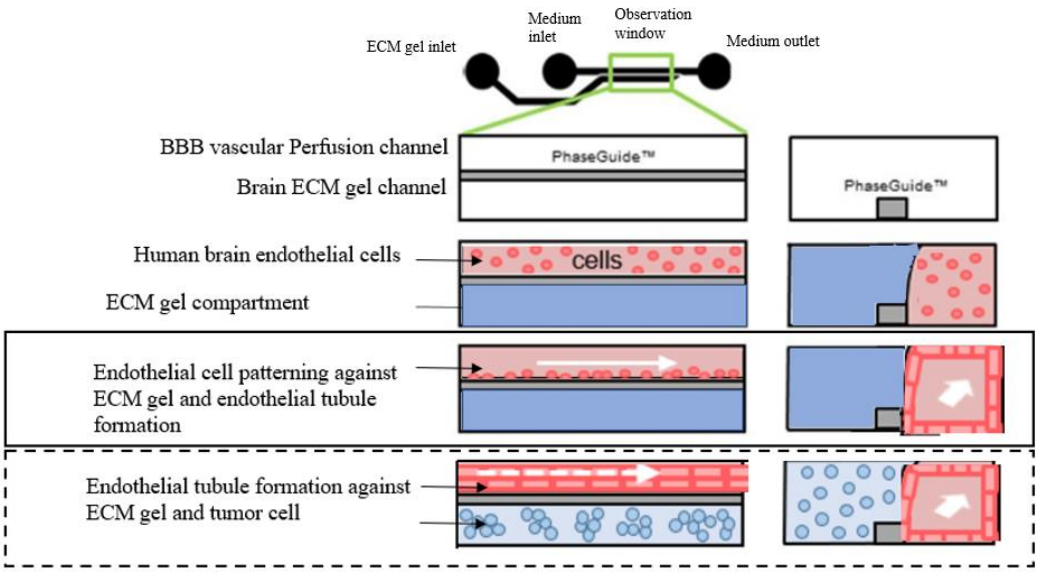

Figure 4: Qualitative representation of MimetasTM 2-lane microfluidic organoplate. (OrganoPlate® 2-Lane 96, n.d.)

1.8 Three Lane Microfluidic Plate.

The three lane organoplate has a similar 384 well plate format, however, it contains only 40 microfluidic testing units (*OrganoPlate® 3-Lane 40*, n.d.). The plate contains only 40 testing units due to the presence of a third channel below the ECM lane (refer to Figure 5.). The presence of a third channel allows for access to both basolateral and apical sides of tubules (*OrganoPlate® 3-Lane 40*, n.d.). Therefore, experiments requiring basolateral sampling can now be performed. Multiple cell types can be seeded within each channel, and this can create, for

example, a neurovascular unit which enables complex cellular modeling. This complex modeling can capture cell-cell or cell-ECM interactions. Perfusion can be applied in the first perfusion lane and/or third lane if desired which gives freedom in designing culture systems (*OrganoPlate® 3-Lane 40*, n.d.). In both cases, plates are placed on an organo-rocker which is a simple rocker system where inclination and interval time can be manually set to create bidirectional fluid flow that best suites the cellular type and assay (*OrganoPlate® 3-Lane 40*, n.d.).

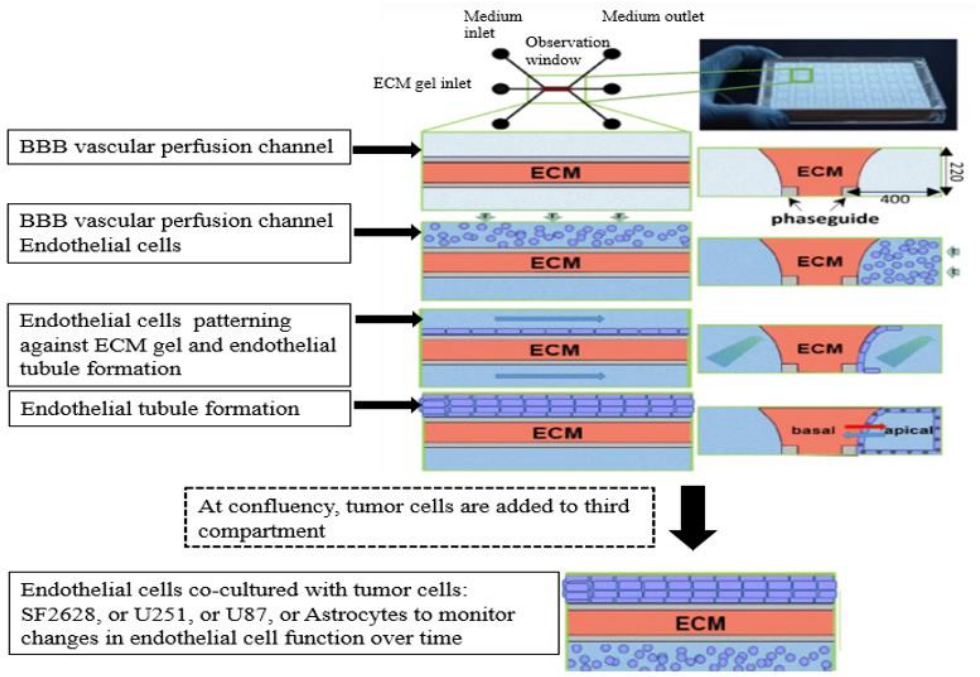

Figure 5: Qualitative representation of MimetasTM 3-lane microfluidic organoplate (OrganoPlate® 3-Lane 40, n.d.)

1.9 Rationale and Objectives.

Novel approaches to drug discovery and assessment of their biological membrane permeability are paramount to improve drug delivery to the brain. The DMF offers a high throughput platform whereby multiple different drugs can be added to independent culture chips and their permeability assessed. The dynamic microfluidic system has the ability to culture several

different cell types which can model CNS architecture *in vivo*. Multicellular culturing can allow insights into inter and intracellular drug transport. Clinically, this could provide valuable insights into drug action and efficacy. Therefore, evaluating novel ways to increase BBB permeability of select therapeutics while limiting toxic effects is of importance. Throughout our work, cadherin peptides were found to be effective at increasing BBB endothelial cell permeability to both various sized solutes and therapeutics such as Avastin and lipid nanoparticles. Lastly, these cadherin peptides were also found to be selective for BBB endothelial vasculature and effective during heterogenous co-culture.

Simplistic microfluidic organo-on-a-chip models pair well with common laboratory equipment and can form simple to complex cellular microenvironments. This will enable replication of cell-cell and cell-ECM interactions that are difficult to capture with other *in vitro* techniques. Forming more complex cellular interactions could closely capture physiological conditions occurring *in vivo*, allowing for a representative analysis of molecular and functional changes occurring within the microcellular environment. Additionally, creation and validation of a dynamic BBB-GB co-culture model that more closely captures *in vivo* BBB conditions can allow for greater understanding of the altered microenvironment that occurs during GB progression. This model can be used to monitor changes in endothelial cell function over time in response to tumor cell progression. Lastly, this BBB-GB co-culture model can provide a more realistic model for examining treatment options in GB patients.

The objectives of the current study were to develop a DMF- BBB- brain tumor co-culture model using the microfluidic platform. As BBB function is not static, but responsive to the microenvironment, the proposed studies will aid in the identification of molecular and functional changes occurring in BBB endothelial cells in response to tumor cell progression and the tumor

microenvironment. The data generated in the DMF model was compared to traditional Transwell™ inserts to determine if the DMF provides improved barrier properties and can identify tumor-induced modulation of the BBB. Various tumor cell lines were selected to encompass the tumor heterogeneity observed *in vivo*.

It was hypothesized that the 3-D microfluidic model of the BBB would provide improved barrier properties and increased gene expression of BBB specific genes compared to traditional Transwell™ inserts and provide a more accurate assessment of *in vivo* conditions. The 3-D microfluidic BBB-GB co-culture model was also hypothesized to aid in identifying tumor-induced modulation of the BBB. The results of these studies showed that in monoculture conditions, the DMF model produced permeability values similar to that observed *in vivo* with significantly increased barrier properties compared to Transwell™ inserts. It was determined that U251 co-culturing in both models did not result in significant changes in endothelial cell permeability. In contrast, the U87 co-culture model seemed to cause endothelial cell leakiness, potentially due to inflammatory cytokine release or increased secretion of triglycerides and fatty acids. Finally, SF8628 co-culture enhanced BBB endothelial cell barrier properties. This was likely the result of sonic hedgehog release from tumor cells acting indirectly to regulate other factors or signaling pathways.

2.0 Methods

2.1 Materials.

Cell culture media was purchased from either Thermo Scientific (Waltham, MA, USA) or Lonza (Muenchensteinerstrasse, Switzerland). Cell culture flasks, plates and dishes were obtained from either Corning incorporated (Corning, NY, USA), Sigma (Oakville, ON, Canada), or ThermoScientific (Waltham, MA, USA). The 2-lane and 3-lane microfluidic organoplates and organorocker were purchased from Mimetas^{TM} (Gaithersburg, MD, USA). Mesoscale plates for cytokine analysis were purchased from Mesoscale discovery (Rockville, MD, USA). Reverse Transcriptase- Polymerase chain reaction kit was purchased from BioRad (Mississauga, ON, CA), Qiagen RNeasy micro column kit (Toronto, ON, CA), Trizol (Thermo Scientific), and primers were designed using NCBI/Primer-BLAST and manufacture by Invitrogen. Matrix Metalloproteinase inhibitor (MMP) was purchased from Abcam (Toronto, ON, Canada) and cultrex 3-D Culture Matrix Rat Tail Collagen I 5mg/mL was purchased from R&D systems (MN, USA). The fluorescent dye, non-pegylated IRdye was purchased from Licor (NB, USA), FDX70,000 TheromoScientific and Rhodamine 800 Exciton (OH, USA). The fatty acids oleic acid, palmitic acid, steric acid, fatty acid free BSA and L-serine were purchased from Sigma (Oakville, ON, Canada) while fluorescently labelled albumin, BSA Alexa fluor 488 conjugate was purchased from ThermoFisher (Ottawa, ON, Canada). Endocytosis inhibitors were purchased from Sigma (Oakville, ON, Canada). Cadherin peptides and monoclonal antibody were provided from our collaborator, Dr. Teruna Siahaan, at the University of Kansas. Nanoparticles were manufacture at the University of Manitoba by Dr. Vinith Yathindranath as described previously (Yathindranath et al. Cancers 2022).

2.2 Cell Culture.

The cell lines used consisted of the human cerebral microvascular endothelial cell line (hCMEC/d3), a human diffuse intrinsic pontine glioma (DIPG) pediatric cell line (SF8628), human glioblastoma (GB) cell lines (U251 and U87), Madin-Darby canine kidney-multi drug resistance (MDCK-MDR) epithelial cell line, primary human astrocyte cells (HA), and primary lung endothelial cells. Cells were cultured according to manufactures directions. Briefly, cells were plated in a T-75 flask and grown in Endothelial Basal Media (EBM)-2 (hCMEC/d3), Dulbecco's Modified Eagle Medium (DMEM) (SF8628), DMEM-F12 (U251 and U87), DMEM + colchicine (MDCK-MDR), Astrocyte media (HA cells), and Endothelial cell medium (ECM, primary lung endothelial cells) respectively. Cells were grown and maintained in incubator conditions of 37^{O}C with 5% CO_2, media was changed every other day.

2.3 Monoculture and Co-culture in Transwell™ and Microfluidic Model.

2.3.1 Transwell Insert Monoculture and Co-Culturing.

The hCMEC/d3 cells were seeding at 40,000 cells/cm^2 in 6 well 0.4µm 4.67 cm^2 Transwell™ insert and grown for 3-4 days until confluent. Cellular visualization on Transwell™ inserts is difficult, therefore, a 6-well cell culture plate was seeded at the same cell density and used as a control to monitor confluency over time using a phase-contrast microscope (Evos). Media was added, 1.5 and 2.5 mL respectively, to apical and basolateral sides of inserts every other day until cells were confluent. To create Transwell™ co-culture conditions, U251, SF8628, U87, or astrocytes were seeded at cell densities of 20,000, 32,000, 20,000 and 32,000 cells/cm^2 within a 6-well cell culture plate using appropriate culture media. At endothelial cell confluency, the Transwell™ inserts were transferred to the 6-well culture plates containing the tumor and

astrocyte monolayers to create co-culture conditions. Additionally, 12-well Transwell^{TM} inserts 0.4µm with a growth area of 1.12cm^2 were used. Endothelial cells were seeded at the same cell/cm^2 density and co-culturing followed the same protocol as above. Co-cultured cells were grown in EMB-2 media on both apical and basolateral sides for 24 hours.

2.3.2 BBB Dynamic Microfluidic 2-Lane and 3-Lane Monoculture.

The microfluidic BBB culture model was established using two and three-lane organoplate plates (Gaithersburg, MD, USA). The plates are configured in a 384-well format in which the two-lane and three-lane plates consist of 96 and 40 microfluidic units respectively. Within each unit, both plates contain a top channel (capillary perfusion lane), and an extracellular matrix gel. A main factor distinguishing the two-lane plate from the three-lane plate is the presence of a third channel (brain extracellular space) in the three-lane organoplate underneath the middle ECM channel. Each channel has inlet and outlet ports as well as an observation window for examining barrier formation/integrity. The top and bottom channels have dimensions of 300µm x 220µm (WxH) and the gel 350µm x 220µm. A phase guide separates the top and bottom channels from the gel channel in the microfluidic chamber and is used to pattern the ECM gel into the middle compartment (100 x 55µm WxH). Within the observation window, 50µL of HBSS was added to aid in cellular viewing. Prior to seeding the hCMEC/d3 cells into the microfluidic unit, a 2 µL solution of ECM was dispensed into the middle channel. The ECM consisted of Cultrex 3D rat tail collagen (R&D systems). A ratio of 8:1:1 composed of collagen (5 mg/mL), 100 mM HEPES, and 37 g/L$NaHCO_3$ (pH 9.5) were mixed to form the final 4 mg/mL rat tail collagen dispended onto the microfluidic wells. The plate was incubated for 15-minutes at 37ºC 5% CO_2. Following incubation, 30 µL of HBSS was added to the gel inlet to prevent gel from drying out and placed back into the incubator for an

additional 1.5-hours to establish the ECM gel in the middle channel. After the incubation the HBSS was removed from gel inlet and human endothelial cells (hCMEC/d3) or pulmonary endothelial cells (HPMEC) were seeded into the top channel inlet of the microfluidic unit by dispensing 2 µL of cell suspension (10,000 cell/µL). For the MDCK/MDR cells, a cell suspension containing 8000 cells/µL were dispensed into the top channel inlet. Following cell seeding, 50 µL of appropriate cellular media was added to top channel inlet and the plate was placed on its side in an incubator to allow cells to pattern and attach against the ECM gel. Following a 2.5-hour side incubation, 50 µL of media was added to the top channel outlet and the plate was then placed on a Mimetas^{TM} interval rocker undergoing +7 and -7 inclinations every 8-minutes, to provide bidirectional fluid flow. Cells were grown to confluency in 37°C 5% CO_2 incubator with media changes every other day.

2.3.3 Creating BBB-GB Co-culture Conditions in Two and Three Lane Organoplate.

In the 3-lane organoplate at endothelial cell confluency, a 2 µL cell suspension of SF8628, U251, U87 or astrocyte cells were seeded in the third channel at a cell density of 5000 cells/µL, 3500 cell/µL, 3500 cells/µL and 5000 cells/µL. The plate was then incubated upside down on its side for 1.5-hours to allow the cells to attach to the ECM gel. Following cell attachment, the plate was then placed back on the rocker for the necessary co-culture time period, 24, 48 or 72-hours. In contrast, in the 2-lane organoplate tumor cells were suspended within the ECM gel and seeded at the same time as endothelial cells. Tumor cell suspensions were created at the above cell densities and re-suspended in the ECM gel to create in gel tumor co-culture conditions. A final volume of 2 µL of the tumor cell/gel mixture was added to the gel

inlet. Subsequently, endothelial cells were then seeded in the perfusion inlet as previously described.

2.4 Permeability Assessments.

2.4.1 Determination of Leak Tight Vessels using Barrier Integrity Assay 2-Lane Organoplate.

Endothelial cells were cultured in the 2-lane organoplate as previously described. At endothelial cell confluency, 20 µL of media was added to gel inlet and outlet ports as a pre-wetting step. Following that, 70 µL of FDX 70,000 (1 µM) in EBM-2 media was added to the top channel, in which 40 µL and 30 µL of the solution was dispensed in the inlet and outlet port respectively. Immediately the plate was taken to an EVOS microscope (GFP channel) and pictures of the perfusion and gel channel were taken at 10x objective every 5-minutes for a total of 30-minutes. Generated images were added to ImageJ FIJI software where regions of interest were defined for apical and basolateral regions. This was standardized for all images to allow quantification of fluorescent dye leakage from the endothelial microvessel into gel channel. Fluorescent pixel intensities of each perfusion and gel region were measured to ensure the image was in the detectable range and relative ratio of fluorescence in the gel channel to fluorescence in the perfusion lane were plotted over time. Values below 0.4 with a relatively constant ratio were considered leak tight vessels. Apparent permeability for the barrier integrity assay was calculated using the equation: $Papp\left(\frac{cm}{s}\right) = \frac{\Delta\left(\frac{Igel}{Iperfusion}\right)}{\Delta t} * Vgel * \frac{1}{Area}$, whereby, $I_{gel}/I_{perfusion}$ is the ratio between the intensity in the gel and perfusion channel, V_{gel} is the volume of gel in contact with perfusion lane ($4.54x10^{-4}cm^3$), and A indicates the surface area of the perfusion lane containing

the microvessel that is in contact with the gel ($1.21x10^{-2}cm^2$). To create no flow "static" conditions, the plate was not placed on the rocker and was left to lay flat inside the incubator.

2.4.2 Permeability Assessments using Transwell™ Inserts and Microfluidic Model.

At endothelial cell confluency, a final concentration of FDX (70,000 MW) 1 µM, non pegylated IR dye (900 MW) 10 µM, and Rhodamine 800 0.1 µM were added to the Transwell™ apical compartment and inserts were swirled to ensure dye distribution. At time 0, 20µL of the apical compartment media was sampled and diluted 5-fold, while 100 µL of the basolateral compartment was sampled with media replacement. Basolateral samples were taken at 0,15, 30, 60, 90 and 120-minutes. Throughout the experiment the plate was placed on a shaker at 50 RPM to ensure dye distribution and disruption of the water layer. Samples taken were placed in a ninety-six well black plate and read on varioskan lux plate reader with excitation emission spectrum of FDX70,000 480/520, IRdye 785/812 and rhodamine 800 685/712. In the three-compartment microfluidic model, 20 µL of media was first added to inlet and outlet of gel and third channel which formed a pre-wetting step. Subsequently, 70 µL of media containing the three florescent dyes at a final concentration previously described was added to the perfusion channel, 40 µL to the inlet port and 30 µL to the outlet port. For experiments requiring sodium fluorescein (Na-F), a final concentration of 100 µg/mL was used. The perfusion compartment was sampled at time 0 to assess initial starting concentrations, whereby 10 µL was sampled, replaced, and diluted 5-fold in 384-well black plate. Passage of dye into the third compartment was monitored by taking basolateral samples from gel and third channel inlet and outlet ports. Plates were read under the same conditions on the Varioskan Lux plate reader to determine permeability under various conditions and formation of leak tight vessels.

Apparent permeability equation 1: $Papp(\frac{cm}{s}) = \left(\frac{\Delta Cr}{\Delta time}\right) * \left(\frac{Volume}{Area * \Delta Cd}\right)$

Endothelial cell permeability equation 2:$\left(\frac{1}{pcell}\right) = \left(\frac{1}{Papp}\right) - (\frac{1}{Pblank}$

2.5 Cellular Uptake Studies.

Cells were plated in 24-well culture plates at a cell density of 26,000 cells/cm^2 and incubated for 5/6 days until confluent. Elacradir (GF), a P-glycoprotein inhibitor, was added to cells at a concentration of 3.2 µM and incubated for 30-minutes. Following incubation, fluorescent dyes were added at the same concentration as previously described and incubated for either 30,60,90 or 120-minutes. Cells were subsequently washed in PBS, followed by Triton-X exposure to solubilize the cells. Solubilize cells were then placed in -20C overnight. Quantification of protein was done using Pierce BCA protein assay kit and protein absorbance of 590 nm was read on Gen5 plate reader. Samples of 20 µL were taken from the 24-well plate and diluted 5-fold into 96-well black plates using Triton-X to determine fluorescent dye uptake on a Varioskan Lux plate reader.

2.6 Endothelial RNA Extraction.

2.6.1 RNA Extraction in Transwell™ Inserts and Analysis of Blood Brain Barrier Specific Genes using Reverse Transcriptase- Polymerase Chain Reaction (RT-PCR).

Cells were harvested and total RNA was obtained using TRIzol reagent according to the manufacture's instructions. Concentration and absorbance purity ratios (260/280) of RNA were read on a nanodrop machine. Total RNA samples were stored at -80ºC for future use. Collected

RNA at a final concentration of 300 ng/µl was used for RT-PCR experiments. Protocol was followed according to BIO RAD iTaq™ Universal SYBR Green One-step Kit directions. Briefly, a master mix was created using iTaq universal SYBR green reaction mix which included DNA polymerase, fluorophore SYBR green for detection, nucleotides, iScript reverse transcriptase, RNA, and nuclease free water. Forward and reverse primers were added at a concentration of 300 nM to form a total of 10 µL reaction mix. Reactions were carried out on QuantStudio™ system. Thermocycler conditions are shown on Table 2.

Table 2. Thermocycler conditions

Step	Time	Temperature
Reverse transcription	10 minutes	50ºC
Initial polymerase activation and DNA denaturation	60 seconds	95ºC
Denaturation	15 seconds	95ºC
Annealing and extension	60 seconds	60ºC
Denaturation, annealing/extension:	40 cycles	

Primers for BBB specific genes were designed using NCBI/Primer-Blast and manufactured by Invitrogen. Primer sequences can be found on table 3.

Table 3. Primer list and sequence for BBB specific markers

Primer	Forward	Reverse	Product length base pair
Occludin	TGC CTT CAC CCC CAT CTG AC	TCA GGA ACC GGC GTG GAT TT	124
Zonula Occludens-1 (ZO-1)	CAA CTG AAG AAG TGG GCA	GAF GAT CCC CTT CTG CCG	119
Protein (BCRP)	AGCCACAGAGATCATAGAGCC	TCCTCACCCCCGGAAGTTG	129
P-glycoprotein (P-gp)	ATATCAGCAGCCCACATCAT	GAAGCACTGGGATGTCCGGT	153
Glucose transporter type 1 (GLUT-1)	CCAACGCAGAGAGAACGAGC	CGTTTATAGGACCCCGGCCAT	199
Claudin 1	TTTACTCCTATGCCGGCGAC	GAGGATGCCAACCACCATCA	133
Claudin 3	GCCACCAAGGTCGTCTACTG	CGTAGTCCTTGCGGTCGTAGG	105
Claudin 5	AGGCGTGCTCTACCTGTTTTT	AACTCGCGGACGCACAATGTT	77
Ve-cadherin	GTTCGGCTGACAGGTCCACA	CGATGTGGGGAGGAGCATCA	147
Mfsd2a	TCCTCCAAAGCACTGAACGT	ACTTCCTCATCCTTGTGAGCCA	184
Dynamin	CTTACATCCGGGAACGGGAG	ACCAGGATCTCCCCCTGATT	175

Caveolin1	GGGGTGTTCCGAGAGAGGTA	CGGTGTAGAGATGTCCCTGCG	111
Plasmalemma vesicle associated protein	CGATGVVTTGCTCTTCATGC	TTGTTCAGCAGCACGCTTTC	183

2.6.2 RNA Extraction in Microfluidic Organoplate using RNeasy Micro Column Kit:

Cells were harvested from the microfluidic organoplate using Trypsin-EDTA (0.25%). Trypsin was used to more accurately separate and detach different adherent cells during co-culture modeling in the 3-D plate. Trypsin was neutralized using media and cells were centrifuged at 1000 RCF and resuspended in fresh media containing 10% DMSO and stored in -80ºC until future use. Cellular RNA was extracted from cells in the 3-lane microfluidic plate using Qiagen RNeasy micro column kit according to manufactures direction. Concentration and purity ratios of harvested RNA were determined using 260/280 absorbance ratios on a nanodrop machine. An absorbance ratio of 1.8-2 was accepted as pure. Collected RNA was converted to cDNA. Once cDNA was formed, a PCR was conducted as previously described for 20 cycles to amplify the small amount of cDNA. The amplified cDNA was then used as the template DNA for a subsequent PCR to determine gene expression of BBB specific genes.

2.7 Mechanistic identification of Changes During Tumor Co-Culturing.

2.7.1 Inflammatory Cytokine Release from Tumor Cells to Elucidate Functional Changes in Endothelial Cells in Response to Tumor Cell Proliferation using Mesoscale Discovery (MSD) Platform.

Mesoscale discovery (MSD) was used to assess inflammatory cytokine release when endothelial cells are co-cultured with tumor cells in the three lane organoplate. Protocol was followed according to manufacturers direction. Briefly, the MSD platform uses biotinylated capture antibodies that are linked to a U-PLEX linker at the bottom of the plate. Capture antibodies and detection antibodies conjugated with electro-chemiluminescent labels bind the analyte in the sample to form a sandwich. Once the immunoassay sandwich has formed, the plate is read on MSD instrument. When voltage is applied to electrodes on the plate, labels emit light. Intensity of emitted light is determined proportional to the analyte concentration. Endothelial cells (hCMEC/d3) were grown in the three-lane organoplate as previous described. At endothelial cell confluency, tumor cell or support cells were added to the third channel to create co-culture conditions at cell densities and protocols previously described. Co-cultures consisted of hCMEC/d3 + U87 or U251 or SF8628 or astrocytes. At 24-, 48- and 72-hour co-culture time points, 20 µL EBM-2 media was added to gel and third compartment inlet and outlet ports and allowed to equilibrate in 3-lane organoplate for 60-minutes. Subsequently, 50 µL of media from each of the perfusion inlet and outlet ports and 20 µL from each inlet and outlet ports from the gel and third channel were collected to form a total end volume of 80 µL for a basolateral sample and 100 µL for apical. Samples were frozen at -80ºC for future use. The MSD U-plex platform was used which contained four analytes: Interleukin-6 (IL-6), Interleukin-8 (IL-8), Monocyte chemoattractant Protein-1 (MCP-1), and Vascular Endothelial Growth Factor-A (VEGF-A). Instructions were followed according to manufactures directions.

2.7.2 Intracellular and Secreted Lipid Profiling.

Endothelial cells were co-cultured with tumor cells in 0.4µm 6-well Transwell™ inserts as previously described. At endothelial cell confluency, both tumor and endothelial cells were washed 3x in cold PBS, 500 µL of methanol was added, and cells were scrapped and harvested in microcentrifuge tube. Methanol was evaporated and cells were dried using centrifugal vacuum concentrator for 2.5-hours. Following drying, cells were purged with nitrogen gas for 30-seconds to ensure lack of oxygen. Microcentrifuge tubes containing cells were stored at -80 ºC and shipped to the metabolomics innovation center (TMIC) at the University of Alberta for lipid profiling assessments using LC/MS as previously described (Zardini Buzatto et al., 2021).

2.7.3 Functional Assessment of Serine and Fatty Acids on Endothelial Cell Permeability.

In the lipidomic analysis, intracellular phosphatidyl-serine was elevated in endothelial cells, therefore, we sought to assess the impact of adding L-serine on endothelial cell permeability. Three different concentrations, 14 mg/L, 140 mg/mL, and 1400 mg/L were mixed in EBM-2 media, this was placed on endothelial cells seeded in 0.4µm Transwell™ inserts. Serine was present for the entire culture period until confluent. At endothelial cell confluency, 1 µM FDX 70,000, 10 µM non-pegylated IR dye, and 0.1 µM rhodamine 800 were added to the endothelial cells and a permeability assessment for 60-minutes was performed as previously described. Additionally, secreted levels of triglycerides/fatty acids were elevated during U87 co-culturing. We therefore sought to test the effects of palmitic acid, steric acid and oleic acid or a combination of all three on endothelial cell permeability. Treatments were added to confluent endothelial cells grown on 0.4 Transwell™ well inserts for either 3-hours or 24-hours and

palmitic acid was added to the 3-lane microfluidic plate for 24-hours, and permeability assessments were performed using 24-hour U87 co-culture as a positive control. A final concentration of 150 mM stock solution was made for each fatty acid by dissolving the appropriate amount of fatty acid in 1 mL of 100% ethanol. A final working solution of 0.1 mM were added to the cells which was prepared by mixing the fatty acids with 10% fatty acid free BSA and EBM-2 media.

2.7.4 Elucidating the Role of Tight Junctions or Endocytosis during Endothelial Cell Co-Culture:

To further investigate the functional changes occurring in endothelial cells in response to tumor co-culturing, endothelial cells were grown in 0.4μm Transwell™ inserts as previously described. At confluency, albumin from bovine serum (BSA) Alexa Fluor™ 488 was added to the cells to examine the endocytosis pathway and it's role in the barrier altering effects during various co-culture conditions. A final concentration of 10 μg/mL BSA, 0.1 μM rhodamine 800 and 10 μM non-pegylated IRdye were added to the cells for 2-hours. Samples were taken as previously described. Additionally, vesicular uptake of the various dyes was also assessed (previously described). To determine which mode of endocytosis was responsible for the changes in permeability observed, various endocytosis inhibitors were used. Endocytosis inhibitors were applied apically to endothelial cells for a pre-treatment of 30-minutes before permeability and uptake experiments in Transwell™ inserts. Chlorpromazine at a final concentration of 7 μg/mL was added to investigate clathrin mediated endocytosis. Genistein at a final concentration of 200 μM was used to investigate caveolae mediated endocytosis and monensin at a final concentration of 25 μM was used to inhibit endosome maturation. Endothelial cells were grown in monoculture conditions or in co-culture with either astrocytes,

GB U87 cells or SF8628 DIPG cells. Endocytosis inhibitors were added to each co-culture and monoculture condition. Endocytosis inhibitors at the same concentration were also added to endothelial cells grown in co-culture (24-hours) in the three-lane organoplate and permeability of the three fluorescent markers were assessed as previously described. Lastly, to assess molecular changes in vesicular RNA during various co-culture conditions, endothelial cells were grown in monoculture or in co-culture with U87, astrocytes or SF8628 in Transwell™ inserts, and an RNA extraction and subsequent qPCR was performed for *caveolin1 dynein2, Mfsd2a,* and *plasmalemma vesicle associated protein* (PVLAP).

2.7.5 Inhibition of Sonic Hedge Hog Signaling Pathway to Elucidate Mechanisms of DIPG Endothelial Cell Modulation.

Endothelial cells in 6-well 0.4µm Transwell™ inserts and 3-lane microfluidic culture plates were cultured as previously described. Tumor condition media from SF8628 cells was concentrated 2x and mixed with EBM-2 media in a 1:1 ratio. Vismodegib, a sonic hedge hog (SHH) receptor antagonist was added to this mixture at a final concentration of 1 µM. Separate studies examined the effects of Ruski-201, an agent that blocks the release of SHH from tumor cells. For these studies, Ruski-201 was added to SF8628 cells grown on a culture plate when they were 90% confluent. Tumor cells (SF8628) were cultured in DMEM media in the presence of RUSKI-201 for 24 hours, media was then changed. Tumor cells were then cultured in the presence of RUSKI-201 for an additional 24-hours and this media was collected to make the tumor conditioned media (TCM) + RUSKI-201 condition. The TCM + RUSKI-201 media was collected, concentrated 2x and diluted 1:1 with EBM-2 media and added to endothelial cells. In another treatment condition, confluent tumor cells previously cultured in the presence of RUSKI-201 for 24 hours were also placed co-culture with endothelial cells on Transwell™ inserts and

grown in EBM-2 media containing RUSKI-201 for another 24 hours. The total RUSKI-201 treatment on SF8628 tumor cells was 48-hours. Recombinant human sonic hedge hog (rhSHH) was added to EBM-2 media at a final concentration of 1 µg/mL and added to endothelial cells. All the treatments were applied to endothelial cells when confluency was reached for 18-hours before subsequent permeability experiments. Final treatments were:

1) Tumor condition media from SF8628 cells or SF8628 cells in co-culture with hCMEC/d3
2) 1 µM Vismodegib + TCM
3) 1 µg/mL recombinant human sonic hedge hog (rhSHH**)**
4) 1 µM RUSKI-201 + TCM

2.8 Endothelial Cadherin Peptide Modulation.

2.8.1 Endothelial Cell Permeability Modulation using Cadherin Peptides.

Brain endothelial and tumor cell co-culture conditions in the 3-lane microfluidic plate were cultured as previously described. At cell confluency, media in perfusion channel was aspirated and 20 µL media was added to gel and third channel inlet and outlet. Following that, a final concentration of 0.01, 0.1, and 0.5 mM cadherin peptide was prepared in media containing FDX70,000 1 µM, IRdye non pegylated 10 µM and Rhodamine 0.1 µM or Na-F 100 µg/mL. The solution containing the dyes was added to the perfusion inlet and outlet, 40 µL and 30 µL respectively. A volume of 10 µL was sampled from the apical compartment and replaced. Apical samples were diluted 5-fold in 384-black plate. Basolateral samples were taken at time 0 and 30 minutes to determine permeability in the presence of cadherin peptides, ADT5, TPP, HAVN1, and HAV6. For qualitative examination, images were taken immediately after the dyes were

added and every 5 minutes thereafter for a total of 30-minutes using an EVOS microscope with 10x objective and GFP channel to monitor passage of FDX70,000 across microvessels.

2.8.2 Determination of Monoclonal Antibody BBB Permeability in the Presence of Cadherin Peptide HAVN1.

Endothelial cells (hCMEC/d3) were grown in the three-lane organoplate. To determine antibody permeability from the blood to brain compartments (A-B), 20 µL of EBM-2 media was added to gel and bottom channel inlet and outlet ports. After a 5-min equilibration period, FDX 70,000, Avastin and Fab in EBM-2 media (final concentration of 1 µM) were added to the top channel of the microfluidic unit by placing 40 µL and 30µL into the inlet and outlet ports, respectively. A sample (10 µL) was immediately removed from the inlet port to determine apical concentrations. This was diluted 5-fold with EBM-2 media in a black 384-well plate. To determine permeability of the macromolecules, 20 µl samples were collected from the middle and bottom chamber inlet and outlet ports at 60-minutes to assess permeability. To determine permeability from the brain to the blood (B-A) 20 µL of solutions containing the same compounds and concentrations as mentioned above were added to the gel and bottom channel inlet and outlet ports while EBM-2 media was added to the inlet and outlet ports of the top chamber, 40 and 30 µL respectively. A sample (10 µl) was taken immediately and replaced from the basolateral side to determine initial starting concentrations. At 60-minutes, 40 and 30 µL samples were removed from the inlet and outlet ports of the top channel to determine permeability. To generate serum free conditions, EBM-2 media was used that contained all the necessary supplements except FBS. Samples were read on Varioskan Lux plate reader, FDX70,000 480/520, Fab 685/712 and Avastin 785/812.

2.8.3 Blood Brain Barrier Permeability of Fluorescently Tagged Nanoparticles Loaded with Chemotherapeutics in the Presence of Cadherin Peptides.

Endothelial cells (hCMEC/d3) were grown in the three-lane organoplate to confluency. Nanoparticles were formulated by Dr. Vinith Yathindranath. Nanoparticles were either loaded with doxorubicin or SAT1 siRNA. Serum free media was used to formulate a final nanoparticle concentration of 5 µL/mL, and non-pegylated IRdye (10 µM) was added as a control to ensure cells behaved as expected. Permeability of nanoparticles were assessed by sampling 10 µL of the apical compartment, replacing, and diluting it 5-fold in 384-well black plate. After 60-minutes, samples were collected from the basolateral chambers and read on Varioskan Lux plate reader. Nanoparticles 485/520 and IRdye 785/812.

2.9 Statistical Analysis.

All data was expressed as mean ± standard error of the mean (SEM) or standard deviation (SD). Data comparison was evaluated using T-tests with Bonferroni multiple comparison correction when two groups were compared or one-way Anova with Dunnett's correction when comparing three or more groups to control. One-way Anova with Bonferroni correction was also performed when all data was compared to one another. The tests were performed using GraphPad Prism, version 6.02. A p value of less than 0.05 was considered statistically significant and represented by asterisks on graphs.

3.0 Results

3.1 Assessment of Leak-Tight Barrier Formation in the 2-Lane Microfluidic BBB Culture Model.

To assess endothelial cell barrier function both qualitatively and quantitatively, barrier integrity assays were performed on confluent monolayers in the 2-lane Mimetas^{TM} organoplate. These experiments assessed the barrier properties of the hCMEC/d3 human brain endothelial cell line in a microfluidic model under static and of bi-directional fluid flow conditions. The microfluidic BBB culture model formed a leak-tight endothelial barrier as demonstrated by the absence of FDX 70,000 fluorescence in the ECM channel (Figure 6-A and B). Qualitative evidence of a leak-tight barrier was observed by monitoring FDX70,000 dye passage out of the perfusion lane into the ECM lane using a fluorescent microscope. Phenotypically, the dye was retained within the perfusion lane indicating leak-tight barrier formation (Figure 6-A). Flow across endothelial cells was necessary to create these tight, leak-proof, tubular structures as demonstrated by the increased permeability of FDX70,000 in the absence of flow and compared to cells that were cultured under bi-directional fluid flow conditions on the rocker platform. (Figure 6-B). Establishment of tubular structures were followed from 4 to 11 days after seeding to determine the approximate duration of barrier properties. Barrier integrity studies indicate that hCMEC/d3 endothelial cells cultured in the 2-lane organoplate established a leak-free barrier by

day 4 and maintained barrier properties for up to 11 days of culture (Figure 6-C

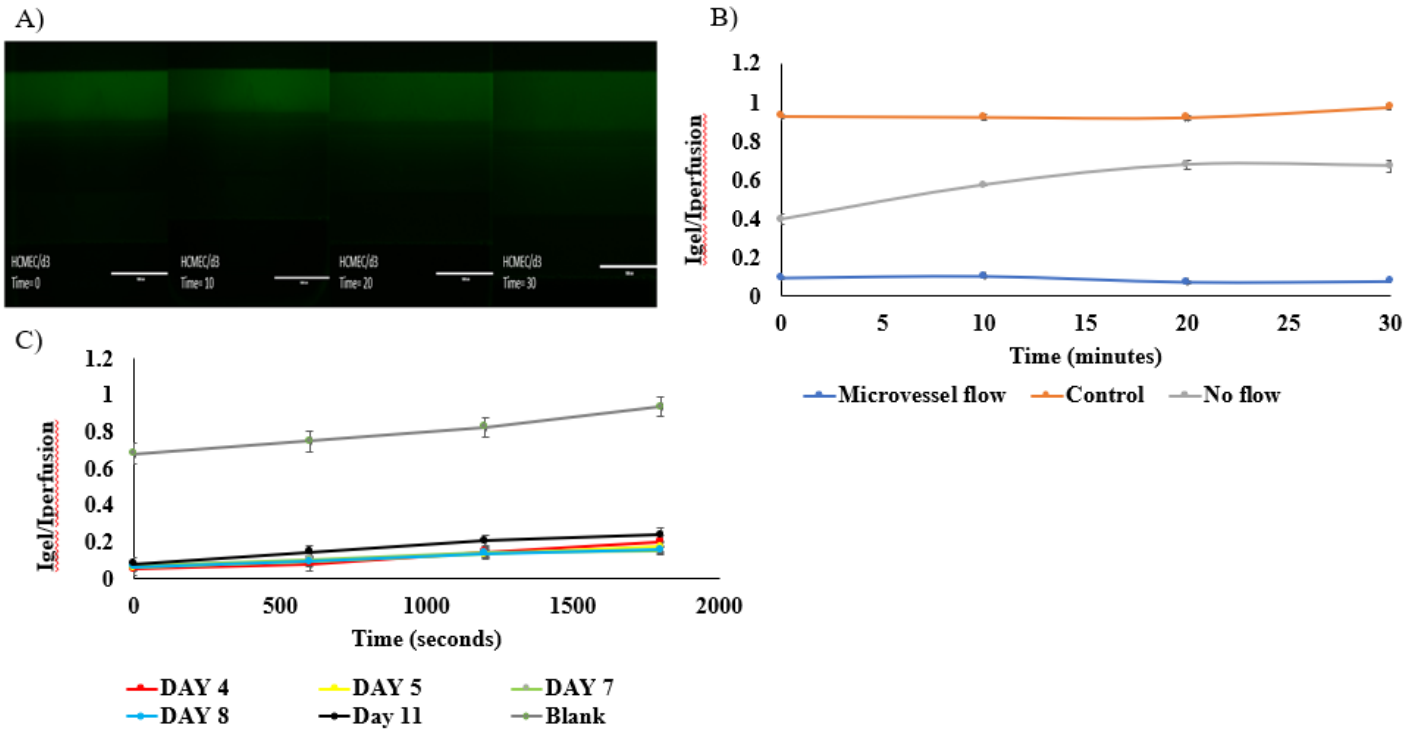

Figure 6: Barrier integrity assays in MimetasTM microfluidic 2-lane organoplate using the paracellular permeability marker FDX 70,000. Qualitative assessment of leak-tight barrier formation using fluorescent imaging of microfluidic chambers over a 30-minunte period (Panel A); Quantitative assessment of barrier properties under flow and no-flow conditions in confluent hCMEC/d3 microvessels (Panel B); and quantitative assessment of barrier properties as a function of days in culture (Panel C). For quantitative permeability assessments, the relative ratio of fluorescence in the gel channel was compared to perfusion channel at various times indicated and expressed as mean +/- SD of three independent microfluidic wells.

3.2 Three-Lane Microfluidic Modeling.

3.2.1 Comparison of Barrier Properties Between 3-D Microfluidic BBB Model, 2-D Transwell™ Inserts, and *In Vivo* Studies.

As fluid sampling from the ECM compartment was difficult with the 2-lane microfluidic plates, and co-culture options were limited to cells that could be embedded in ECM, the BBB

microfluidic culture model was transferred to the 3-lane microfluidic format. Endothelial cells were cultured under monoculture conditions and leak tight barrier formation was confirmed using fluorescent microscopy and FDX70,000 fluorescent dye (Figure 7-A). Following confirmation of a leak-tight barrier, a more comprehensive examination of the permeability of a series of paracellular and transcellular solutes were measured and compared in the 3-lane DMF and 2-D Transwell™ culture models. A substantial decrease in the apparent permeability coefficients were found for all three dyes tested in the microfluidic model compared to Transwell™ inserts (Figure 7-B). As it is possible that the extracellular gel matrix could be contributing to the decreased permeability observed with the DMF model, studies were performed in the microfluidic model with endothelial cells as well as in the cell free ECM. These studies showed the decreased permeability for all three dyes examined in the DMF model was attributable to enhanced barrier properties of the endothelial cells in the microfluidic model (Figure 7-C). In comparison to *in vivo* permeability assessments using the both small molecule and large molecule permeability probes, Na-F and FDX 70,000, respectively, the Transwell™ model was significantly leakier to both dyes, while three-lane microfluidic model displayed comparable apparent permeability values to previously published *in vivo* studies (Figure 7-D)

Comparison of the expression of selected BBB genes known to have a role in maintaining barrier integrity identified several junctional adhesion molecules and carrier/transporter systems that had higher expression in the DMF model. The expression of *ZO-1, BCRP, claudin-5, claudin-3* and *Ve-Cadherin* were increased in the microfluidic model (Figure 7-E). However, important to note, to obtain gene expression data in the microfluidic model, multiple wells had to be pooled together. Therefore, the microfluidic data represents one pooled sample that was examined in three technical replicates. This gene expression data supported the functional studies

performed and indicated enhanced endothelial cell barrier properties in the 3-lane microfluidic model.

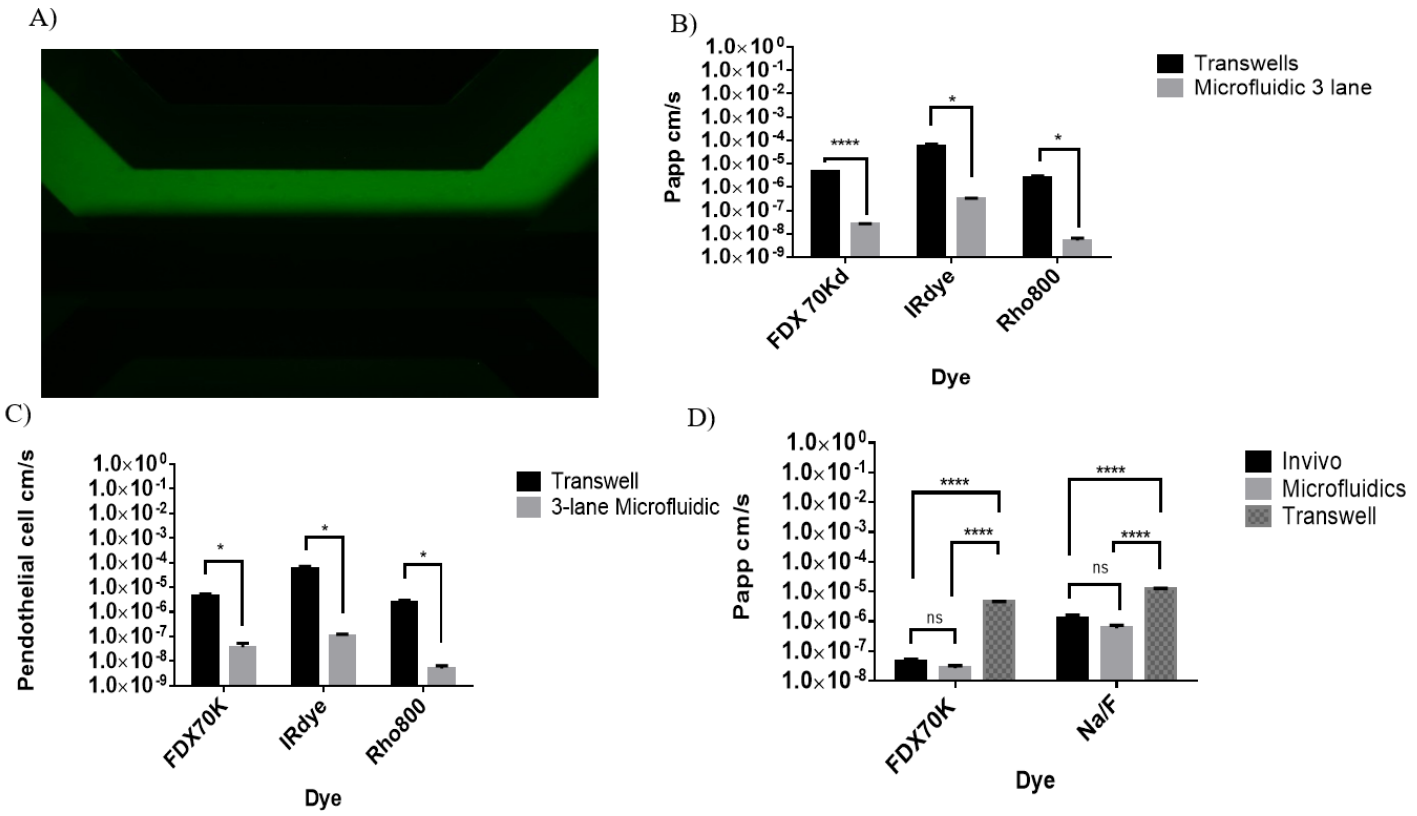

E)

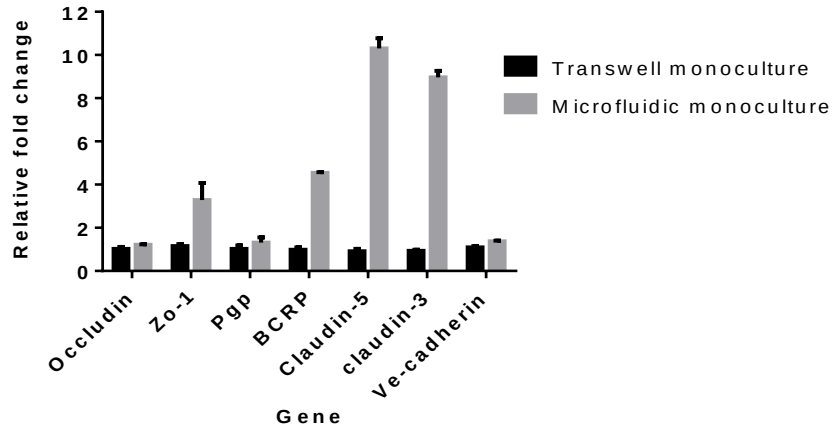

Figure 7:Comparison of DMF and Transwell™ models. Leak-tight endothelial barriers were established in the 3-lane Mimetas™ organoplate using FDX70,000 as fluorescent probe (Panel A). The barrier properties were determined in the 3-lane microfluidic and Transwell™ culture models using FDX 70kD, IRdye 800 and R800. Both apparent permeability coefficients (Panel B) and endothelial cell permeability coefficients (Panel C) were determined as described in methods. Comparison of the apparent permeability coefficients for both Na-F and FDX70kDa in Transwell and 3-lane microfluidic models were compared to in vivo values reported by Shi et al 2014 (Panel D). Examination of relative fold change in expression compared of select BBB related genes in brain endothelial cells grown in Transwell™ inserts and 3-lane microfluidic organoplate (Panel E). For expression studies in the microfluidic model, values represent one pooled sample from 6 different units with three technical replicates. Panel B and C were evaluated using unpaired students T-test, correct for multiple comparisons using Bonferroni method, while Panel D was evaluated using a one- way Anova with Bonferroni correction. Values represent mean ± SEM of three samples per treatment. *$p<0.05$, ** $p<0.01$, $p<0.001$***, $p<0.0001$****

3.2.2 Establishment of the BBB-GB Co-Culture Model in Mimetas™ Microfluidic 3-Lane Organoplate.

Permeability studies using FDX 70,000 established confluent and leak-proof barriers. The fluorescent dye, FDX70,000 was added to the perfusion lane and visual inspection of dye leakage into the gel and third compartment was monitored over 30-minutes (Figure 8). The 3-lane organoplate was investigated for feasibility since it allowed for sampling from both basolateral and apical compartments. In contrast, the 2-lane model was incapable of fluid sampling from the basolateral chamber, therefore studies moving forward focused on the 3-lane microfluidic model. Using the three-lane organoplate, we found fluorescent dye to be retained within the perfusion channel indicating a phenotypically leak-tight vessel (Figure 8-A). Qualitative depiction of a confluent microvessel in the perfusion channel was captured at both 10x and 4x objective (Figure 8-B and C). The BBB-GB co-culture model was established using hCMEC/d3 for microvessel formation and either astrocyte, GB (U251 or U87) or DIPG (SF8628) cell co-cultures (Figure 8-D).

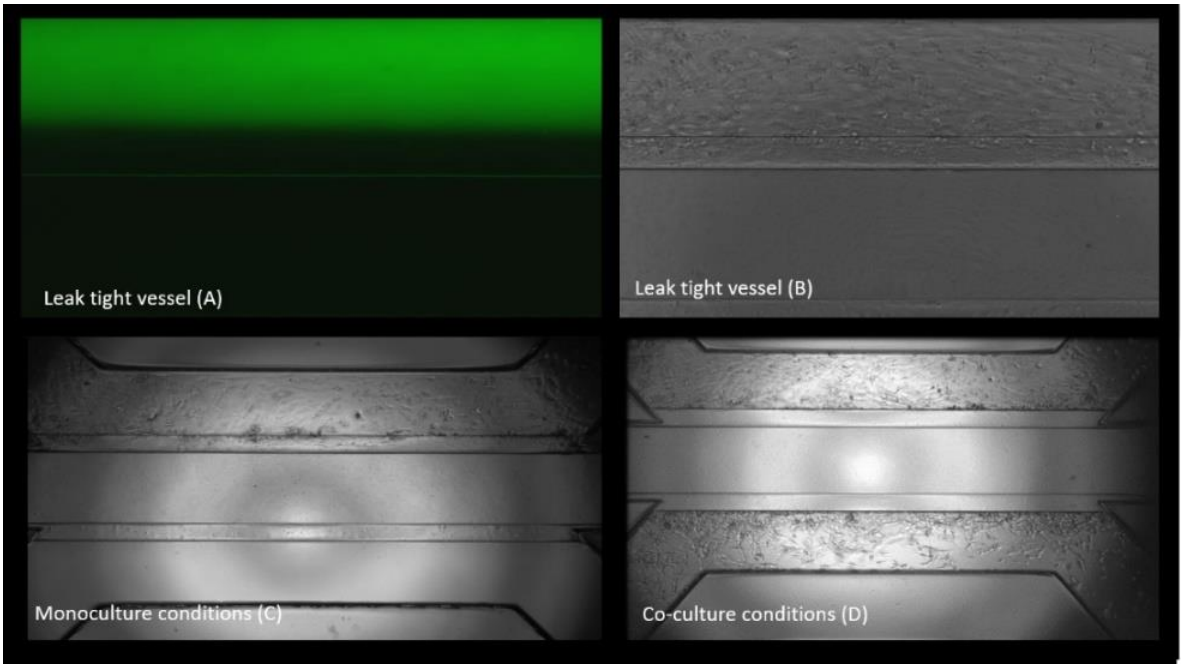

Figure 8:Qualitative establishment of leak tight barrier using the paracellular marker FDX 70,000 in the 3-lane organoplate (A), confluent microvessel at 10x objective (B) and 4x objective (C), and establishment of endothelial cell- GB co-culture model (U87) (D)

3.3 Establishment of Co-Culture Conditions.

3.3.1 Establishment of the BBB-GB Co-Culture Model in Transwell™ Inserts.

In Transwell™ inserts, endothelial cells were co-cultured with GB cells (U251, U87), DIPG cells (SF8628) or human astrocytes (HA) for 24-hours. At the end of the culture period, apparent permeability was assessed to determine changes in endothelial barrier properties in response to tumor co-culture conditions and the tumor microenvironment (Figure 9). Mechanistically, SF8628 DIPG co-culture enhanced barrier properties for both large and small paracellular permeability markers in brain endothelial cells. In contrast, endothelial cells co-cultured with GB (U87) cells displayed increased permeability for the same paracellular markers

and diminished barrier properties. Human astrocytes (HA) and U251 GB co-culture had no significant effect on endothelial cell apparent permeability (Figure 9).

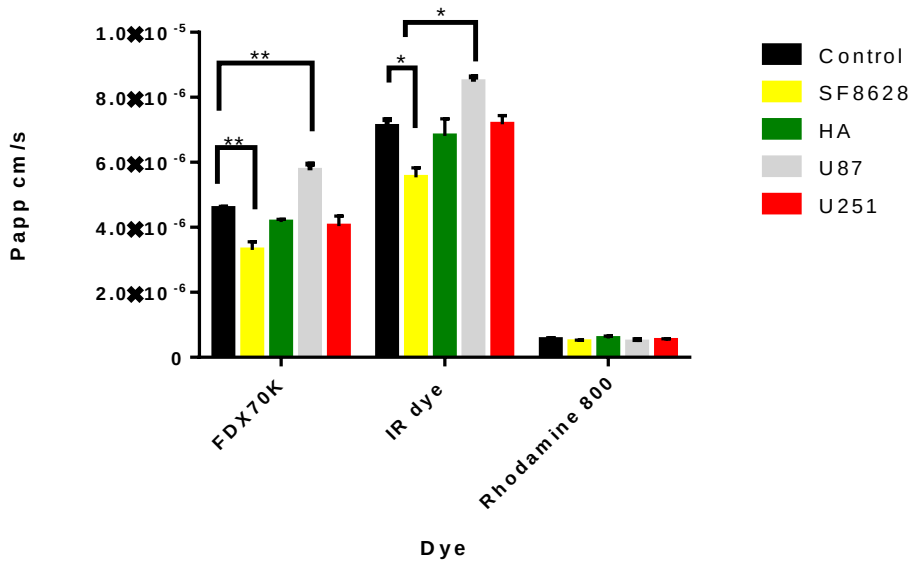

Figure 9: Apparent permeability of FDX70kDa, IRdye, and Rhodamine 800 was determined in Transwell™ inserts on confluent endothelial monolayers co-cultured with GB, DIPG and human astrocytes for 24 hours. Values represent mean ± SEM of three samples per treatment. *p<0.05, ** p<0.01, p<0.001***, p<0.0001**** (One-way Anova with Dunnets corrections)

3.3.2 Functional Assessment of Tumor Co-Culturing in the DMF Model over 24-, 48- and 72-hour Co-Culture Time Points.

Tumor co-culturing was also examined in the DMF model. As the endothelial cells cultured in the DMF model retained BBB properties for an extended period of time compared to Transwell™ inserts, co-culture studies with human astrocytes (HA), GB cells (U251 and U87) or DIPG cells (SF8628) were performed for 24, 48 and 72-hours. Results indicate significant changes in permeability occurred in endothelial cells at 24, 48, and 72-hours of co-culture (Figure 10-A, B and C). Similar to the Transwell™ model, it was found that endothelial cells co-cultured with U87 human GB tumor cells displayed increased paracellular leakiness to FDX70,000 and IRdye, while U251 did not impact permeability, and SF8628 co-culture lead to

significant decreases in permeability reflecting a barrier enhancing impact on endothelial cell function (Figure 10-A).

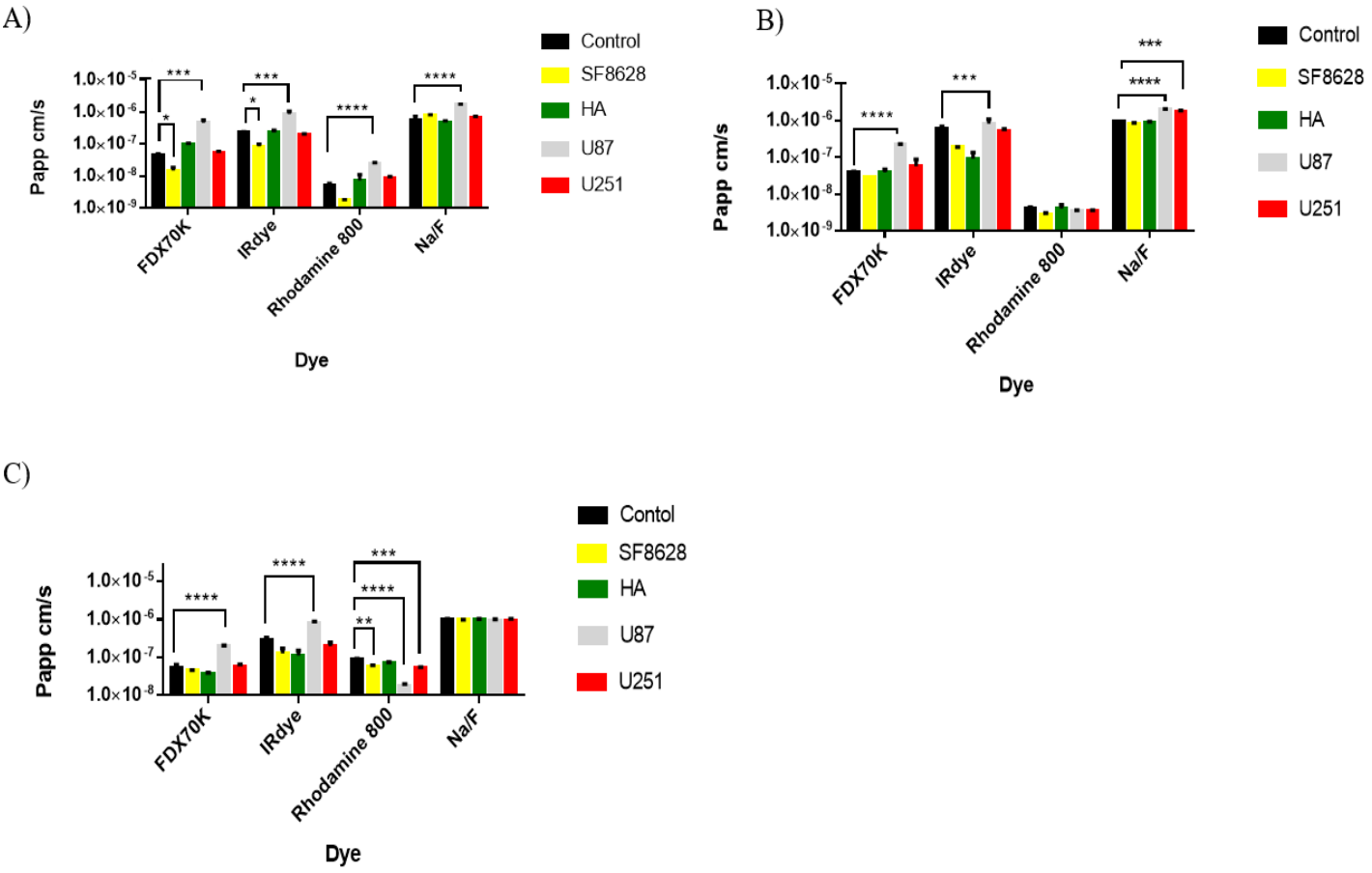

Figure 10: Apparent permeability of confluent endothelial cell microvessel co-cultured with GB (U251, U87), DIPG (SF8628) and human astrocytes (HA) at (A) 24 hours of co-culture, (B) 48 hours of co-culture and (C) 72 hours of co-culture. Values represent mean ± SEM of three samples per treatment. *p<0.05, ** p<0.01, p<0.001***, p<0.0001**** (One-way Anova with Dunnets correction).

3.4 Gene Profiling for Blood-Brain Barrier Specific Markers in Transwell™ Inserts and Mimetas™ 3-Lane Microfluidic Plate Following Co-Culture Conditions.

Gene expression studies of endothelial cells following co-culture with U87, U251, and SF8628 were performed in Transwell™ inserts (Figure 11-A). Expression of BBB genes were also determined in endothelial cells co-cultured with SF8628 in the Mimetas™ 3-lane organoplate (Figure 11-B). In Transwell™ inserts, all endothelial cell co-cultured treatments had significantly increased expression of *GLUT1* (Figure 11-A). Expression of *occludin, ZO-1,* and *claudin-1* were significantly decreased when endothelial cells were co-cultured with U87 GB cells (Figure 11-A). While expression of *claudin-3, claudin-1, occludin,* and *ZO-1* were found to be significantly increased during both U251 and SF8628 co-culturing. Lastly, SF8628 co-culturing resulted in increased expression of *BCRP* in endothelial cells (Figure 11-A). In the microfluidic 3-lane organoplate, compared to control, endothelial cells co-cultured with SF8628 displayed increased expression of *occludin, ZO-1, P-gp¸ BCRP,* and *claudin-5* (Figure 11-B). The molecular data correlated with functional permeability data supporting improved barrier properties in the 3-lane organoplate, with SF8628 co-culturing enhancing barrier integrity and

U87 having diminished barrier effects

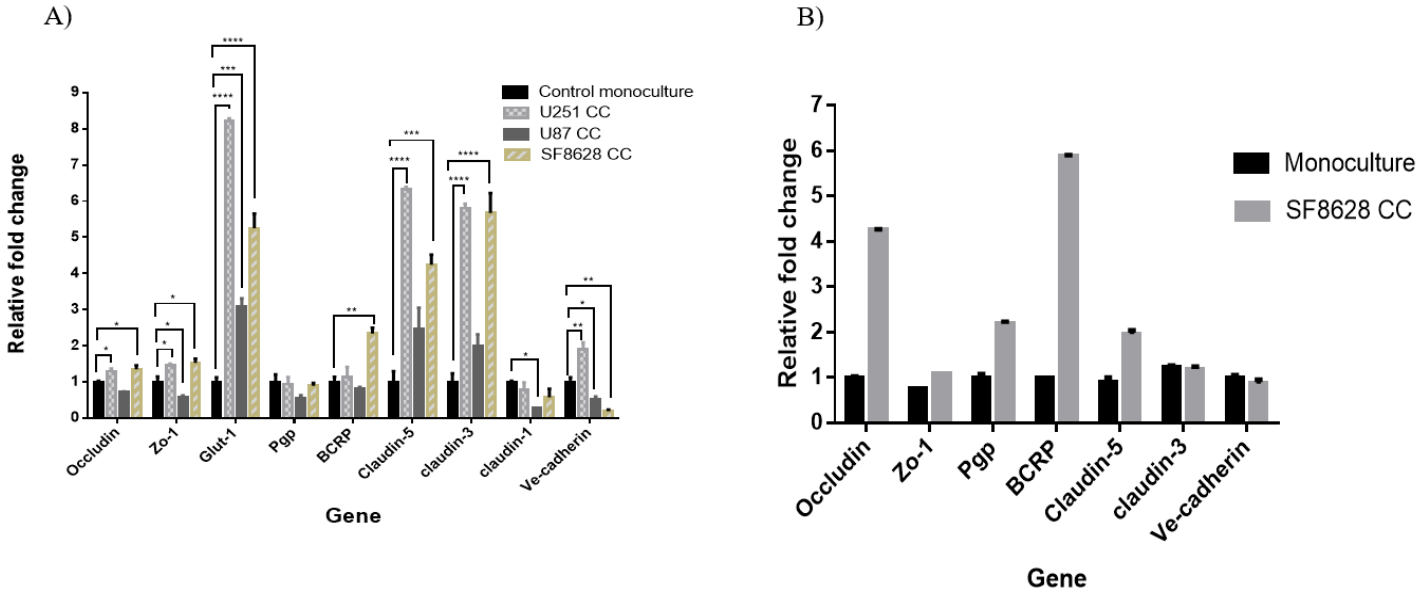

Figure 11: Examination of relative fold change to GAPDH expression of select BBB related genes in brain endothelial cells under different culture conditions. Endothelial cell gene expression was determined in various co-culture conditions in Transwell^{TM} inserts (Panel-A) and during SF8628 co-culture in three-lane microfluidic model (Panel-B). The ΔΔCT method was employed and genes were normalized to GAPDH to determine relative fold change in expression. For Transwell^{TM} inserts values represent mean ± SEM of three samples per treatment. *p<0.05, ** p<0.01, p<0.001***, p<0.0001**** (One-way Anova, Dunnets correction). For microfluidic data, values represent one pooled sample from 6 different units with three technical replicates.

3.5 Factors Impacting Endothelial Cells During Co-Culture Conditions.

3.5.1 Investigation of Cytokine Release during BBB-GB Tumor Co-Culturing in the 3-Lane Organoplate.

A mesoscale discovery (MSD) platform was used to assess various cytokines released during tumor co-culture in the 3-lane microfluidic organoplate. Cytokines were assessed to better understand the tumor-endothelial cell microenvironment and elucidate molecular and functional changes occurring in endothelial cells in response to the tumor microenvironment. Based on MSD plate compatibility and factors known to play a role in BBB permeability, interleukin-6

(IL-6), interleukin-8 (IL-8), monocyte chemoattractant protein-1 (MCP-1) and vascular endothelial growth factor alpha (VEGF-a) were assessed. It was found that SF8628 co-culture resulted in significantly increased levels of IL-6, IL-8 and VEFG-A at 24-hours of co-culture (Figure 12-A), with similar trends showing increased levels of IL-6 continuing following 48 and 72-hours of co-culture (Figure 12-B and C). In contrast, U251 co-culture resulted in reduced levels of IL-6 and IL-8 and increased levels of VEGF-A at 24-hours. These trends were transient as cytokine levels in U251 co-culture were similar to monoculture (control) at both 48 and 72-hours of culture (Figure-12 B and C). When endothelial cells were co-cultured with U87 cells, results showed significantly lower MCP-1 levels and higher VEGF-A levels at 24-hours, while IL-8 levels were increased at 48 and 72-hours (Figure 12-A and B). Lastly, in astrocyte co-culture, IL-8 levels were increased at 24-hours (Figure 12-A). Increased IL-8 levels persisted at 48 and 72-hours of culture, although these increases were not significant. Additionally, MCP-1 was significantly increased at all three astrocyte co-culture time points (Figure 12-A, B and C). Taken together, these results indicate varying cytokine release in heterogenous tumor-endothelial cell co-culture.

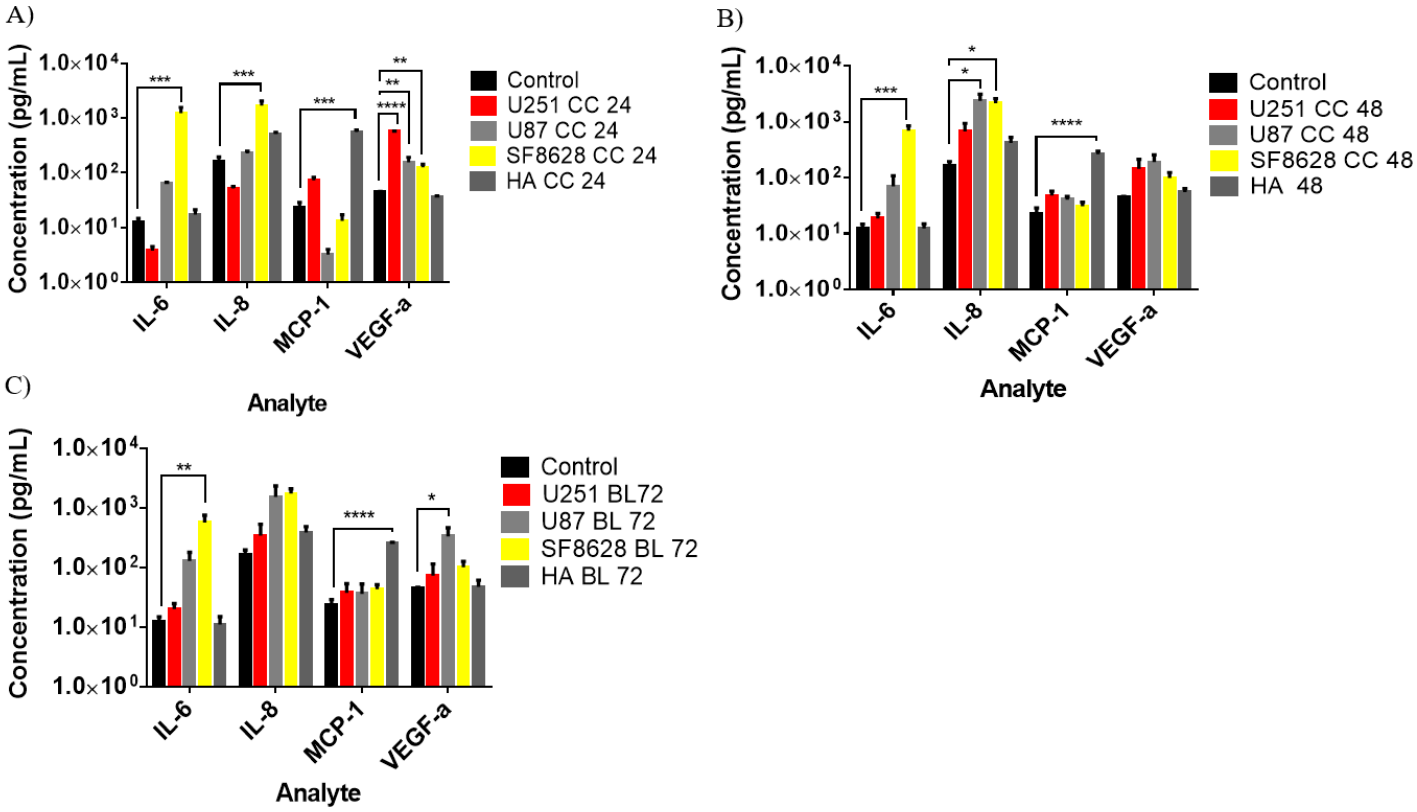

Figure 12:Cytokine concentration of basolateral media samples collected from three tumor co-culture and astrocyte co-culture conditions at 24 (Panel-A), 48 (Panel-B) and 72-hours of co-culture (Panel-C). Values represent mean ± SEM of three samples per treatment.

3.5.2 Profiling of Intracellular and Secreted Lipids in Brain Endothelial Cells Under Monoculture and Tumor Co-Culture Conditions.

When examining changes in intracellular lipid concentrations in brain endothelial cells, the biggest change was found during SF8628 co-culturing with a large increase in the amount of phosphatidylserine (PS) compared to control and other GB co-culture conditions (Figure 13-A). The best matched PS was PS 45:1, however other possibilities were PS 45:2 or ceramide 1-phosphate. This increase in PS during SF8628 co-culture was significant compared to monoculture and both U251 and U87 co-culture. Examination of the secreted lipids present in the basolateral media compartment from the various tumor microfluidic co-cultured models showed high amounts of triglyceride (TG) secretion in U251 and U87 co-cultures compared to

SF8628 co-culture and hCMEMC/d3 monoculture models (Figure 13-B and C). Comparing the secreted TG levels, U87 co-culturing had the largest increase in TG and fatty acids compared to other co-culture conditions (Figure 13 B). This was in contrast to the secreted lipid profile found in the media collected from the apical compartment in which few changes were observed in the various co-culture models (Figure 14-A). This suggests that the brain endothelial microvessel compartment remains relatively stable in regard to lipid profiles during various GB co-culturing. However, when examining the class distribution of significantly altered lipids in the basolateral "brain" compartment, large differences between the various classes of lipids were observed (Figure 14-B). Taken together, the variability of secreted lipids in the basolateral chamber reflects the heterogenous nature of various GB co-culture microenvironments and therefore heterogeneity in brain tumors.

A)

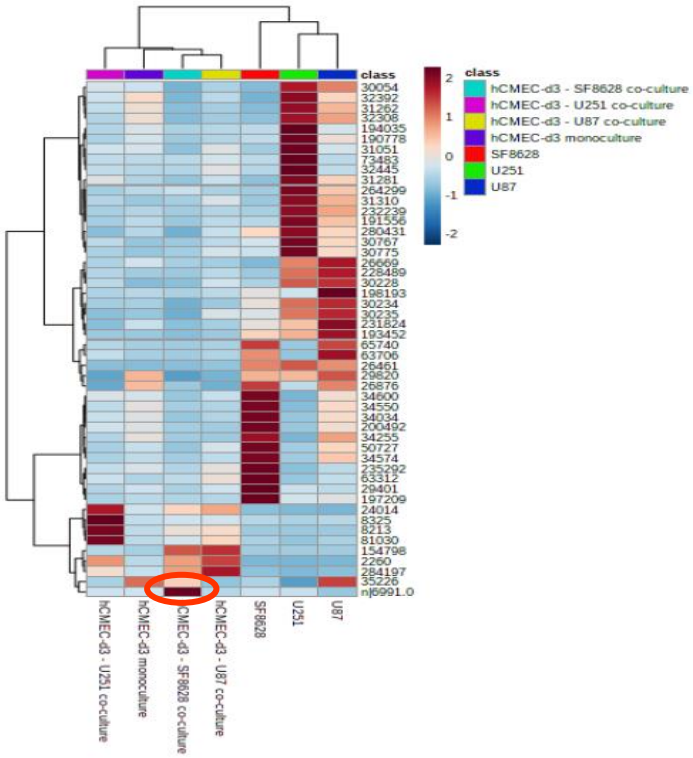

Table 4. Identity of lipids on heat map

Number	Lipid Class	Lipid identity	Tier	Other possibilities
30054	Triglyceride	TG 47:4	3	TG 47;5
32392	Triglyceride	TG 48;6	3	HexCer 45;6 or TG 48;7
31262	Triglyceride	47;3	3	TG 47;4
32308	Triglyceride	46;5	3	HexCer 43;5 or TG 46;6
194035	Phosphatidylcholine	18;1	2	PS 20;1
190778	Phosphatidylcholine	18;1	2	PS 20;2
31051	Sphingolipid	40;2	3	PE-Cer 43;2 or SM 40;1
73483	Phosphatidylcholine	33:1	3	PE 36:1, PA 38:2 or PE 34:1
32445	Phosphatidylcholine	38:2	3	PE 41:2, PC 38:3 or DG 50:12

31281	Triglyceride	48:7	3	TG 48:8 or HexCer 45:6
264299	phosphatidylethanolamine	PE 18:1	2	PE 20:2
31310	Glycosphingolipids - Hexosyl ceramides	45:3	3	HexCer 45:2 or 45:6
232239	Phosphatidylcholine	PC 14:1	1	
191556	Phosphatidylcholine	PC 18:1	1	
280431	Phosphatidylcholine	PC 15:1	2	PC 22:6
30767	Phosphatidylcholine	34:1	3	PE 37:1, PA 39:2 or PC 34:2
228489	Phosphatidylcholine	14:0	1	
30228	Sphingolipid	42:4	3	SM 40:1. SM 42:3 or PE-Cer 45:4
198193	Hexosyl ceramides	42:1	3	HexCer 42:0
30234	Ceramide-1 phosphate	53:6	3	HexCer 45:4, HexCer 45:3
30235	Ceramide phosphoinositols	41:0	3	PI-Cer 41:2
231824	phosphatidylethanolamine	18:1	2	PE 22:4

193452	Glycosyldiacylglycerols	16:1	1	
65740	Triglyceride	62:12	3	PC 50:3, DG 62:13, PE 53:3, or TG 62:13
63706	Triglyceride	62:8	3	DG 62:9, TG 62:9, or DG 62:10
26461	Phosphatidylserine	40:5	3	PG 40:7, PS 38:2 or PS 40:6
29820	Phosphatidylcholine	38:5	3	PC 36:2, PE 41:5 or PE 39:2
26876	Hexosyl ceramides	40:3	3	HexCer 40:4
34600	Triglyceride	64:5	3	PI 53:0
34550	Triglyceride	62:4	3	TG 62:3
34034	Triglyceride	57:5	3	TG 57:3 or PI 46:0
200492	Triglyceride	20:4 or 20:5	1	
34255	Triglyceride	57:5	3	PI 36:0
50727	Sphingolipid	38:0	3	PE-Cer 41:1

34574	Phosphatidylcholine	57:5	3	PE 60:5, TG 69:14, or PA 62:6
235292	Sphingolipid	SM 14:0	2	SM 23:1
63312	Cardiolipins	72:7	3	
29401	Sphingolipid	38:2	3	PE-Cer 41:2 or SM 38:1
197209	Hexosyl ceramides	18:1 or 22:0	1	
24014	Triglyceride	39:9	3	TG 39:10, PG 29:1 or PI-Cer 29:0
8325	Ceramide - phosphoinositols	38:0	3	PG 41:0
8213	Fatty acid	FA 42:4	3	FA 42:12
81030	Taurines	31:5	3	ST 28:4, ST 30:7 or ST 28:5
154798	Phosphatidylcholine	22:6	3	ST 30:5, PE 25:5, LPS 24:6
2260	Sterol lipid	22:6	3	ST 30:5, PE 25:6
284197	Hexosyl ceramides	37:1	3	HexCer 37:3

35226	Triglyceride	57:5	3	Acer 60:5, DG 57:6
n|6991	Phosphatidylserine	45:1	3	PS 45:2, CerP 51:3

Table 5. Lipid abbreviation with corresponding lipid name

Abbreviation	**Lipid identity**
TG	Triglyceride
PS	Phosphatidyl Serine
PC	Phosphatidylcholine
PE	Phosphatidylethanolamine
PI	Phosphatidylinositol
HexCer	Hexosyl Ceramide
CL	Cardiolipin
ST	Sterol Lipd
DG	Diacyl glycerol
Acer	Acyl Ceramide
LPS	lysophosphophosphatidylserine
PA	Phosphatidic acid
PG	Phosphatidylglycerol
PI- Cer	Ceramide phosphoinositol
FA	Fatty Acid

SM	Sphingomyelin
PE- Cer	Ceramide phosphoethanolamine

B)

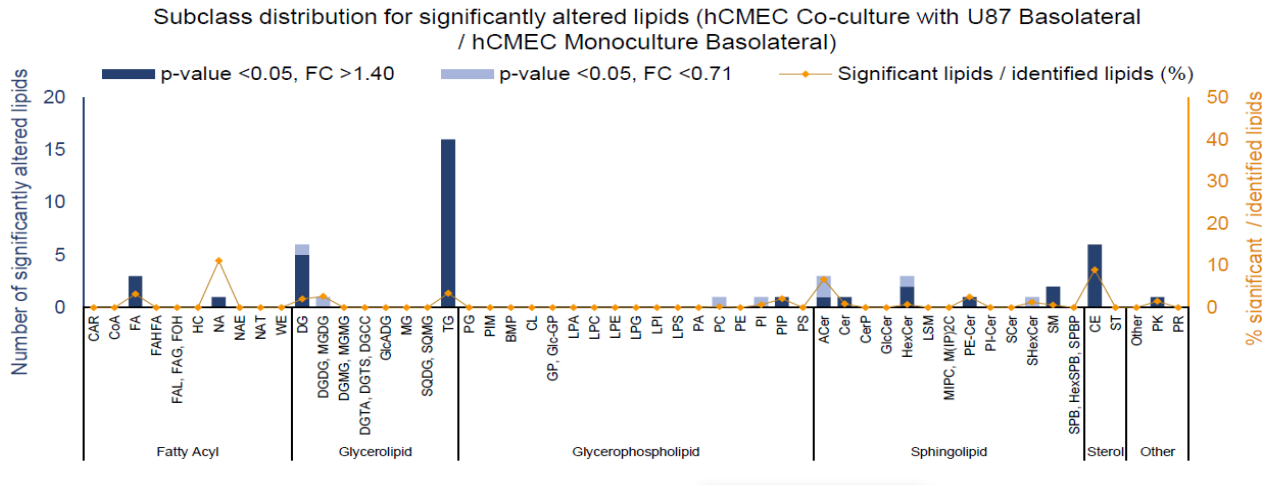

C)

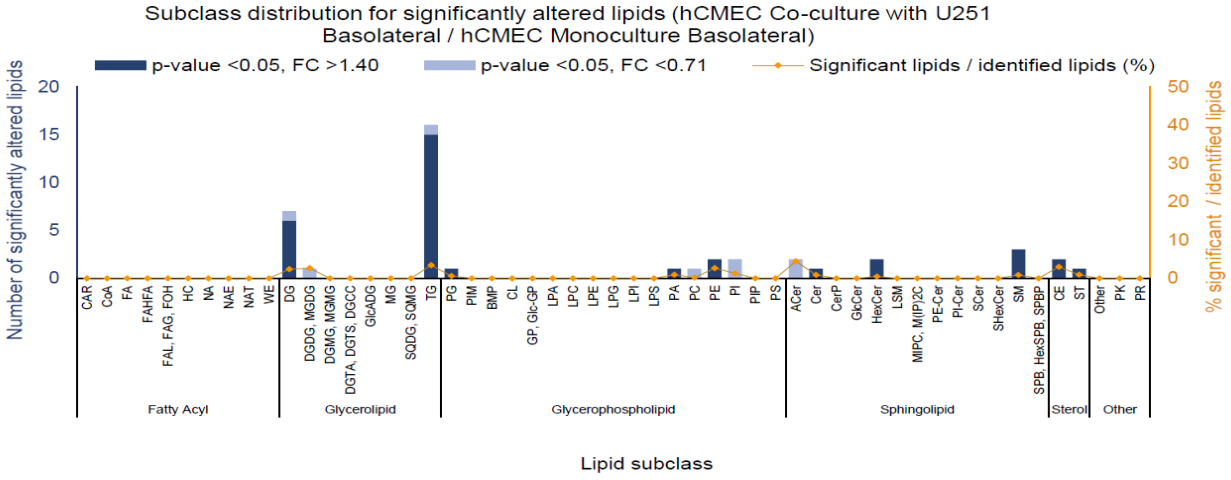

D)

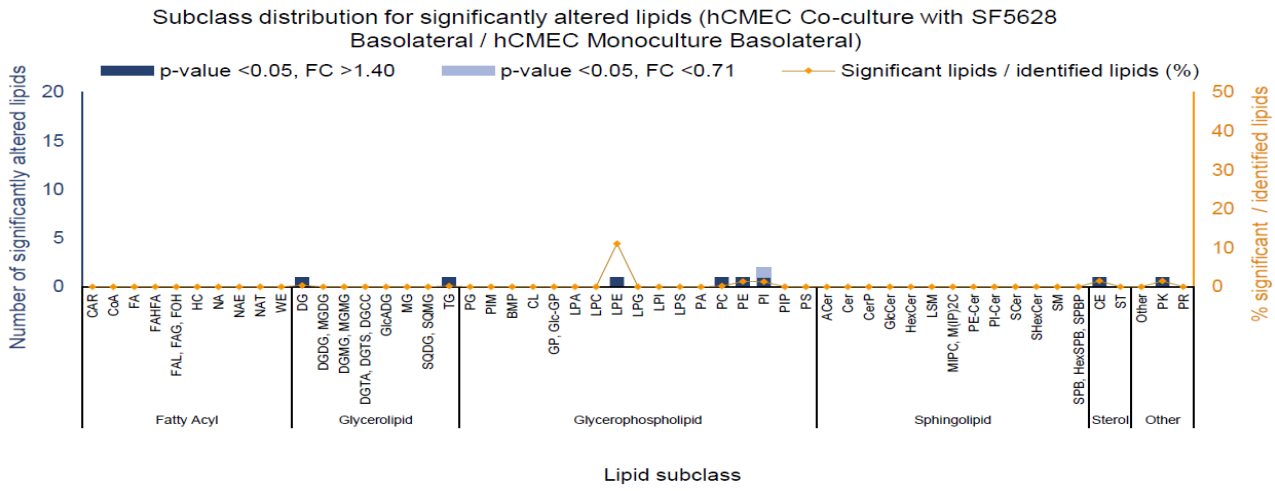

Figure 13: Heat map of endothelial cell intracellular lipid concentrations when endothelial cells were co-cultured with GB tumor cells for 24-hours in Transwell™ inserts (Panel-A). Secreted lipid profiles in 3-lane microfluidic plate of endothelial cell co-cultured with U87 (Panel-B) U251 (Panel-C) and SF8628 (Panel-D). Intracellular lipids that were increased are represented in light pink to dark red the higher the expression. Down regulated lipids are shown in light to dark blue depending on the degree of down regulation.

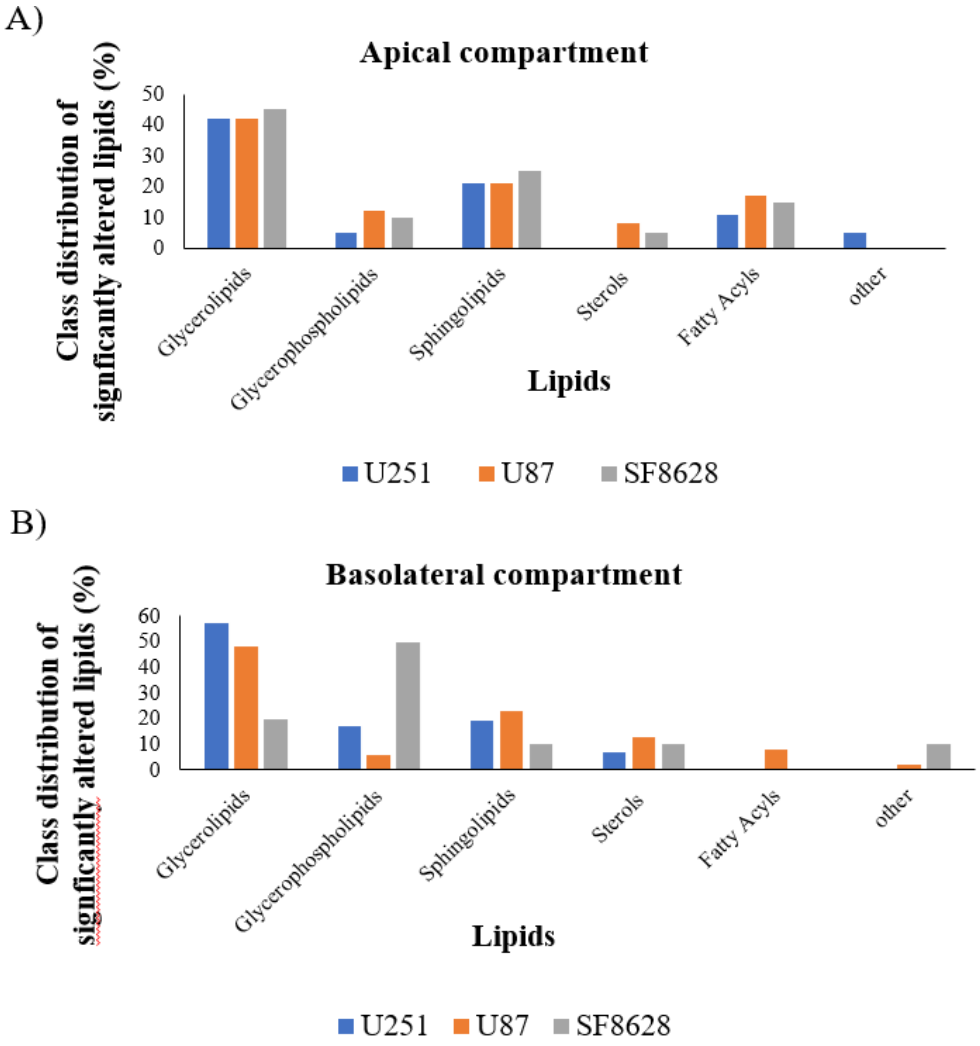

Figure 14: Categorization of secreted lipid profiles in three different endothelial cell-GB co-culture conditions. Examination of secreted lipids of the apical compartment in the three-lane organoplate during SF8628, U251 and U87 co-culturing respectively (Panel-A). Basolateral distribution of secreted lipids in the same co-culturing conditions (Panel-B). All secreted lipids were compared to hCMEC/d3 monoculture conditions.

3.5.3 Investigation of Lipid Exposure on Endothelial Cell Permeability.

During endothelial cell co-culturing with U87 in the microfluidic 3-lane plate, high levels of secreted triglycerides and fatty acids were found compared to the monoculture and other co-culture conditions. Therefore, to elucidate if these high triglyceride/fatty acid levels contributed

to the increase in endothelial cell permeability, oleic acid, steric acid, palmitic acid, or a combination of all three were added to confluent EC grown in Transwell™ inserts for 3 or 24-hours to mimic co-culture conditions and permeability was assessed. Treatment with steric acid, palmitic acid, or oleic acid increased EC permeability to both large and small molecular weight paracellular markers (Figure 15-A and B). These permeability increases were similar in magnitude to the permeability increases observed following co-culture of the endothelial cells with GB U87 tumor cells (Figure 15-A and B). Interestingly, while any three of the fatty acids alone resulted in permeability increases, when the three triglycerides were combined, no significant changes in permeability were observed (Figure 15-A and B). To draw comparisons between the microfluidic model and Transwell™ inserts, palmitic acid was added to endothelial microvessels in the 3-lane organoplate and changes in permeability were assessed (Figure 15-C). Similar to results obtained in Transwell™ inserts, palmitic acid significantly increased paracellular and transcellular permeability of fluorescent markers (Figure 15-C). Increased endothelial cell permeability in the presence of palmitic acid showed similar trends to the increases in permeability observed in endothelial cells co-cultured with U87 (GB) cells (Figure 15-C).

When endothelial cells were co-cultured with SF8628 (DIPG) cells, increased levels of intracellular phosphatidylserine were observed in comparison to monoculture and other co-culture conditions. To elucidate if intracellular phosphatidylserine was playing a role in EC tightening, serine was added to the endothelial cell culture media at 14, 140, and 1400 mg/ml concentrations. Adding serine to the culture media did not result in decreased endothelial permeability. Interestingly, the addition of serine to endothelial media increased paracellular

permeability of both large and small molecular weight markers in the monoculture model (Figure 15-D).

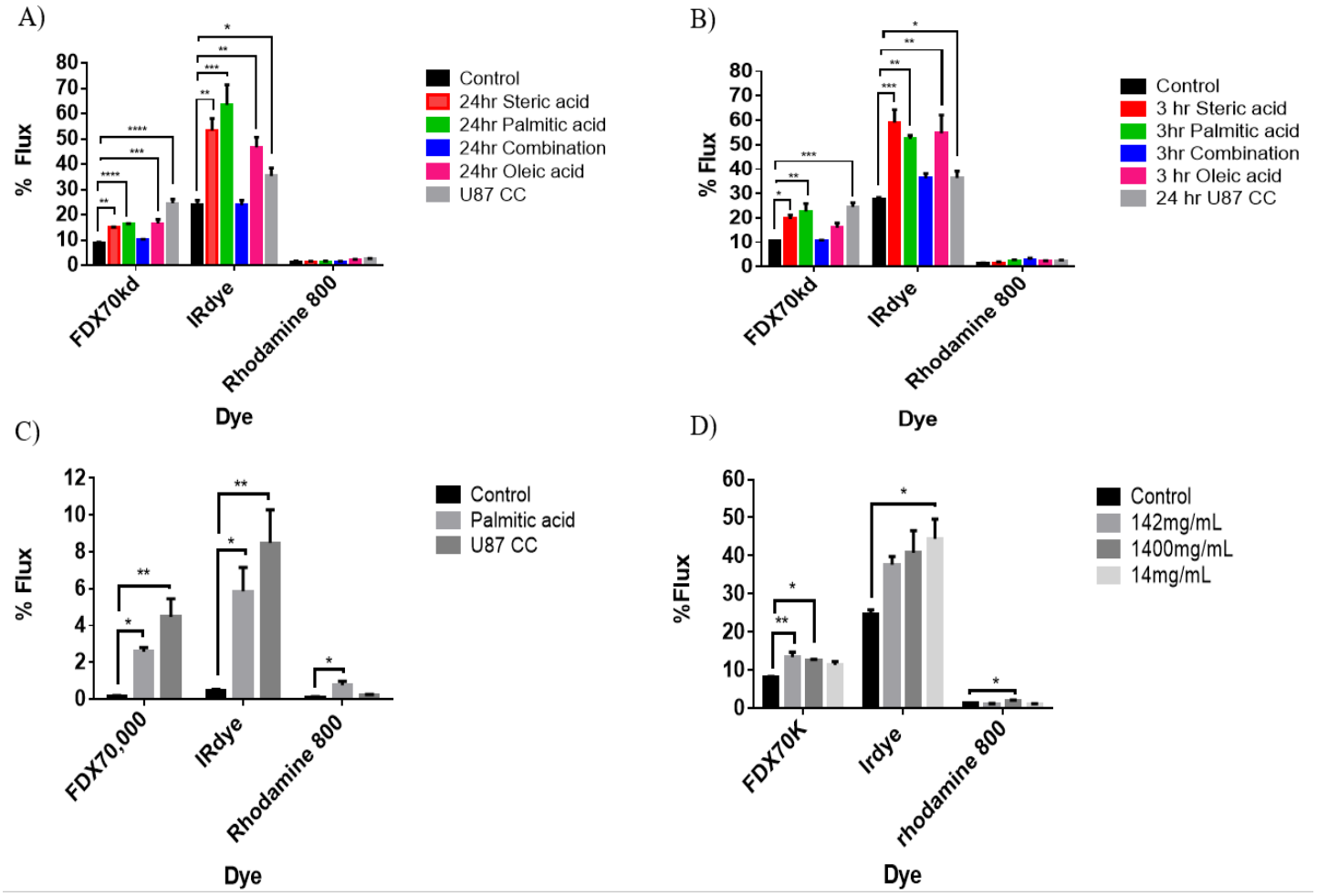

Figure 15: Endothelial cells cultured on Transwell™ inserts in the presence of three fatty acids, steric acid, palmitic acid, oleic acid or a combination of the three. Treatments were applied to endothelial cells for either 24-hours (Panel-A) or 3-hours (Panel-B). Flux across endothelial barriers was assessed for FDX70,000, non-pegylated IR dye and rhodamine 800. Apparent permeability of the same dyes was assessed in the 3-lane organoplate in the presence of palmitic acid and compared U87 co-culture (Panel-C). Serine was applied to endothelial cells and flux across endothelial barriers of the three fluorescent molecules were compared (Panel-D). Values represent mean ± SEM of three samples per treatment. *p<0.05, ** p<0.01, p<0.001***, p<0.0001**** (One-way Anova, Dunnets Correction)

3.5.4 Role of Endocytosis in Permeability Changes Observed Under Various Co-Culture Conditions.

To understand if the changes in brain endothelial cell permeability observed with the various tumor co-culture models were attributed to changes in vesicular transport processes, the cellular uptake and permeability of fluorescently labeled bovine serum albumin (BSA) was examined. In addition to BSA, paracellular transport of non-pegylated IR dye and transcellular transport of rhodamine 800 were assessed (Figure 16-A). When the endothelial cells were co-cultured with U87 tumor cells, significantly increased permeability of BSA and IRdye were observed compared to control/monoculture conditions (Figure 16-A). One possible explanation for the increased BSA permeability could be increased vesicular activity in endothelial cells due to the presence of U87 tumor cells. In support of altered vesicular transport contributing to the loss of barrier function under U87 co-culture conditions, increased endothelial cell uptake of BSA was observed in the U87 co-culture model compared to monoculture conditions (Figure 16-B). To identify which vesicular transport processes were altered, uptake and permeability of fluorescently labeled BSA was examined in the presence of various endocytosis inhibitors. Chlorpromazine (inhibits clathrin mediated endocytosis) was found to decrease endothelial cell permeability and uptake of BSA during monoculture and SF8628 co-culture conditions, while monesin (inhibits endosome maturation) and genistein (inhibits caveolae) increased permeability and uptake in monoculture, SF8628 and astrocyte co-culture (Figure 17-A). In contrast, genistein and monesin significantly decreased BSA uptake during U87 co-culture (Figure 17-A and B). Minimal changes in endothelial cell permeability and uptake were observed during various culture conditions when IRdye was examined (Figure 17-C and D), indicating the vesicular transport inhibitors had minimal impact on paracellular diffusion.

To compare results from Transwell™ inserts to the three-lane organoplate, the same experiments were performed. Permeability in the microfluidic plate was assessed quantitatively (Figure 18 A-C) and qualitatively (Figure 18 D-G). Similar to results in Transwell™ inserts, chlorpromazine decreased BSA permeability while monesin significantly increased permeability in monoculture (Figure 18-A). In contrast to Transwell™ inserts, chlorpromazine significantly increased BSA permeability in both astrocyte and SF8628 co-culture (Figure 18-A). Additionally, both monesin and genistein decreased permeability of BSA in U87 co-culture conditions (Figure 18-A). This was supported qualitatively with visual representations of the microfluidic co-culture units using an EVOS microscope GFP channel (Figure 18-C,D,E,F) While minimal significant changes in IR dye permeability were observed in Transwell™ inserts, in the microfluidic model, chlorpromazine increased paracellular permeability of IRdye in monoculture, astrocyte and SF8628 co-culture conditions (Figure 18-B). Lastly, both chlorpromazine and monesin decreased IRdye permeability in U87 co-culture (Figure 18-B). In summary, it seems that both vesicular and paracellular transport processes are playing a role in both the increased permeability during U87 co-culture as well as enhanced barrier properties in SF8628 co-culture.

Lastly to further elucidate changes in endocytosis and junctional proteins, RNA expression profiles for paracellular, transcellular, and vesicular markers in brain endothelial cells grown in Transwell™ inserts and three-lane organoplate were examined (Figure 19). Data suggested increased expression of *GLUT-1* in all three tumor co-culture conditions (Figure 19-A). While SF8628 co-culture increased expression of *claudin-5*, *BCRP* and *Ve-cadherin* (Figure 19-B) and U87 co-culture increased expression of *caveolin-1* (Figure 19-C). Lastly, the level of *Mfsd2a* in monoculture conditions was undetectable, while the highest level of expression was

found in endothelial cells co-cultured with SF8628 (Figure 19-D). In the three-lane organoplate, both SF8628 co-culture and tumor conditioned media (TCM) increased expression of *occludin, claudin-5, P-gp, and cav-1* (Figure 19-E) suggesting a role of both junctional proteins and vesicular transport processes.

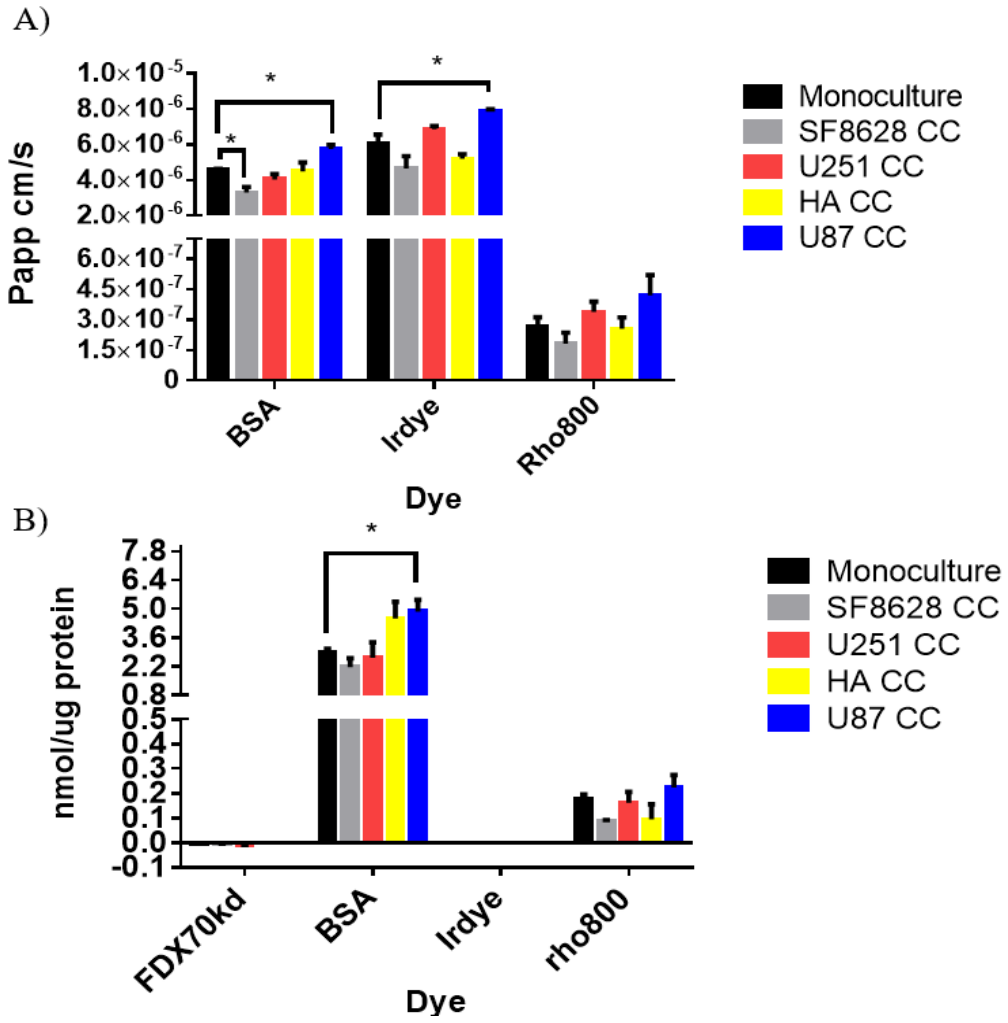

Figure 16: Endothelial cells were co-cultured with various GB and support cells Transwell™ inserts. To assess the role of endocytosis, BSA was used as a marker. Permeability of BSA, IRdye, and rhodamine 800 was determined in monoculture and co-culture with GB cells (U251, U87), DIPG (SF8628) or astrocyte cells (Panel-A). Uptake was also assessed in the same treatment groups (Panel-B). Values represent mean ± SEM of three samples per treatment. *p<0.05, ** p<0.01, p<0.001***, p<0.0001**** (One-way Anova, Dunnets correction)

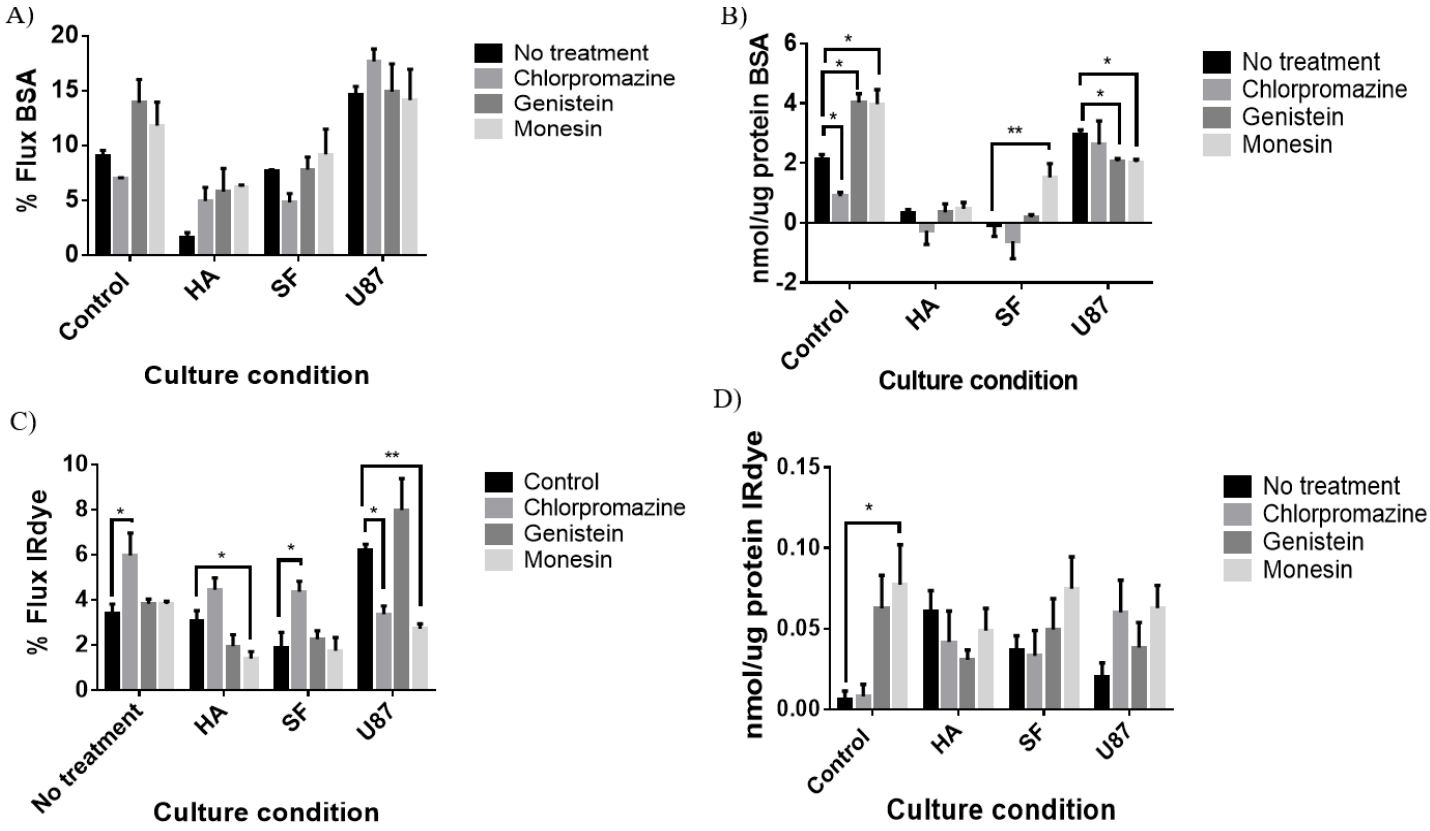

Figure 17: Endothelial cells were co-cultured for 24 hours with HA (astrocyte cells), U87 GB cells or DIPG SF8628 cells in Transwell^{TM} inserts. At endothelial cell confluency, cells were pretreated for 30-minutes with various endocytosis inhibitors. After 30-minutes, fluorescent markers were added, and permeability and uptake were assessed at 2-hours. Permeability and uptake were assessed for BSA (Panel-A and B) and IRdye dye (Panel-C and D). Values represent mean ± SEM of three samples per treatment. *p<0.05, ** p<0.01, p<0.001***, p<0.0001**** (One-way Anova, Dunnets Correction)

A)

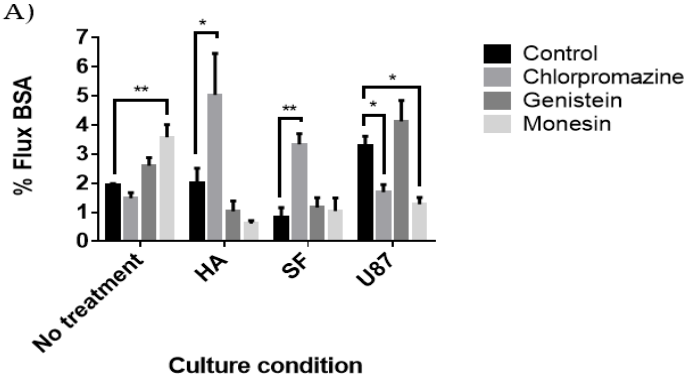
% Flux BSA
Control
Chlorpromazine
Genistein
Monesin
No treatment
HA
SF
U87
Culture condition

B)

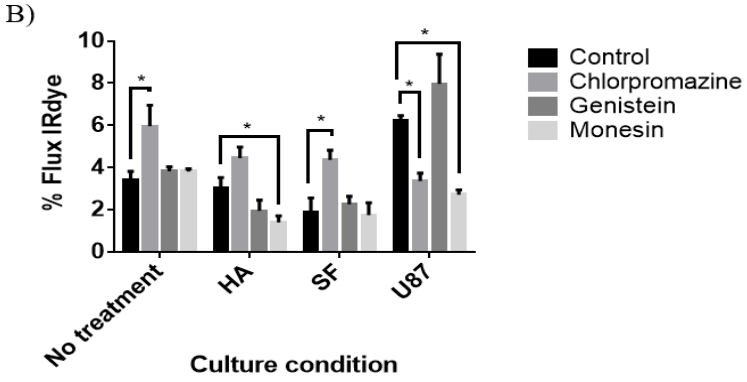
% Flux IRdye
Control
Chlorpromazine
Genistein
Monesin
No treatment
HA
SF
U87
Culture condition

C)


Monoculture
No treatment
Monoculture+
Chlorpromazine
Monoculture+
Genistein
Monoculture+
Monesin

D)

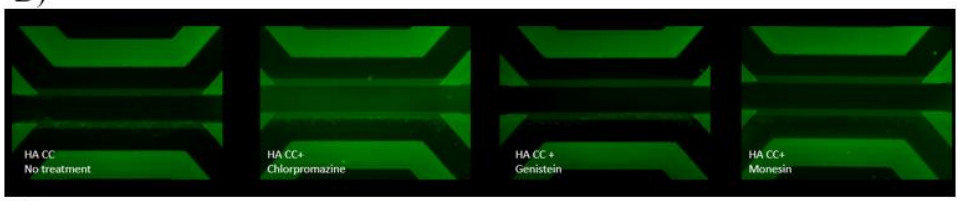
HA CC
No treatment
HA CC+
Chlorpromazine
HA CC +
Genistein
HA CC+
Monesin

E)

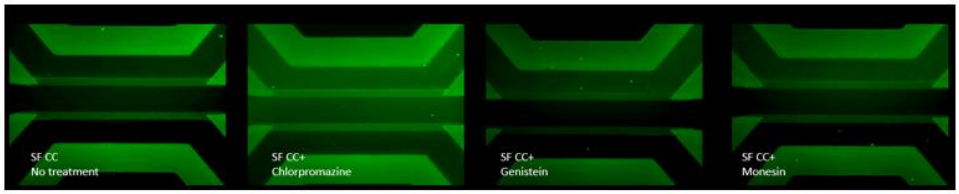
SF CC
No treatment
SF CC+
Chlorpromazine
SF CC+
Genistein
SF CC+
Monesin

F)

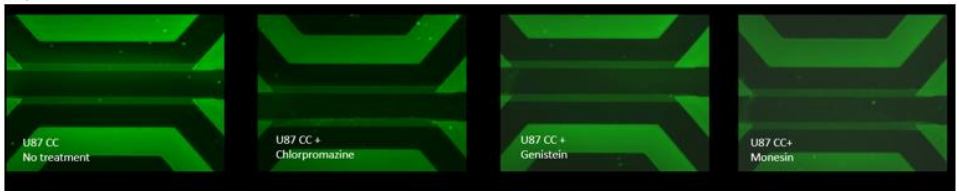
U87 CC
No treatment
U87 CC +
Chlorpromazine
U87 CC +
Genistein
U87 CC+
Monesin

Figure 18: Examing the impact of endocytosis inhibitors in the three-lane organoplate during various co-culture conditions. Flux of BSA (Panel-A) and IRdye (Panel- B) were determined. Qualitative examination of BSA permeability in monoculture conditions (Panel- C), endothelial co-cultured with astrocytes (Panel-D), SF8628 (Panel-E) and U87 (Panel-F). Values represent mean ± SEM of three samples per treatment. *p<0.05, ** p<0.01, p<0.001***, p<0.0001**** (One-way Anova, Dunnets correction)

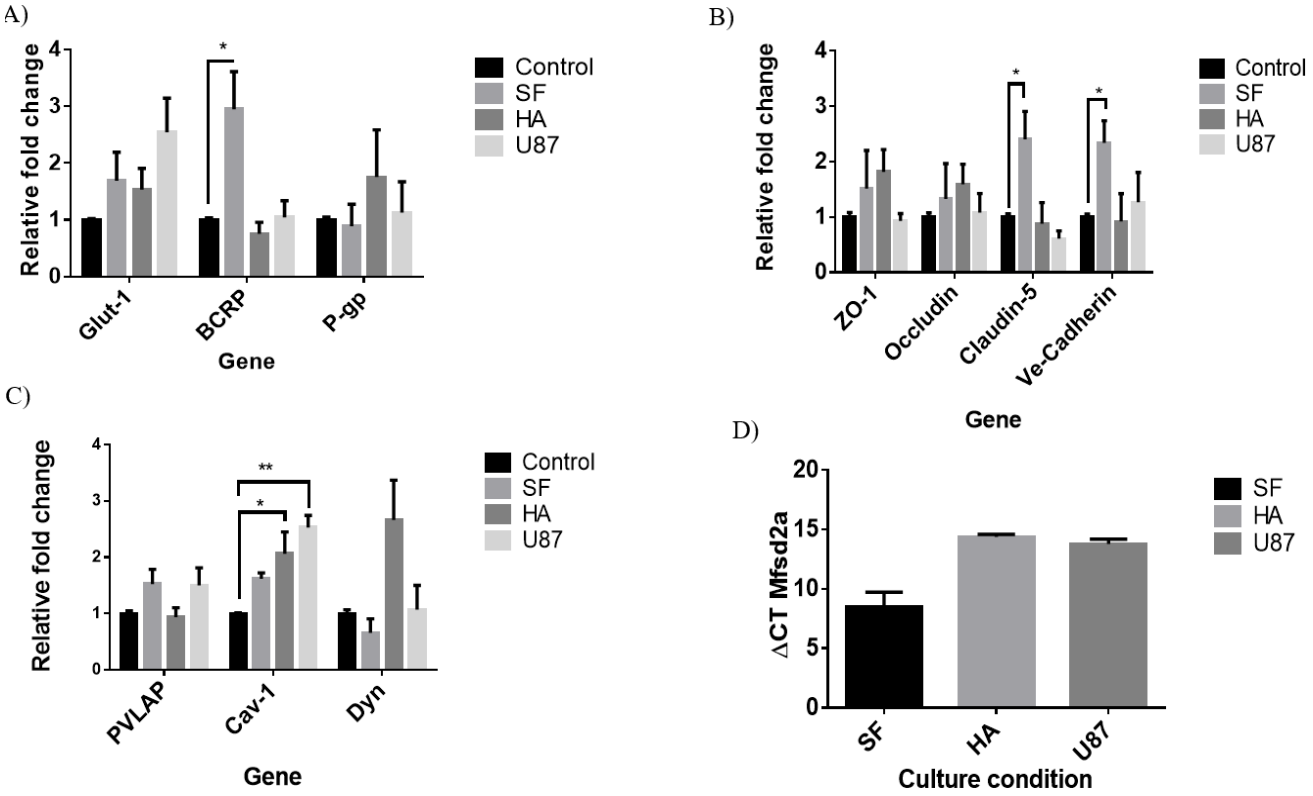

E)

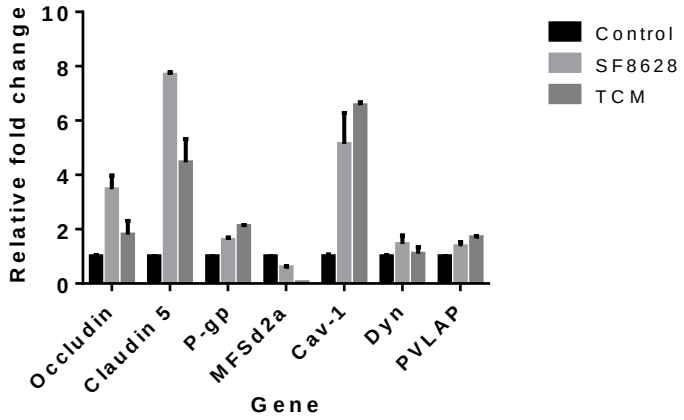

Figure 19: Relative fold change in expression to GAPDH of paracellular, transcellular or vesicle gene expression during various co-culture conditions in 12-well Transwell™ inserts and three-lane microfluidic organoplate. In Transwell™ inserts, changes in endothelial cell expression during monoculture (control) and co-culture conditions were examined for transcellular markers (Panel-A), paracellular markers (Panel-B) and vesicular markers (Panel-C). Changes in mfsd2a expression were also examined (Panel-D). Values reported as ΔCT, the data was normalized to GAPDH. Additionally changes in relative fold change to GADPH of paracellular, transcellular, and vesicular markers in the three-lane microfluidic plate in control monoculture conditions, SF8628 co-culture and tumor conditioned media conditions were examined (Panel-E). All genes were normalized to GAPDH and compared to monoculture control conditions to obtain relative fold change in expression. Values represent mean ± SEM of three samples per treatment in Transwell™ inserts *p<0.05, ** p<0.01, p<0.001***, p<0.0001**** (One-way Anova, with Dunnets correction). In the microfluidic model, data represents 6 pooled microfluidic units to create one biological replicate.

3.5.5 Role of Sonic Hedgehog (SHH) in Barrier Enhancing Effect of DIPG Co-Culture Model.

To elucidate mechanisms of SF8628 DIPG tumor cell induced modulation of endothelial cells, the sonic hedgehog pathway was investigated. To assess various SHH conditions, apparent permeability in the 3-lane organoplate was determined using FDX70,000 and IRdye, as paracellular markers and Rhodamine 800 as a transcellular marker. Tumor conditioned media (TCM) from SF86828 cells and DIPG co-culturing were investigated to elucidate differences between endothelial-tumor cell-cell interactions and effects of TCM media. Various sonic hedgehog inhibitors were also examined including RUSKI-201 which blocks sonic hedgehog release from tumor cells and Vismodegib which acts as a sonic hedgehog receptor antagonist. Vismodegib was used to assess binding of SHH to endothelial cell receptors and RUSKI-201 to determine the impact of blocking the production of SHH from DIPG (SF8628) tumor cells. Compared to control, both TCM and SF8628 (DIPG) tumor co-culture reduced endothelial cell permeability for all three-dyes tested (Figure 20-A, B and C). Additionally, RUSKI-201 restored

barrier properties which approached control/ monoculture values. However, Vismodegib did not restore permeability for IRdye and FDX70,000 (Figure 20-A and B). Interestingly, Visomodegib increased rhodamine 800 permeability (Figure 20-C).

Lastly, recombinant human sonic hedgehog (rhSHH) was added to endothelial cells. If SHH was directly acting on endothelial cells, it was expected that recombinant human sonic hedgehog would decrease endothelial permeability. Interestingly, rhSHH did not have a barrier enhancing effect (Figure 20-A, B and C). Taken together, these results suggest both TCM and co-culturing reduced apparent permeability and improved barrier properties (Figure 20-A, B and C). Blocking SHH release from SF8628 cells resulted in permeability values similar to control levels (Figure 20-A and B). However, treatment with the SHH receptor antagonist had no significant impact on permeability values (Figure 20-A and B). These results indicate SHH is likely acting indirectly on endothelial cells to decrease permeability. It is suspected that blocking SHH release from tumor cells might impact or prevent activation of other downstream factors. This was also supported by the observation that rhSHH did not impact apparent permeability relative to control (Figure 20-A, B and C).

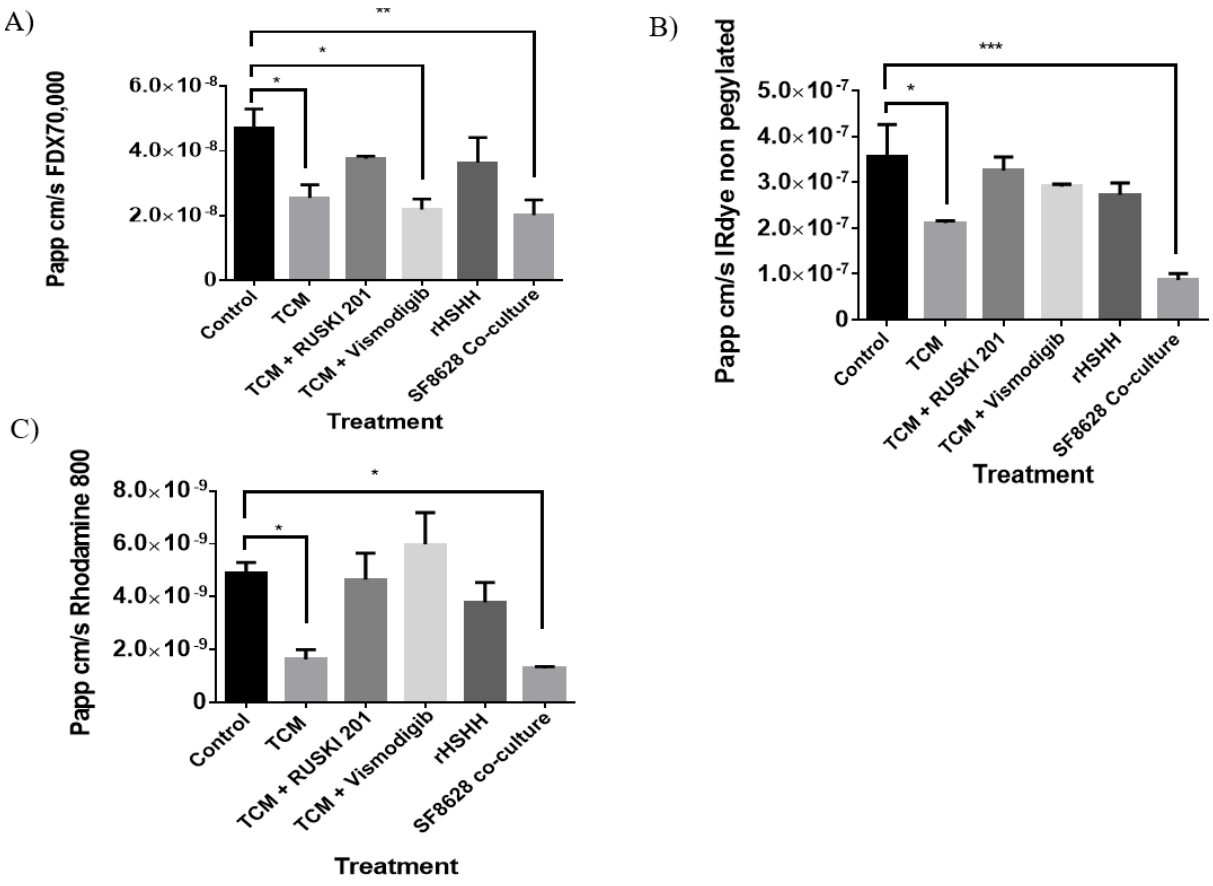

Figure 20: Endothelial cells were cultured in the three lane organoplate in the presence of tumor conditioned media, SF8628 cells, recombinant human sonic hedgehog, Vismodegib (sonic hedgehog receptor antagonist), and RUSKI-201 (blocking sonic hedgehog release from tumor cell). Apparent permeability was measured in the various conditions for FDX70,000 (Panel-A), IRdye (Panel-B) and rhodamine 800 (Panel-C) to determine effects on endothelial cell barrier integrity. Values represent mean ± SEM of three samples per treatment. *p<0.05, ** p<0.01, p<0.001***, p<0.0001**** (One way anova, Dunnets correction)

3.5.6 Sonic Hedge Hog Receptor Antagonist Interaction with P-glycoprotein

Uptake studies using elacridar, a P-gp inhibitor, confirmed rhodamine 800 as a p-glycoprotein substrate. Evidence was based on the increase in rhodamine 800 permeability in the presence of elacridar. Furthermore, Vismodegib and RUSKI-201 were also investigated for P-gp

binding activity. In the presence of elacridar and the various sonic hedgehog inhibitors, RUSKI-201 did not influence rhodamine 800 transport, suggesting unlikely interactions with P-gp. However, Vismodegib significantly increased rhodamine 800 uptake, suggesting Vismodegib's role in P-gp interaction and inhibition (Figure 21).

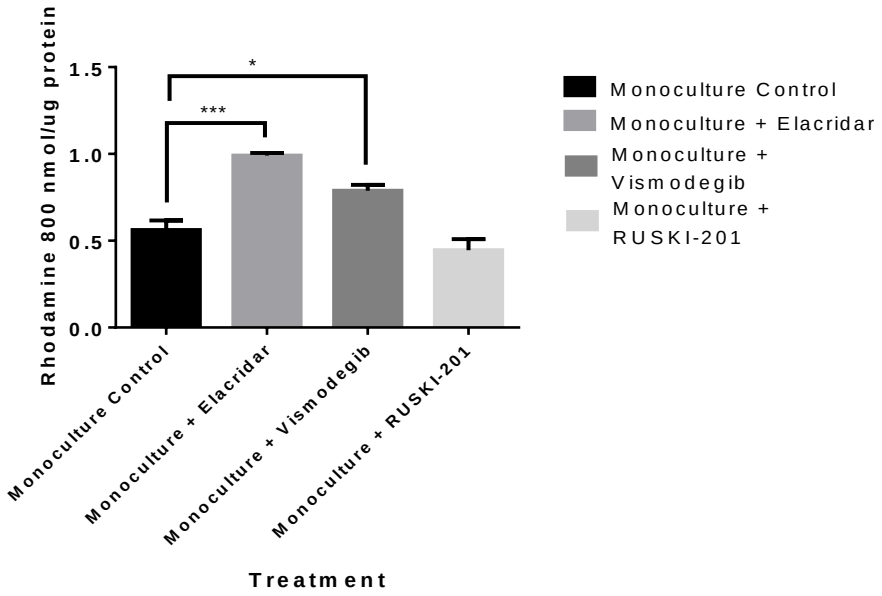

Figure 21: Endothelial cell uptake of rhodamine 800 in the presence of elacridar, a P-gp inhibitor, and various sonic hedgehog inhibitors. Values represent mean ± SEM of three samples per treatment. *p<0.05, ** p<0.01, p<0.001***, p<0.0001**** (One way anova, Dunnets correction)

3.5.7 DIPG Tumor Induced Changes in BBB gene Expression.

To further investigate DIPG tumor induced effects on endothelial cells, examination of RNA expression was determined for BBB specific genes. Expression profiles were examined in endothelial cells co-cultured with SF8628 cells, TCM, and various SHH inhibitors in 6-well Transwell^{TM} inserts. Findings indicate that both TCM and DIPG co-culture significantly increased expression of *occludin, ZO-1, GLUT-1, BCRP, claudin-1,* and *claudin-5* (Figure 22-A). While TCM treatment increased expression of *P-gp* (Figure 22-A). Many expression changes

were observed in both TCM and DIPG co-culture, mechanistically suggesting a secreted factor responsible for the alterations in endothelial expression changes. However, these increases in gene expression were highest when endothelial cells were in co-culture with DIPG tumor cells, indicating some inter-cellular cross talk not captured with TCM (Figure 22-A). Results support the functional studies performed and supported the hypothesis that SF8628 DIPG cells induces endothelial cell tightening, likely by a secreted factor. To further investigate the role of sonic hedgehog, changes in endothelial cell gene expression in the presence of sonic hedgehog inhibitors were examined. The findings suggest that in the presence of RUSKI-201, there was decreased expression of *claudin-5* and *claudin-3* compared to TCM alone (Figure 22-A and B). At the BBB the most dominant junctional protein for barrier integrity is claudin-5 with minor contributions from claudin-3 and claudin-1 (Berndt et al., 2019). Therefore, it is not surprising that when sonic hedgehog release from the tumor cell is inhibited with RUSKI-201, the effects of SF8628 co-culture conditions on both barrier formation and junctional protein expression is

reversed (Figure-20, 22-B).

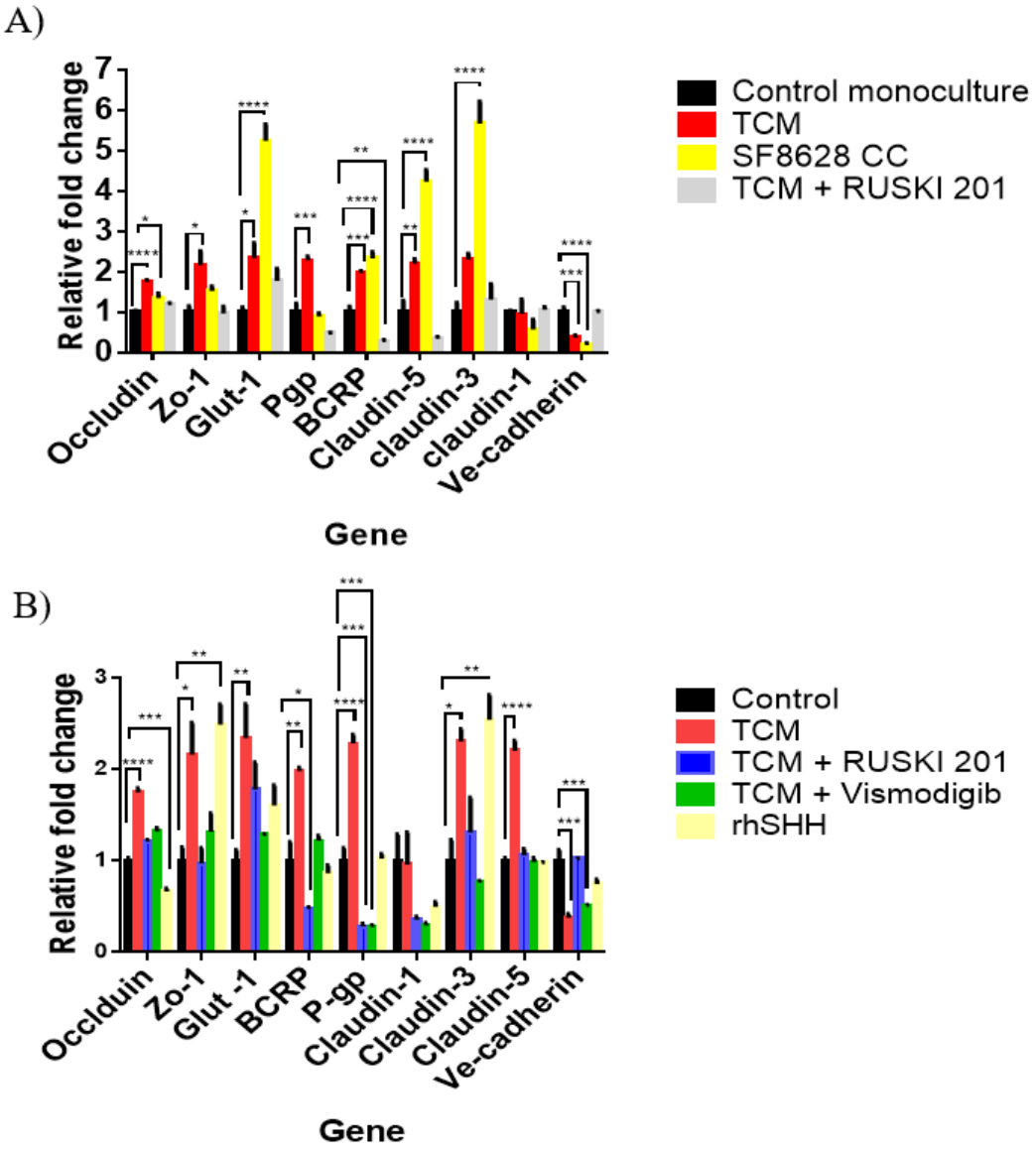

Figure 22: Relative fold change to GADPH of gene expression of selected BBB specific genes. Changes in gene expression were examined in monoculture conditions, SF8628 co-culture conditions and TCM from SF8628 cells (Panel-A). Additionally, changes in endothelial cell gene expression in the presence of various sonic hedgehog inhibitors was also examined (Panel-B). Genes were normalized to GAPDH and the ΔΔCT method was employed to determine relative fold change. Values represent mean ± SEM of three samples per treatment in Transwell™ inserts. *p<0.05, ** p<0.01, p<0.001***, p<0.0001**** (One-way Anova, Dunnets correction)

3.6 Clinical Applications of the Model.

3.6.1 Quantitative Examination of Cadherin Peptide Modulation.

Cadherin peptides were formulated by collaborators at Kansas University and developed to bind to the extracellular domains of cadherin, preventing homodimer formation and causing opening of cadherin peptide junctions between vascular endothelial cells. Through reversible interaction of the cadherin peptides with the endothelial cell cadherin proteins at the tight junction, transient increases in BBB permeability occur that can be utilized to aid in drug delivery to the brain. A quantitative examination of endothelial cell permeability in the three lane organoplate under normal conditions and following exposure to various concentrations of HAVN1 cadherin peptide for 30-minutes was assessed (Figure-23). A concentration dependent effect was observed whereby increasing concentrations of HAVN1 cadherin peptide resulted in increased amounts of FDX70,000 leaking from the vascular compartment into the gel and third lane (Figure 23-B). These results suggested cadherin peptides disrupted vascular cadherin junctions resulting in increased endothelial cell permeability (Figure 23-A and B).

A)

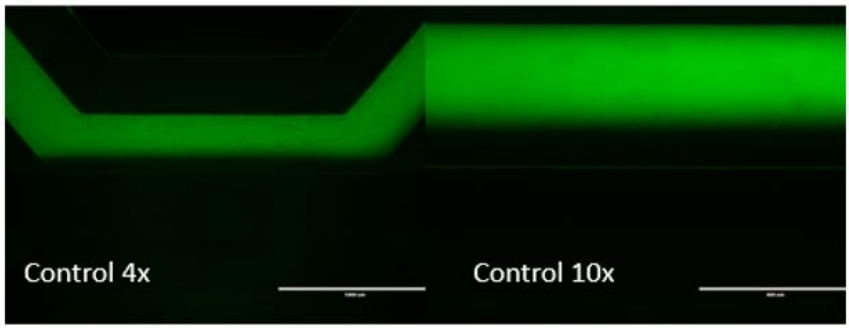

B)

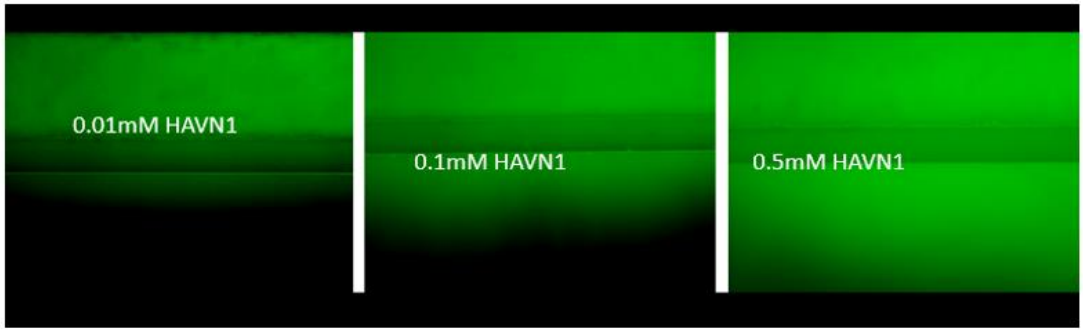

Figure 23: Qualitative examination of endothelial cell permeability of FDX 70,000 in microfluidic monoculture model under control conditions (Panel-A) and in the presence of increasing concentrations of HAVN1 cadherin peptide at 30 minutes (Panel-B).

Based on these initial studies with HAVN1, a more extensive evaluation of the extent of permeability modulations produced by the cadherin peptides were performed with the microfluidic BBB culture model. Endothelial cell permeability of a large paracellular marker (FDX 70,000), a small paracellular marker (IRdye, 900Da) and transcellular rhodamine 800 in the presence of various cadherin peptides, HAVN1, ADTC5, TPP, and HAV6 were assessed in the 3-lane organoplate. Various peptides were examined to assess cadherin peptide efficacy with regard to disruption of cadherin junctions and increasing permeability of various sized markers. The peptide HAV binds the extracellular cis domain of cadherin preventing homodimers, ADTC5 prevents trans binding while TPP has components of both. The data suggests the most

effective cadherin peptide concentration to increase paracellular permeability was 0.5mM (Figure 24- A and B). Additionally, at the 0.5mM concentration, cadherin peptides HAVN1 and HAV6 were shown to be most effective for increasing permeability of large molecular weight molecules (Figure 24-D) while both ADTC5, HAV6 and HAVN1 significantly increased IRdye permeability (Figure 24-E). Interestingly, ADTC5 (Figure 24-E) increased transcellular transport of rhodamine 800 (Figure 24-F). Lastly, TPP had little effect on permeability for any of the dyes tested (Figure 24-D, E and F).

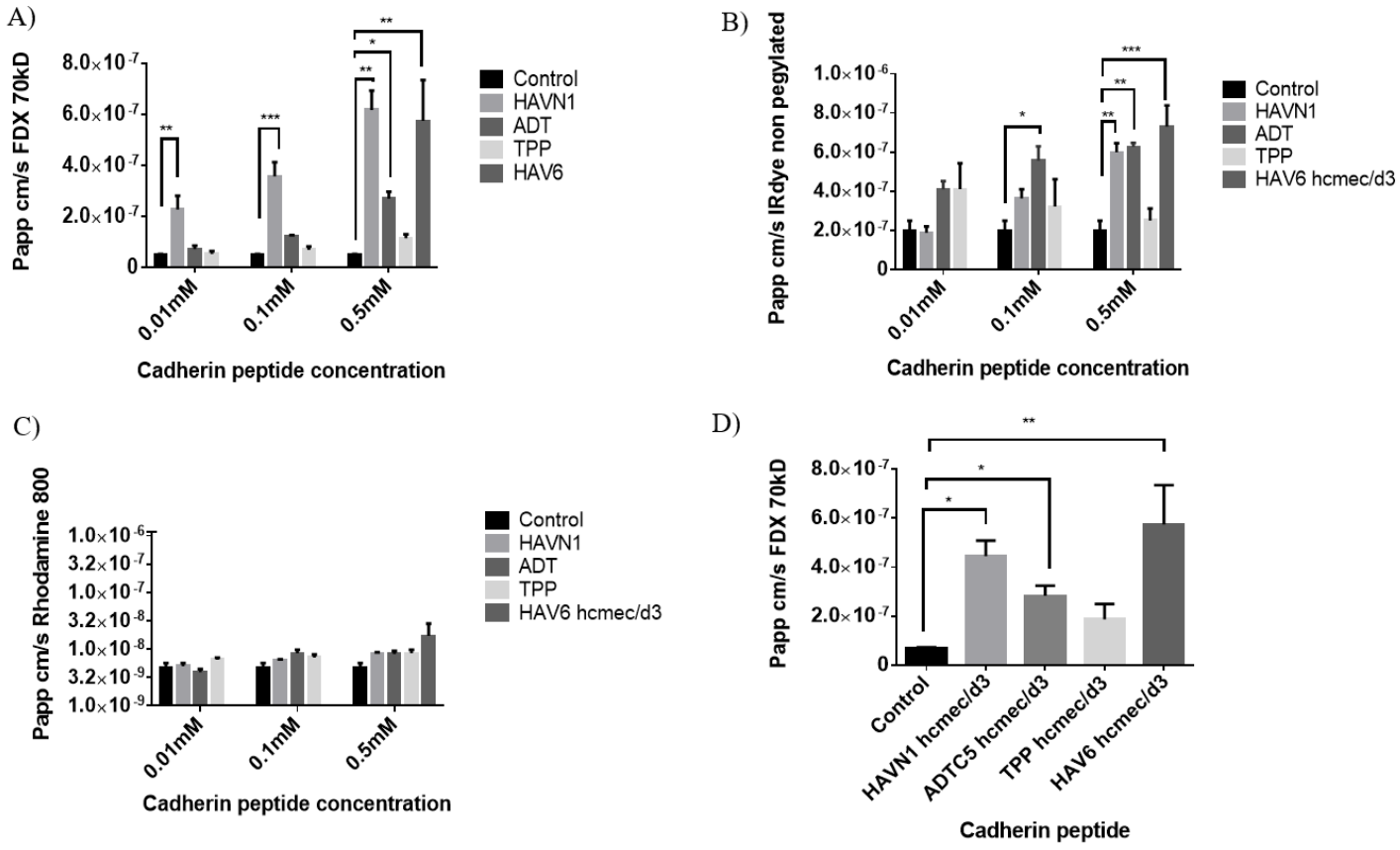

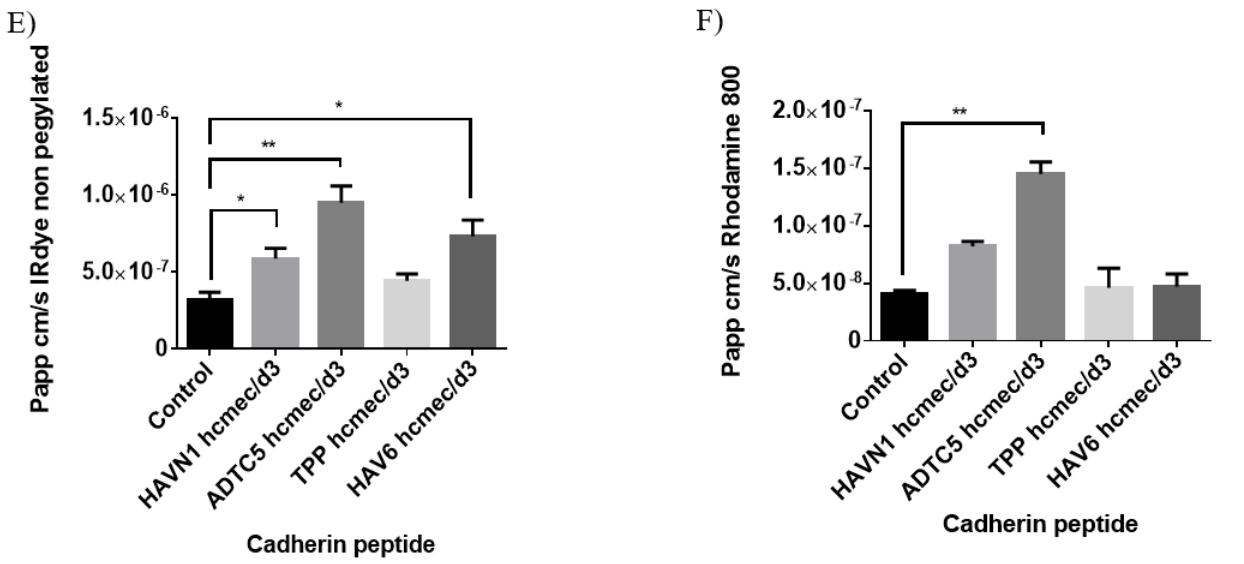

Figure 24: Investigation of the impact of cadherin peptides using various concentrations of HAVN1, ADTC5, and TPP in the three-lane organoplate using FDX70,000 (Panel-A), IRdye (Panel-B) and Rhodamine 800 (Panel-C). Using 0.5mM concentrations, cadherin peptides (HAVN1, ADTC5, TPP and HAV6) were evaluated for their impact on endothelial cell permeability in the same culture model and using the same fluorescent dyes: FDX70,000 (Panel-D), IRdye (Panel-E) and rhodamine 800 (Panel-F). Values represent mean ± SEM of three samples per treatment. *p<0.05, ** p<0.01, p<0.001***, p<0.0001**** (One-way Anova, Dunnets correction)

3.6.2 Endothelial Cell Specificity of Cadherin Peptide.

As cadherin peptides are found in both vascular endothelial cells and epithelial cell barriers, cadherin peptides that are selective for endothelial cells would minimize adverse toxic effects. To determine cadherin peptide endothelial selectivity, permeability studies were performed in a 3-lane organoplate using both a vascular brain endothelial cell line (hCMEC/d3), kidney epithelial cell line (MDCK-MDR) and pulmonary vascular cells. Apparent permeability in hCMEC/d3 and MDCK cell lines were determined for both paracellular markers FDXK70,000 and IRdye (Figure 25-A and B), and a transcellular marker rhodamine 800 (Figure 25-C) in the presence and absence of cadherin peptides. In the presence of HAVN1, ADTC5 or HAV6, significantly increased permeability of FDX70,000 was observed in hCMEC/d3 brain endothelial

cells (Figure 25-A). However, these increases were not observed in the epithelial cell culture model (Figure 25-A). Similar results were obtained with the small paracellular marker, where significant increases in vascular BBB endothelial cell permeability but not epithelial cell permeability were observed in the presence of HAVN1, ADTC5 and TPP (Figure 25-B). With regard to transcellular transport, significant increases in rhodamine 800 permeability were observed in the presence of ADTC5 in BBB endothelial cells. While there was also a trend towards increased permeability to rhodamine 800 in the MDCK/MDR1 epithelial cells, such alterations were not statistically significant (Figure 25-C). Additionally, pulmonary endothelial cells were cultured in the 3-lane microfluidic plate and permeability was determined for paracellular and transcellular fluorescent markers in the presence of 0.01mM, 0.1mM and 0.5mM HAVN1. Compared to hCMEC/d3 brain endothelial cells, the HAVN1 cadherin peptide had no significant effect on paracellular or transcellular permeability in pulmonary endothelial cells (Figure 25-D,E,F). Collectively, these data suggest cadherin peptides appear to be selective at increasing paracellular permeability in vascular endothelial cadherin junctions and indicate a selective increase in permeability of BBB vasculature when compared to epithelial and pulmonary endothelial cells.

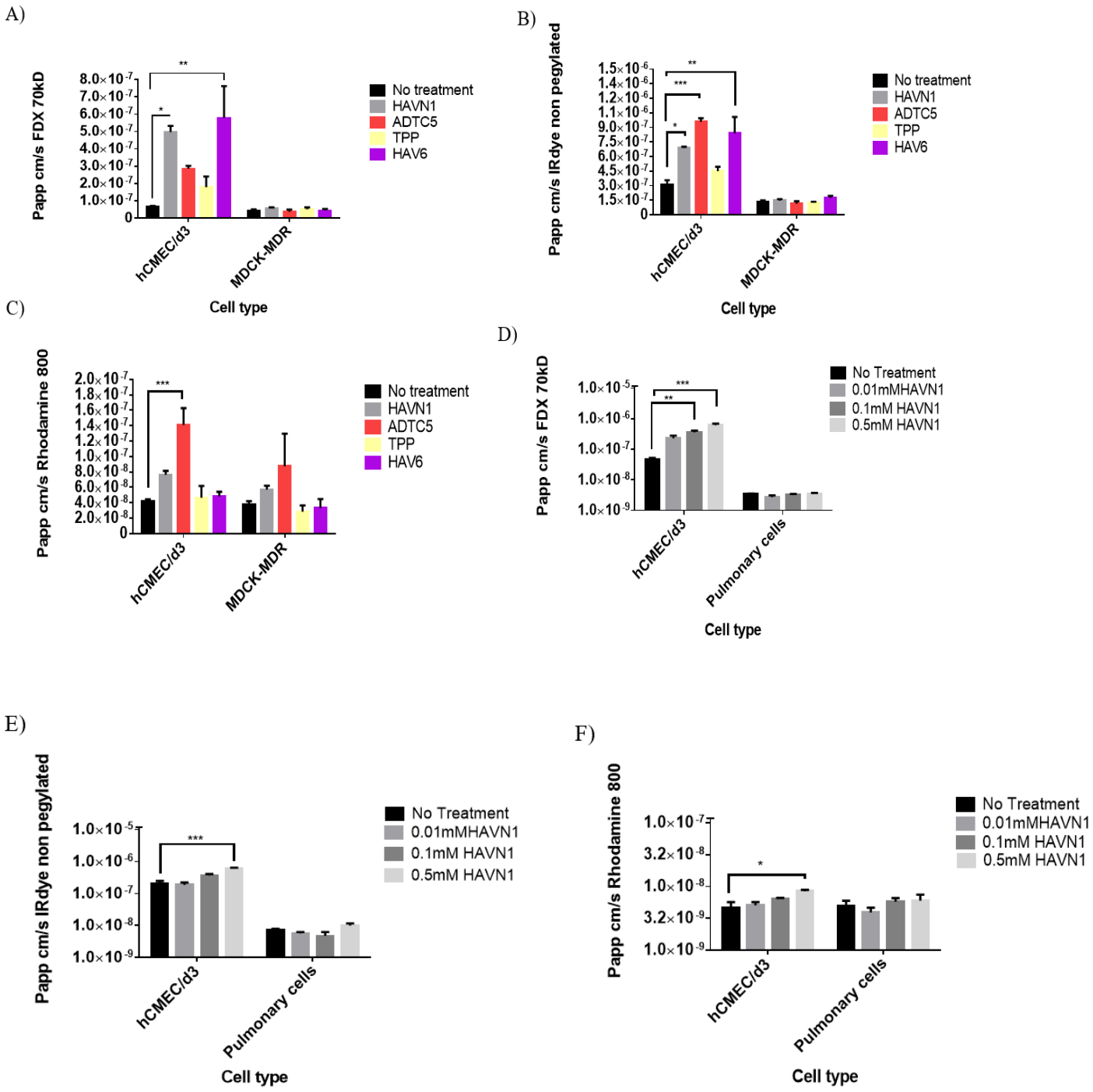

Figure 25: Determination of apparent permeability in hCMEC/d3 and MDCK-MDR cell lines for FDX70,000 (Panel-A), IRdye (Panel-B) and rhodamine 800 (Panel-C) in the presence of HAVN1, HAV6, ADTC5, and TPP. Permeability of FDX70,000 (Panel-D), IRdye (Panel-E), and rhodamine 800 (Panel-F) in pulmonary endothelial cells and hCMEC/d3 brain endothelial cells in the presence of 0.01mM, 0.1mM and 0.5mM HAVN1 concentrations. Cultured model used was the three-lane organoplate. Values represent mean ± SEM of three samples per treatment. *p<0.05, ** p<0.01, p<0.001***(One-way Anova, Dunnets correction)

3.6.3 Investigation of Monoclonal Antibody Permeability in the DMF Model in the Presence of HAVN1.

Avastin is a monoclonal antibody (mAb) that blocks vascular endothelial growth factor (VEGF) from binding its receptor (Chamberlain, 2011). Vascular endothelial growth factor is important in angiogenesis and required for tumor cell growth and proliferation (Chamberlain, 2011). Glioblastoma is a highly vascularized cancer and studies have shown administration of Avastin to block VEGF can improve the quality of life for GB patients (Nagpal et al., 2011). However, the BBB poses a major restriction in the amount of Avastin reaching the brain to block VEGF in therapeutic concentrations. Therefore, we tested the ability of HAVN1 to increase Avastin BBB permeability. Endothelial cells were cultured in the three-lane organoplate and permeability of Avastin, a monoclonal antibody fragment (Fab) and FDX70,000 were assessed in the presence or absence of HAVN1 (Figure 26). Permeability studies were conducted in both the blood (apical-A) to brain (basolateral-B) direction (A→B) and brain to blood direction (B→ A) to determine if there was any directional transport of mAb or Fab in the BBB. We previously observed expression of the neonatal Fc receptor (FcnR) in hCMEC/d3 cells. This receptor is reported to aid in scavenging mAb and prolonging circulation time (Pyzik et al., 2023). The Fc receptor is believed to be responsible for binding IgG and pumping antibodies out of the brain back to the blood (Cooper et al., 2013). Albumin, which is present in serum, may also be a FcnR substrate (Nilsen et al., 2018). The fragment (Fab) is not likely transported by the FcnR, therefore if FcnR is involved in BBB transport, the fragment would be less effected than the antibody.

To elucidate the role of the FcnR, serum free conditions were examined for each condition. Results show a 0.5 mM concentration of HAVN1 increased Avastin permeability to the greatest extent when compared to FDX 70,000 and Fab in the A→B direction (Figure 26). We also observed significantly increased permeability of Avastin and Fab in the B→A direction when compared to FDX70,000 (Figure 26). However, Avastin had the highest increase in permeability in the B→A direction when compared to Fab, suggesting FcnR's role in removing the antibody from the brain back to the blood (Figure 26). Lastly, HAVN1 was able to significantly increase permeability of FDX70,000, Avastin and Fab in the A→B direction (Figure 26). Taken together these results suggest the ability of Avastin to be transported from the brain back to the blood. The cadherin peptide HAVN1 was also shown to significantly improve blood to brain permeability of Avastin.

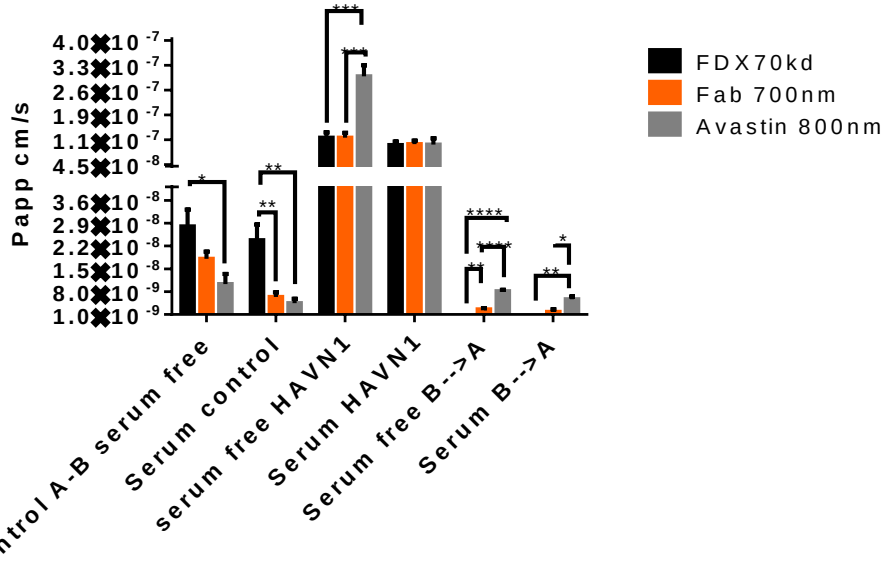

Figure 26: Endothelial permeability of Avastin, Fab, and FDX70,000 in the three-lane organoplate was assessed at 60 minutes in the A→B direction (blood to brain) and B→A direction (brain to blood). Permeability impacts of 0.5mM HAVN1 were also determined. Fluorescence of compounds were read on varioskan lux plate reader FDX70,000 485/520,

Avastin 785/812 and Fab 685/712. Values represent mean ± SEM of three samples per treatment. *p<0.05, ** p<0.01, p<0.001***, p<0.0001**** (One- way Anova, Bonferroni correction)

3.6.4 Quantitative Examination of Cadherin Peptide Modulation on Nanoparticle Permeability.

To better understand clinical applications of the model, nanoparticles were added to the vascular compartment of confluent endothelial microvessel in the 3-lane organoplate and their passage across endothelial barriers was monitored. Nanoparticles are of interest as potential carriers for both small molecule chemotherapeutics as well as biological and gene therapy payloads (Prados et al., 2012). However, a critical feature is that nanoparticles must be able to cross the BBB to deliver the encapsulated drugs in sufficient concentrations. Therefore, nanoparticle permeability across an endothelial barrier was assessed. Nanoparticle permeability was determined in both control conditions and in the presence of 0.5 mM HAVN1, ADTC5 or TPP (Figure 27-A). Cadherin peptides HAVN1 and ADTC5 significantly increased BBB permeability of nanoparticles loaded with doxorubicin, with the most profound increase in NP permeability seen when HAVN1 was applied (Figure 27-A). Additionally, nanoparticles of different sizes loaded with SAT1 siRNA were assessed for BBB permeability (Figure 27-B and C). Again, HAVN1 significantly increased NP permeability across confluent microvessel (Figure 27-B). This was supported by qualitative data in which phenotypically, nanoparticles crossed the endothelial cell barrier and entered the gel and third compartment in the presence of HAVN1 (Figure 27-C).

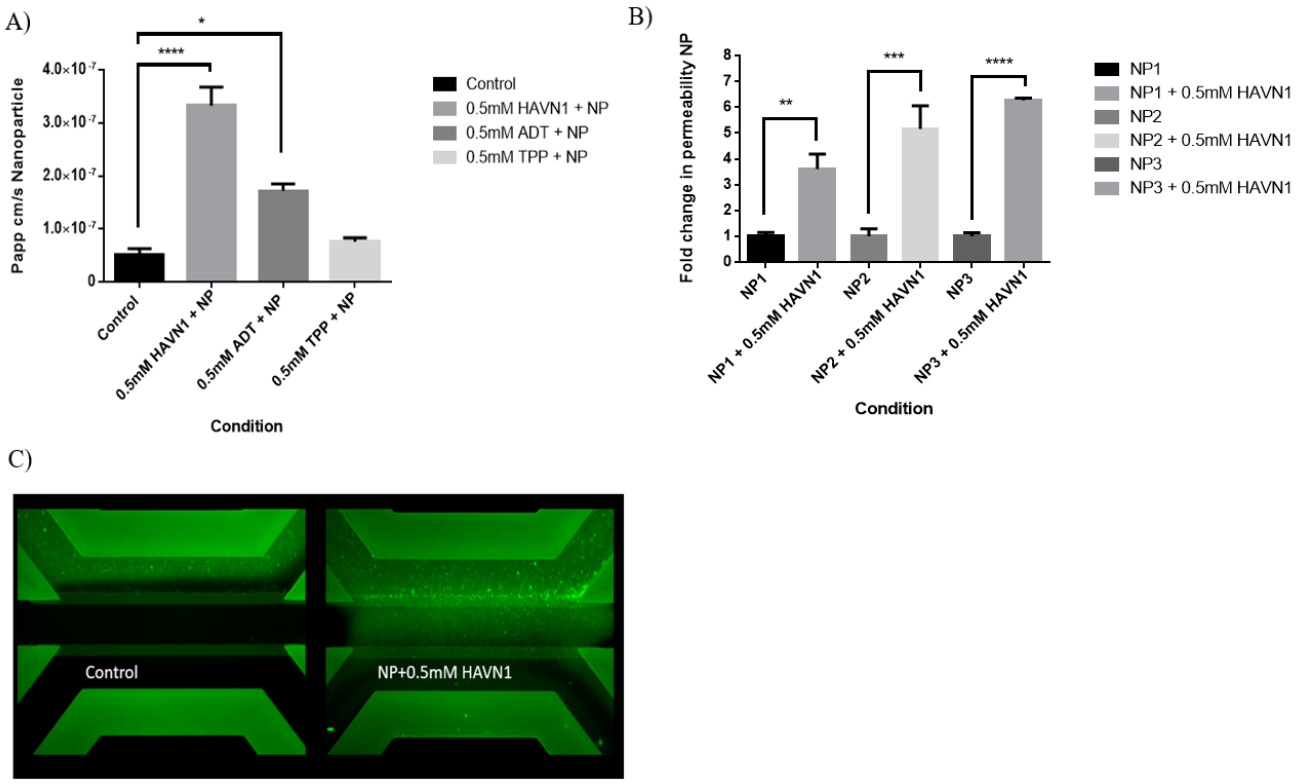

Figure 27: Endothelial cell permeability of nanoparticles loaded with doxorubicin in the presence of 0.5mM HAVN1, ADTC5 and TPP in the three lane organoplate (Panel-A). Quantitative examination of various sized nanoparticles loaded with SAT1 siRNA in the presence of HAVN1 (Panel-B). Qualitative examination of SAT1 siRNA nanoparticles in the presence and absence of 0.5mM HAVN1(Panel-C). Values represent mean ± SEM of three samples per treatment. *p<0.05, ** p<0.01, p<0.001***, p<0.0001**** (One-way Anova, Dunnets correction)

3.6.5 Cadherin Peptide Modulation in BBB-Tumor Co-Culture Microfluidic Model.

The cadherin peptide, HAVN1, was also examined in the microfluidic brain tumor co-culture model to determine the effectiveness of cadherin peptide modulation of brain endothelial cell permeability as a potential approach for improving drug delivery to brain tumors. Co-culture conditions were established in the 3-lane organoplate using both GB cells (U87 and U251) and DIPG (SF8628) cell lines. The HAVN1 cadherin peptide was chosen based on its pervious

performance in producing dramatic alterations in permeability to a wide range of solutes. Across all tumor co-culture models examined, HAVN1 produced significant increases in brain endothelial cell permeability to FDX70,000 (Figure 28).

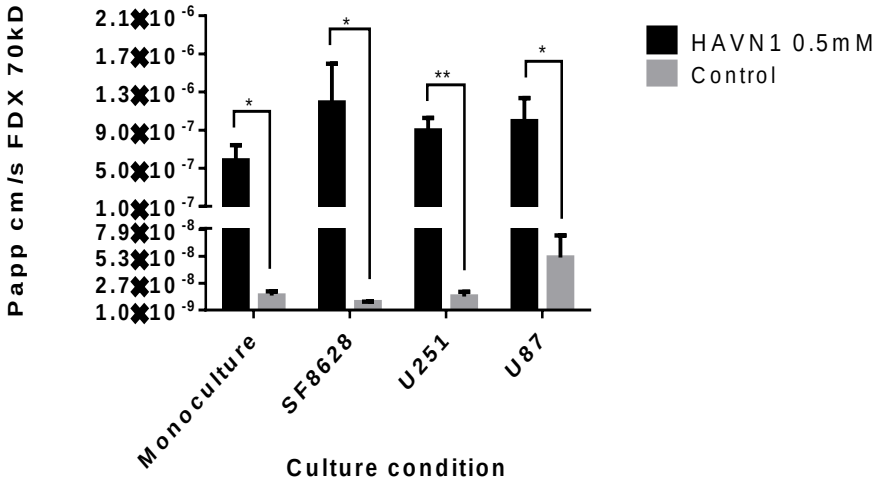

Figure 28: Endothelial permeability of FDX70,000 in the 3-lane organoplate. Cells were grown in monoculture or co-culture with GB (U87 and U251) cells or DIPG (SF8628) cells and permeability was determined in the presence or absence of 0.5 mM HAVN1. Values represent mean ± SEM of three samples per treatment. *p<0.05, ** p<0.01, p<0.001***, p<0.0001**** (unpaired students T-test, correct for multiple comparisons using Bonferroni method)

3.6.6 Size Based BBB Permeability using Various Cadherin Peptides.

Various cadherin peptides were formulated and tested to determine the peptide most effective at increasing endothelial paracellular permeability. As mentioned, HAV binds extracellular cis domains of cadherin preventing homodimers, ADTC5 prevents trans binding while TPP has components of both. A quantitative BBB permeability assessment in the three-lane organoplate revealed binding of the peptides to either trans, cis or both cadherin domains increased permeability for small molecular weight markers (Figure 28-A). When plotting

endothelial permeability against size of molecular markers, data revealed difference in cadherin peptide modulation of endothelial permeability (Figure 28-B). The results indicate that peptide binding to cadherin cis domains using HAVN1 is most effective and produces the most dramatic increases in endothelial cell permeability of large molecular weight markers (Figure 28-B)

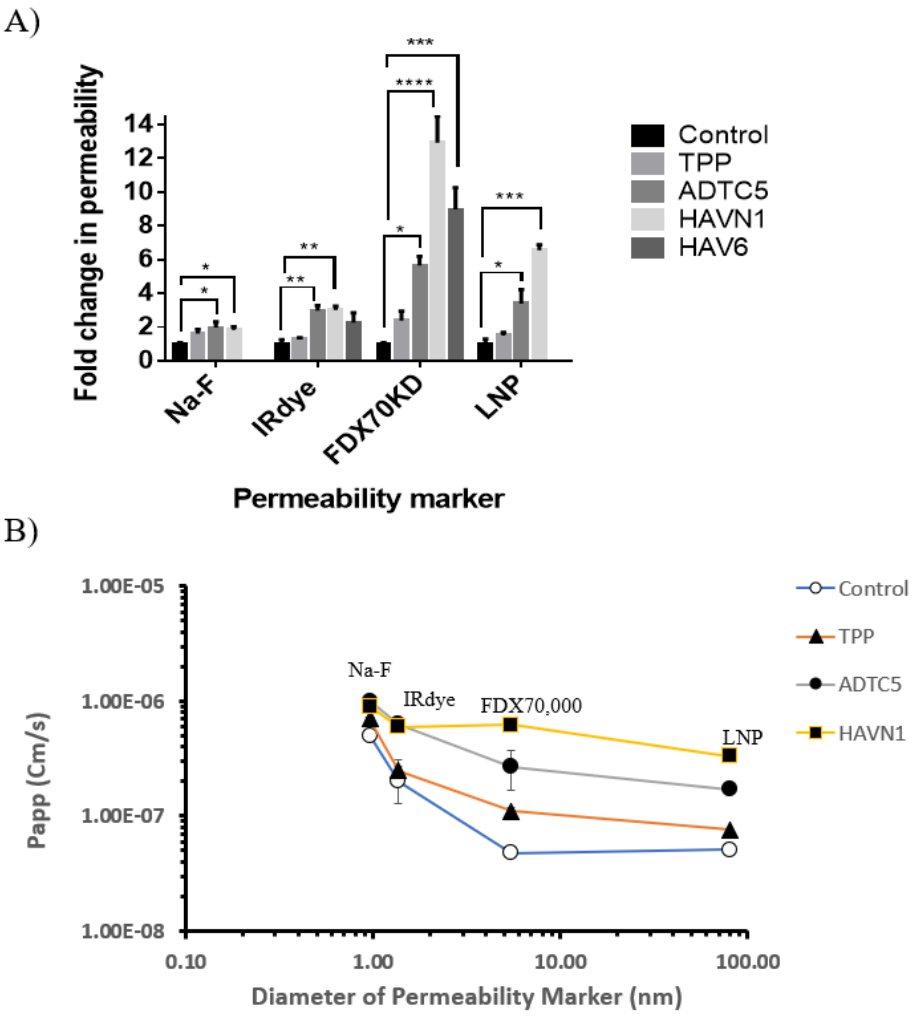

Figure 29: Endothelial cell permeability in the three-lane organoplate using various size molecules and cadherin peptides (Figure 28 A and B). Values represent mean ± SEM of three samples per treatment. *p<0.05, ** p<0.01, p<0.001***, p<0.0001**** (One-way Anova, Dunnets correction)

4.0 Discussion

Cell culture models have been essential to understanding cellular biology, mechanisms of disease, drug action and discovery (Kapałczyńska et al., 2018). Two-dimensional cell culture models are extensively used for *in vitro* cellular analysis. However, these traditional cell culture models do not capture all the complexities of the neurovascular unit. Many of the current culture models for the BBB are single monolayers of endothelial cells, requiring semi-permeable membranes support structures which makes cell- cell contact difficult, and are grown under static "no flow" conditions (Kapałczyńska et al., 2018). These limitations of 2-D models make replicating *in vivo* physiological conditions challenging. Emerging microfluidic technology has provided methods for 3-D culture systems that allow a better understanding of BBB function under normal conditions and pathological conditions such as brain tumors where the tumor microenvironment can alter permeability. In the present study, the main objectives were to develop a BBB barrier dynamic microfluidic model and compare the 3-D Mimetas^{TM} organoplate to 2-D Transwell^{TM} inserts to characterize differences. The 3-D Mimetas^{TM} microfluidic organoplates were chosen in this study because of the relatively simple design and ease of set up, direct cell-cell contact abilities, fluid sampling from both vascular and non-vascular compartments, absence of artificial membrane, ability to create bidirectional fluid flow in the absence of pump mechanisms and compatibility with common laboratory equipment. Additionally, this study aimed to characterize molecular and functional changes in endothelial cells in response to the heterogenous tumor microenvironment and determine clinical applications of the model.

4.1 The Microfluidic System as a BBB Model.

The human brain endothelial cell line (hCMEC/d3) was used for the *in vitro* models and to characterize functional and molecular changes resulting from the various treatments examined. The hCMEC/d3 is a well-established cell line used previously in BBB cell culture models that demonstrate the expression of key junctional proteins such as claudin-5 and ZO-1 which are known to be expressed under physiological conditions (Eigenmann et al., 2013; Weksler et al., 2013).

The initial assessment of the Mimetas^{TM} microfluidic BBB model were performed in 2-lane organoplate plates on confluent microvessels. Based on the data, placing the plate on a rocker platform to create flow was necessary to form leak-tight barriers. This was shown by the marked increase of fluorescence in the gel channel under no flow conditions compared to conditions where flow was present during culture. Based on previous literature, a confluent microvessel is formed when the ratio of relative fluorescence in the gel to the perfusion lane remains constant and below 0.4 over time (Duinen et al., 2017). Using the 0.4 cut-off value, the microfluidic BBB monoculture model was able to maintain a leak-tight barrier from culture days 4 to 11. Barrier properties were retained for several days in the microfluidic model which was in contrast to what is observed with traditional BBB culture models, a possible explanation for this is the ability of the microfluidic system to support culturing under fluid flow conditions in contrast to static monolayers in traditional 2-D culture models.

While the 2-lane microfluidic provided valuable data, due to the plate format, sampling from the basolateral compartment was not feasible. Therefore, permeability assessments were limited to molecules that can be examined on the EVOS microscope. Additionally, to create co-culture conditions in the 2-lane plate, in-gel tumor cells needed to be seeded at the same time as

endothelial cells. Due to the timing of co-culture, assessing molecular and functional changes on confluent microvessesls in response to the tumor microenvironment was not possible. The presence of a third channel in the three-lane microfluidic plate enabled basolateral sampling. Sampling from basolateral compartments removed limitations for fluorescent markers that could be viewed microscopically and allowed for expansion of permeability markers that can be quantitatively measured using different analytical platforms. Lastly, due to the plate structure, endothelial cells can be grown to confluency before co-culture treatments in the 3-lane model which allowed for examination of the tumor microenvironment over an extended period of time.

To compare permeability between two different culture systems, endothelial cells were grown in monoculture conditions in Transwell™ inserts and the Mimetas™ three-lane organoplate. Model assessments were also expanded from a single large molecular weight permeability probe to three different fluorescently labelled dyes selected to examine different permeability processes. The permeability markers included FDX70,000, a large molecular weight marker to examine paracellular permeability of macromolecules, non- pegylated IRdye (IRdye 800), a small molecular weight marker for monitoring paracellular diffusion and R800, a transcellular permeability marker that is actively effluxed out of the brain microvessel endothelial cells through a P-gp transporter process (D. S. Miller et al., 2008). Significant reductions in permeability were observed for all three dyes tested in the microfluidic plate compared to Transwell™ inserts. These results suggest an enhanced endothelial barrier effect with the microfluidic system. To confirm the improvements in the microfluidic model were due to enhanced barrier properties of the endothelial cells, permeability was assessed in the microfluidic model without endothelial cells. These studies showed that the ECM in the three-

lane organoplate was not responsible for the enhanced barrier properties observed and provided additional confidence in the microfluidic BBB model system.

The improvements in the barrier properties of the microfluidic BBB model are likely due to the ability of the three-lane organoplate to support culturing under fluid flow conditions in contrast to static monolayers in Transwell^{TM} inserts. In support of this, permeability in the microfluidic model was substantially increased under no-flow conditions. Endothelial cells of the BBB express various tight junction molecules, efflux transporters and solute carriers important for barrier function (Chow & Gu, 2015). Therefore, to assess whether the decreases in permeability were due to transporter function, expression of BBB specific genes was examined. Increased barrier properties observed in the microfluidic model correlated with increased expression of key BBB specific genes such as *ZO-1*, *BCRP*, *claudin-5*, *claudin-3* and *ve-cadherin* compared to brain endothelial cells cultured in Transwell^{TM} inserts. These increases in key BBB tight junction and adhesion molecules could provide insights into the profound tightening effect observed in endothelial cells when they are cultured in the microfluidic model.

The ultimate utility of any *in vitro* BBB model is the extent to which it replicates *in vivo* BBB properties. Most of the current *in vitro* models are substantially leakier with 10-100 fold higher permeability coefficients than observed *in vivo* (Eigenmann et al., 2013; Shi et al., 2014) . Examination of the literature identified a study from Shi et al that examined the permeability of both sodium fluorescein and FDX70,000. Shi's model used multiphoton microscopy to determine solute permeability in the BBB of rats. Injections of sodium fluorescein, FDX70,000 and other fluorescent markers were given through cerebral circulation and BBB permeability was assessed. The apparent permeability of sodium fluorescein and FDX70,000 observed in the

microfluidic model were comparable to values reported *in vivo* (Shi et al., 2014). Compared to the traditional 2-D Transwell^{TM} model, *in vitro* BBB culture model was able to more accurately reproduce the BBB barrier properties observed *in vivo.* Taken together, this data supports the DMF model to be able to form tight structures and *in vivo* physiological relevance.

4.2 Establishment of the BBB-GB Microfluidic Model.

Three different human brain tumor cell lines were chosen to examine the tumor microenvironment driven changes in brain microvessel function in the *in vitro* models. Based on previous studies, conditioned media from U87 GBM cells increased endothelial cell permeability through an increased secretion of IL-8 (Dwyer et al., 2012). This was supported by pharmacological inhibition of IL-8 or RNA interference silencing of IL-8 expression in U87 which decreased endothelial cell hyperpermeability when cultured with U87 TCM (Dwyer et al., 2012; Guequén et al., 2019). Additionally, U87 conditioned media resulted in a rearrangement of endothelial cell VE-cadherin away from the cell junctions, likely adding to the increased permeability observed (Dwyer et al., 2012). Clinically, pediatric diffuse intrinsic pontine glioma tumors are non-MRI contrast enhancing, indicating that the BBB remains intact (Warren, 2018). Therefore, it was hypothesized that DIPG SF8628 co-culture might result in enhanced barrier properties. Lastly, U251 (GB) cell co-culture was expected to produce minimal changes in endothelial cell integrity (Dwyer et al., 2012). Therefore, these three cell lines were chosen to represent the spectrum of tumor effects in the BBB culture model.

Endothelial barrier responses in the microfluidic tumor co-culture followed similar trends in Transwell^{TM} inserts. In both culture models, DIPG co-culture enhanced barrier properties, U87 co-culture diminished barrier properties resulting in endothelial cell leakiness and U251 co-culture did not produce significant changes in endothelial barrier integrity compared to

monoculture. These results were as predicted according to the literature and since data correlated in two different *in vitro* co-culture models, data likely reflects the nature of various tumor cell impacts on BBB endothelial cell integrity.

Although permeability trends during tumor co-culture were similar between the two culture models, there were some notable differences. With the microfluidic culture model, we were able to determine sodium fluorescein permeability. This was challenging in Transwell™ inserts due to the inherent leakiness to small sized permeability probes and an immediate equilibration between the donor and receiver compartments. However, in the microfluidic model we were able to demonstrate partial retention of the dye within the perfusion lane allowing a quantitative permeability assessment. This finding is consistent with the ability of endothelial cells to form tight microvessels in the three-lane organoplate compared to the Transwell™ inserts. Sodium fluorescein was an important molecule to examine in various co-culture conditions since it allowed us to make inferences about small changes in endothelial permeability when endothelial cells are co-cultured with different tumor cell lines. Despite the fact that lipophilic molecules with a molecular weight of 400-600 daltons can readily diffuse across the BBB (Bellettato & Scarpa, 2018), at 24-hour co-culture time points we can see significant increases in endothelial permeability during U87 co-culture compared to monoculture conditions. This data speaks to the value of the microfluidic model to form tight tubular structures and detect changes in endothelial permeability using a small molecular weight marker.

In addition, using the three-lane microfluidic model, were able to examine changes in brain microvessel permeability under co-culture conditions at three different time points – 24, 48, and 72-hours. This allowed for the ability to determine whether the effects on endothelial cell permeability changed as a function of time in co-culture. Based on our results, the tumor-

driven changes in paracellular permeability were consistently observed throughout all time points examined with U87 producing significant increases, and SF8628 causing reductions in brain endothelial cell permeability to both FDX70000 and IRdye800 that were greatest after 24 and 48-hours of co-culture. In contrast, the effects on rhodamine800 permeability varied as a function of days in co-culture, with U87 displaying significantly increased permeability at 24-hours, but significantly reduced permeability at 72-hours compared to monoculture and astrocyte co-culture. Even the U251, which had no effect on R800 permeability at 24-hrs, results showed a significant reduction by 72-hours.

It should be noted that the changes in R800 permeability observed at 48 and 72-hours with the tumor co-culture models were largely driven by increased permeability in the monoculture model. The fact that permeability to R800 is relatively unchanged in the respective tumor co-culture models suggests the reductions in R800 permeability observed in the U87 and U251 co-culture were likely not due to increased R800 accumulation inside the tumor cells compared to monoculture conditions, but rather reflect the potential reductions in P-gp transport in the monoculture group over time. Regardless, these findings are consistent with *in vivo* findings in many brain tumors where increased paracellular leakiness within the tumor vasculature is accompanied by a maintained or enhanced drug efflux activity (Aryal et al., 2017). As many chemotherapeutic agents are subject to drug efflux transport at the BBB (On et al., 2014) this may explain why an otherwise leaky tumor vasculature remains unresponsive to therapeutic treatment.

As tumor cell induced changes in endothelial cell permeability followed the same trends in both the Transwell and microfluidic models, tumor-induced changes in the expression profile of BBB specific genes were examined in Transwell™ inserts. All tumor co-culture conditions

resulted in increased *GLUT-1* expression. This result was expected as tumor cell metabolism and fast rate of proliferation require large amounts of glucose (Alexandru et al., 2014). During SF8628 co-culturing, there was increased expression of *occludin*, *zo-1*, *BCRP*, and *claudin-5/3*. The increased expression of tight junction and adhesion molecules supported the functional permeability data showing enhanced barrier properties of brain endothelial cells with DIPG co-culture. Given that claudin-5 is known to play the most dominant role in barrier integrity at the BBB, the marked increase in *claudin-5* expression correlates with the enhanced barrier properties observed (Berndt et al., 2019). Supporting the functional permeability data, U87 co-culture resulted in decreased expression of tight junction and adhesion molecules such as *occludin, zo-1*, *claudin-1* and *ve-cadherin.* Surprisingly, increased expression of *claudin5/3* and *ve-cadherin* were found during U251 co-culture, but the increased expression of these inter-junctional adhesion molecules did not result in significant changes in endothelial cell permeability. Therefore, although expression of key BBB specific genes may be increased, these changes did not correlate to changes in permeability and it is possible other factors are being released to maintain barrier properties similar to monoculture (control) levels.

Despite challenges in extracting sufficient amounts of RNA from the microfluidic model, the SF8628 microfluidic co-culture model was chosen to further examine differences in endothelial gene expression compared to hCMEC/d3 monoculture conditions. Similar to the Transwell^{TM} model, increased expression of *occludin*, *zo-1*, *p-gp*, *BCRP*, and *claudin-5* were observed in the SF8628 co-culture model. The gene expression data supports the functional paracellular and transcellular permeability values obtained with the SF8628 co-culture model.

4.3 Investigation of Cellular Mechanisms Involved in Tumor Induced Changes in Brain Endothelial Cell Barrier Properties.

The next steps were to investigate the mechanisms behind U87 endothelial cell induced leakiness and SF8628 tightening. A mesoscale discovery U-plex platform was used to assess various cytokine release during different co-culture conditions and at different co-culture time points. Although MDS platforms are quite useful, due to the plate design and antibody compatibility, we were only able to assess inflammatory cytokines IL-6, IL-8, MCP-1 and VEGF-A. Both apical and basolateral media samples were taken, however, only basolateral data was shown since that is where we expected to see the biggest difference in the tumor microenvironment between various tumor co-cultures. Based on previous literature, it was suspected that when endothelial cells were co-cultured with U87, high levels of IL-8 would be present which could explain endothelial cell leakiness (Dwyer et al., 2012). However, based on the data, no significant increase in IL-8 secretion were observed at 24-hour U87 co-culture. However, at 48-hours we saw significantly increased IL-8 secretion which continued to the 72-hour time point. Therefore, IL-8 may be playing a role in inducing endothelial cell leakiness. Interestingly, at 24, 48 and 72-hours of co-culture, DIPG cells, SF8628, had the highest level of IL-8 and IL-6 levels, as well as significantly increased levels of VEGF-A compared to control. High levels of IL-8 in SF8628 co-culture were surprising since IL-8, a proinflammatory cytokine, has been linked to increased endothelial cell permeability (Dwyer et al., 2012). In support, addition of IL-8 to endothelial cells has been shown to down regulate tight junction proteins (H. Yu et al., 2013). Therefore, to explain the decrease in endothelial cell permeability observed during SF8628 co-culturing, another factor must be present that can override the proinflammatory IL-8 effect.

It was not surprising that all tumor co-culture conditions secreted high levels of VEFG-A. Elevated levels of VEFG are characteristic of GBM and VEGF promotes tumorigenesis and angiogenesis (C. Xu et al., 2013). Another surprising finding was the differences in MCP-1 levels during different co-culture conditions. We expected MCP-1 levels to be increased in all tumor co-culture conditions compared to control. The rationale behind this expectation is, MCP, a proinflammatory cytokine, is known to increase levels of macrophages at tumor sites, these macrophages in turn can morph into tumor associated macrophages which participate and function in tumor invasiveness, metastasis, growth, and drug resistance (Pan et al., 2020). However, only 24-hour U251 co-culture increased levels of MCP-1 with decreased levels during U87 co-culture. Otherwise, MCP-1 levels in all tumor co-culture conditions did not differ from the control at 48- and 72-hour time points. A potential explanation for these results is that this is *in vitro* data, and the necessary inflammatory and support cells are not present to continue the signalling cascade. In conclusion, based on this data, it is possible that IL-8 may be playing a role in endothelial cell leakiness in U87 co-culture, however maybe not a major one and the largest increases in proinflammatory cytokine release were observed for SF8628 DIPG co-culturing, therefore other factors must be present that produce an endothelial tightening effect.

The present study also examined the secreted and intracellular lipid profiles from the various co-culture conditions to better understand molecular mechanisms behind the tumor-induced alterations in endothelial cell permeability. When examining intracellular lipids, the most striking differences observed between the tumor co-culture systems occurred in the phosphatidylserine group. Heat maps from the intracellular lipids showed phosphatidylserine was much higher in SF8628 co-culture compared to other conditions. Phosphatidylserine is one of the most abundant negatively charged phospholipids present in biological membranes and

under normal physiological conditions, is localized to the inner leaflet (Leventis & Grinstein, 2010). However, the role of phosphatidylserine has been more extensively studied when it is present on the outer leaflet. When expressed on the outlet leaflet phosphatidylserine plays a role in apoptosis (Leventis & Grinstein, 2010). However, recently, reports have shown that increased levels or accumulation of phosphatidylserine at the plasma membrane inner leaflet can lead to activation of the Akt survival pathway which may be able to counteract apoptotic stimuli (Freed et al., 2008). Additionally, according to Freed et al, cells exposed to shear stress and serine in the medium lead to decreased caspase 3, a marker for apoptosis, in comparison to cells grown with out serine in the media. Additionally, cells grown in shear stress in the presence of serine resulted in increased Akt protein levels, supporting cell survival (Freed et al., 2008). Increased phosphatidylserine in the outer leaflet and increased apoptosis seemed unlikely, given the enhanced barrier properties observed in the SF8628 co-culture model. Therefore, we sought to take the information from the Freed et al studies and add serine to endothelial cells grown in monoculture to see if it produced a tightening effect on permeability. We tested three concentrations of serine concentrations and none of them produced a barrier tightening effect on the brain endothelial cells. While the exposure levels of serine encompassed a range of concentrations previously showing barrier enhancement, we did not examine the phosphatidylserine levels in the cells. Thus, there is a possibility that the supplementation of serine in the media was unable to increase intracellular phosphatidylserine levels to those observed under the SF8628 co-culture conditions. Therefore, it is still possible that increased levels of intracellular phosphatidylserine induced by SF8628 co-culture result in decreased permeability but will require further experimentation to determine if these increases in phosphatidylserine are mechanistically involved in the barrier enhancement observed. Another

limitation of the present studies was that the intracellular lipid profiling was only feasible for Transwell™ inserts since a large number of cells were required for lipidomics analysis.

In contrast, analysis of the tumor secreted lipids was possible for both the Transwell™ and microfluidic co-culture models. Distribution of different lipid classes were examined in both the apical "BBB" and basolateral "brain" compartment in the microfluidic model between the various co-culture models. When examining lipid distribution in the apical compartment, minimal changes were observed between the different co-cultures. The results suggest the brain endothelial microenvironment with regard to lipid composition, remains relatively constant during heterogenous tumor co-culture. However, when examining distributions of lipid classes in basolateral "brain" tumor microenvironment, large differences between the various co-culture conditions were observed, suggesting variability in secreted lipids between different tumor microenvironments. High levels of secreted glycerophospholipids in DIPG co-culture are not surprising. Phosphatidylserine is one of the major lipids produced from glycerophospholipids, supporting the intracellular lipid data. Glycerophospholipids play a role in cerebral structure and cognitive function and studies suggest supplementations with phosphatidylcholine or phosphatidylserine can improve cognitive function in animals (Reddan et al., 2018). Although lipids are important in endothelial vascular metabolism and structure (Rhea & Banks, 2021), there is lack of evidence to support glycerophospholipid or phosphatidylserine directly playing a role in modulating BBB permeability.

A greater distribution of fatty acyls in the basolateral compartment during U87 co-culture were also found compared to monoculture and other tumor co-culture conditions. This was also not surprising since literature suggests increased fatty acids levels may lead to disruption of the

BBB and alterations in tight junction proteins (Rhea & Banks, 2021) which may explain the increase in permeability when endothelial cells were co-cultured with GB U87 tumor cells.

Lipids are involved in a variety of important cellular processes such as signaling and cellular energy utilization in both brain endothelial and glioblastoma cells (Bezawork-Geleta et al., 2022; Rhea & Banks, 2021). Evidence also suggest lipids play a roll in cancer cell plasticity and persistence (Bezawork-Geleta et al., 2022). Therefore, identifying changes in secreted and intracellular lipid profiles may provide foundational knowledge to better characterize tumor cell-driven changes in endothelial cell functions. When examining secreted lipid profiles of the different co-culture systems, we found differences in secreted lipids between the microfluidic system and Transwell™ inserts. As tumor co-culture conditions were qualitatively similar in terms of the barrier changes produced, this would seem to argue against secreted lipid components driving the barrier effect. However, the differences in the secreted lipidomic profiles may reflect the large volume of sample collected from Transwell™ inserts compared to the microfluidics. A large sample volume might result in dilution of the lipids being measured, resulting in the differences in lipid profiles between the culture systems. Preliminary lipidomics profiling in the microfluidics indicated an increased amount of triglyceride and fatty acids in U87 co-culture compared to other co-culture conditions. Although the data was most pronounced in the microfluidic model, U87 co-culture also had increased secreted triglyceride levels compared to SF8628 co-culture in Transwell™ inserts.

Literature suggests increased levels of triglyceride rich lipoproteins and fatty acids are released during lipolysis of triglyceride rich lipoproteins which contribute to pathogenesis of diseases (Lee et al., 2017). Additionally, research has shown these triglyceride rich lipoproteins and their lipolysis fatty acid products, result in increased blood brain barrier transfer co-efficient

(Lee et al., 2017). Lipolysis products such as steric acid, palmitic acid and oleic have also been shown to induce astrocyte proinflammatory cytokine release (Lee et al., 2017). In support, lipid droplets have been observed in high concentrations in human brain tumors, specifically, GBM, and triglycerides, the major component of lipid droplets, serve as a critical source of energy to support GBM cell survival (Bezawork-Geleta et al., 2022).

Therefore, based on the literature and secreted lipid data, we sought to test three fatty acids and their effect on endothelial cell permeability. The rational was to determine if the increased number of triglycerides and fatty acids secreted during U87 co-culture were leading to the endothelial cell permeability increase. Compared to control (no fatty acid treatment), steric acid, oleic acid and palmitic acid all produced significantly increased permeability for both FDX70,000 and IRdye and the magnitude of barrier reduction was similar to that observed in the U87 co-culture positive control group. Interestingly, while these fatty acids were each individually associated with barrier weakening effects on the brain microvessel endothelial cells, when these fatty acids were added together in 1:1:1 combination ratio, no significant affects on permeability were observed. These trends were consistent whether fatty acids were added to endothelial cells for 3 or 24 hours. This data likely suggests that the increased levels of fatty acids or triglycerides seen during U87 co-culture could be resulting in the increased permeability and reduced barrier properties observed. However, it is unclear which fatty acid is responsible for this increase in permeability and further studies are required. To determine if fatty acids resulted in increased permeability across different culture platforms, palmitic acid was added to endothelial cells grown in the microfluidic plate. Data revealed increased endothelial cell permeability for both FDX70,000 and IRdye in the presence of palmitic acid. Again, the magnitude of barrier reduction was similar to that observed in the U87 co-culture positive

control. Since two different culture models produced similar results, the data suggests a strong indication of increased fatty acid levels resulting in the increased permeability values observed during U87 co-culture. Due to time constraints, only palmitic acid was tested in the microfluidic model, therefore, further studies to investigate barrier impacts of oleic acid, steric acid, and a combination of all three are necessary.

To summarize, there seem to be several factors at play causing either the increase or decreases in permeability observed during various tumor co-culture treatments. Taken together, data suggests interaction of multiple secreted components to create either barrier enhancing effects observed during SF8628 co-culture or barrier diminishing effects in U87 co-culture.

4.4 Evidence for Sonic Hedgehog Involvement in DIPG Induced Endothelial Cell Barrier Enhancement.

The SHH pathway regulates many fundamental processes in development including cell differentiation, stem cell maintenance, tissue polarity and cell proliferation (MacDonald, 2012). Studies have demonstrated SHH to be involved in tumorgenesis, in particular, analysis of tissue from patients that suffered from DIPG showed that the SHH signalling pathway is active in DIPG tumor cells and when the SHH pathway is inhibited, this significantly reduced the self-renewal capacity of tumor cells (MacDonald, 2012). Additionally, our collaborators at Cancer Care Manitoba have previously shown that SF8628 DIPG cells secrete a large amount of SHH in comparison to astrocytes and other DIPG cell lines. Secreted as a glycoprotein, SHH participates in numerous physiological processes, in particular, it is known for its role in neurogenesis, and maintenance of BBB integrity and tightness (Xing et al., 2020). Therefore, we suspected SHH might be playing a role in the endothelial cell tightening effect observed during DIPG co-culture.

We assessed endothelial paracellular and transcellular permeability under various treatments to elucidate the role of SHH in DIPG co-culture. Endothelial cells were subjected to different treatments which consisted of SF8628 co-culture, tumor conditioned media from SF8628 tumor cells, addition of rhSHH, or SHH inhibitor molecules. Inhibitor molecules included RUSKI-201, which blocks SHH release from tumor cells, and vismodigib, a SHH receptor antagonist. Our findings suggest that the decreases in permeability observed in the present study with DIPG cell co-culture and SF8628 TCM were likely due to a secreted factor since the permeability of various solutes decreased in the presence of both DIPG co-culturing or TCM. However, we were unable observe any barrier tightening effects when rhSHH was added to the hCMEC/d3 monoculture. Additionally, vismodigib, was unable to inhibit the barrier tightening effects of either TCM or SF8628 co-culturing. Taken together, the data suggest that SHH is likely playing a role in the endothelial cell tightening effect. However, it seems more indirect, given that blocking sonic hedge release from the tumor cell restored permeability to control levels but blocking SHH from binding to its receptors on endothelial cells had no significant effect. Therefore, SHH release from the tumor cell might be impacting down stream factors and this is what may ultimately cause the tightening effect.

Of note, vismodigib did appear to reverse the permeability response selectively for R800. To better understand this, we examined R800 uptake into the brain endothelial cells and these studies indicated that vismodigib might be acting a P-gp/BCRP inhibitor, resulting in the increased R800 permeability observed. When examining the expression profiles of selected BBB genes in the presence of TCM and DIPG co-culturing, the data revealed increased expression of *BCRP*, *claudin-5* and *claudin-3*. In Transwell^{TM} inserts, the increased expression of *claudin-5* when TCM media is added seems to decrease in the presences of RUSKI-201. This is not

surprising since SHH has been shown to upregulate tight junctions in endothelial cells (Xing et al., 2020). Glioma associated oncogene homolog- 1 (Gli-1), a down stream target of sonic hedgehog, has been proven to be an important transcriptional regulator of the expression of key tight junction proteins and BBB formation (Xing et al., 2020). In support of the observed data, SHH has also been reported in astrocyte conditioned medium and when applied to endothelial cells, increased trans endothelial electrical resistance (TEER) and decreased large molecule solute permeability was observed (Feliciano, 2012). Taken together, this data suggests that sonic hedgehog is playing a role in the improved barrier properties observed during SF8628 co-culture and this may be due to increased expression of key BBB genes or activation of other targets.

4.5 Assessment of Vesicular Transport in Various Co-Culture Conditions.

While the paracellular diffusion and cellular transport systems have been more widely studied from a BBB perspective, endocytosis is known to influence BBB permeability, especially during pathological conditions (Ayloo & Gu, 2019a). Multiple routes of vesicular trafficking occur in vascular endothelial cells such as fluid phase endocytosis, absorptive endocytosis (solute binding to cell surface, through non specific binding such as electrostatic interactions), and receptor mediated endocytosis (solutes binding specific cell membrane receptors) (Smith & Gumbleton, 2006). The major types of receptor mediated endocytosis occurring in BBB endothelial cells are clathrin and caveolae-mediated endocytosis (Ayloo & Gu, 2019b). The transcytosis pathway is often overlooked in terms of an entry pathway for solutes as a low rate of transcytosis is reported to occur in BBB endothelial cells relative to peripheral endothelial cells (Andreone et al., 2017). The protein Mfsd2a, a sodium dependent lysophophatidylcholine symporter, is a transmembrane protein of importance for regulating BBB formation by supressing transcytosis (Andreone et al., 2017). Specifically, studies suggest that Mfsd2a inhibits

caveolae-mediated endocytosis through altering the lipid composition of the plasma membrane (Andreone et al., 2017). Tumor co-culture resulted in variable endothelial *Mfsd2a* expression. In monoculture conditions, *Mfsd2a* levels were undetectable, however, SF8628 co-culture resulted in the lowest ΔCT value compared to other tumor co-culture conditions suggesting higher *Mfsd2a* levels. Taken together, increased *Mfsd2a* levels provides a possible explanation for the decreased BSA uptake in SF8628 co-culture. Plasmalemma vesicle-associated protein (PVLAP) has been reported to be endothelial cell specific and involved in endothelial fenestrae and caveolae diaphragms (Guo et al., 2016). Studies suggest PVLAP plays a role in BBB permeability, angiogenesis and migration (Guo et al., 2016). Plasmalemma vesicle-associated protein in endothelial cells has been associated with gliomas which can result in increased fenestration and hyperpermeability (Guo et al., 2016). Additionally, caveolin-1 is the major protein involved in caveolae mediated endocytosis and has a role in both physiological and pathological conditions of the BBB (Zhao et al., 2014). Increased caveolin-1 has been linked to diminished expression of tight junction proteins and increased permeability (Zhao et al., 2014). Lastly, dynamin (Dyn) is a protein involved in mediating membrane fission during clathrin-mediated endocytosis (Sundborger & Hinshaw, 2014). Therefore, we sought to test the expression of these vesicular proteins in tumor co-cultures. When examining changes in vesicular proteins, the data indicated significantly increased expression of caveolin-1 in U87 co-culture compared to monoculture conditions. Therefore, it is possible that the decreased expression of *Mfsd2a* in U87 co-culture compared to SF8628 co-culture and increased expression of *cav-1* could be attributing to the increases in endothelial permeability observed in U87 co-culture.

Previous studies have shown transcellular transport of albumin in brain endothelial cells, therefore, fluorescently labelled bovine serum albumin (BSA) was chosen as a marker for endocytosis in the present study (Vogel et al., 2001). In all of the tumor co-culture models examined, fluorescently labeled BSA permeability was low but measurable and associated with measurable accumulation of BSA in the endothelial cells. In contrast, the cellular uptake of IRdye was negligible despite quantifiable passage across the brain endothelial cell monolayers. Thus, while IRdye 800 permeability is accounted for by paracellular diffusion, the permeability with BSA is a combination of paracellular diffusion and vesicular transport processes that may be impacted by the tumor microenvironment.

Initially, in Transwell^{TM} inserts we found decreased BSA permeability values in SF8628 co-culturing with minimal changes in uptake compared to monoculture, suggesting barrier enhancing effects observed might be due to reduced paracellular leakage. This was also supported with increased expression of tight junction molecules like *claudin-5* that are known to be important for barrier function. In contrast, significantly increased BSA permeability and uptake observed in the U87 co-culture model indicated a potential increase in permeability due to either changes in vesicular transport, paracellular diffusion, or both. In order to determine which potential vesicular transport pathway was involved, various endocytosis inhibitors were added to the co-culture models. When chlorpromazine was present, a molecule that inhibits clathrin mediated endocytosis, permeability and uptake of BSA decreased in both control and SF8628 co-culture conditions. This suggested that clathrin mediated endocytosis was likely contributing to the passage of BSA under these culture conditions. Of note, when the clathrin endocytosis inhibitor chlorpromazine was present in monoculture conditions, the BSA permeability values were reduced to similar levels as found in the SF8628 co-culture model. This may indicate a

potential reduction in clathrin mediated endocytosis under SF8628 co-culture conditions that may contribute, along with the effects on the paracellular pathway, to the barrier enhancement observed. No significant changes in BSA permeability were observed during U87 co-culture, however there seemed to be an increase in permeability in the presence of chlorpromazine. It is possible that dysregulation of clathrin mediated endocytosis might be occurring in U87 co-culture. However, important to note, this is one snapshot in time and if examined at a different time point the data might look different. To conclude, these studies provided a lot of valuable data which suggested changes in clathrin mediated endocytosis during SF8628 and U87 co-culturing in Transwell™ inserts.

According to the literature, *in vitro* and *in vivo* studies have demonstrated anti-cancer properties of chlorpromazine including induction of apoptosis, DNA synthesis, and intracellular signaling pathways (Vlachos et al., 2021). In support, chlorpromazine has been reported to have direct anti-tumor effects on the GB U87 cell line (Vlachos et al., 2021). Therefore, in the microfluidic system, the restoration of BSA permeability values similar to monoculture levels in the U87 co-culture model when chlorpromazine is present is not surprising. An additional consideration, SF8628 co-culture resulted in significantly increased BSA permeability in the presence of chlorpromazine in the microfluidic model. A possible explanation for this is fact that antipsychotics have been reported to inhibit the SHH signaling pathway (Vlachos et al., 2021) and our results have shown SHH to be critical for the enhanced endothelial barrier properties. Lastly, when examining U87 co-culture, BSA permeability in the presence of genistein, a caveolae mediated inhibitor, was significantly decreased. Therefore, data indicates involvement of vesicular pathways during tumor co-culturing, however, the involvement of these pathways might be different under different tumor co-culture conditions.

To summarize, it is possible that vesicular transport may be playing a role in the various co-culture treatments, however further studies are necessary to begin determining more directly which endocytic pathways are impacted by the tumor microenvironment.

4.6 Investigation of Cadherin Peptide Permeability Modulation on BBB Endothelial cells.

Cadherin peptides have been proposed as a method for transiently opening the BBB for the delivery of therapeutics to the brain (Ulapane et al., 2019). These cadherin peptides were formulated to bind intercellular cadherin and prevent cadherin homodimerization. Preventing cadherin homodimerization creates a paracellular opening, therefore, it was speculated that this could increase drug delivery to the brain. The cadherin peptides evaluated in the present study increased brain endothelial cell permeability. These effects were rapid, appearing within the first 30-minutes. This is in contrast to other BBB disrupting approaches, such as osmotic agents like mannitol, which result in the dehydration of endothelial cells leading to enlargement of intercellular junctions. However, after osmotic disruption, the BBB does not return to baseline levels until 6-8 hours following mannitol treatment, which could be problematic for patients (Siegal et al., 2000). Therefore, important characteristics of these cadherin proteins were to increase BBB permeability but for a shorter duration of time.

The present study also looked to characterize the magnitude of the opening that could be achieved with the cadherin peptides by examining permeability changes observed with a range of different sized permeability markers. Based on the studies examining the molecular binding sites for the cadherin peptides, HAVN1 prevents cis binding of cadherin homodimers, whereas ADTC5 prevents the trans binding of cadherin homodimers, and TPP has components of both

(Sinaga et al., 2002; Ulapane et al., 2019). Based on the present study, inhibiting cis or trans binding of cadherin results in paracellular openings for both small or large molecules. However, preventing cis binding appears to be more efficient at increasing the paracellular diffusion of large molecular weight molecules. Additionally, the cadherin peptide TPP, which had components of both cis and trans binding was proven to be least effective at increasing permeability of large or small molecular weight markers.

An additional aspect examined with the cadherin peptides in the present study was BBB vascular selectively. Cadherin junction adhesion molecules are expressed in both epithelial and endothelial cells (Nachtigal et al., 2001). However, to avoid toxicities and other adverse effects, cadherin peptides for BBB based drug delivery applications should ideally be suited to target BBB vascular cadherin. Based on the data, significant increases in permeability were found for large and small molecular weight markers in endothelial cells co-administered with cadherin peptides. However, under the same conditions, these increases were not present in epithelial cells or pulmonary vascular endothelial cells. This data indicates BBB vascular endothelial cell cadherin selectivity, in which these peptides would be well suited to increase BBB permeability with negligible effects on epithelial and non-BBB vascular cadherin junctions.

The restrictive nature of the BBB presents a major obstacle for pharmacological treatment options in patients suffering with GBM. Therefore, the principal behind cadherin peptides was to increase BBB permeability to promote diffusion of chemotherapeutics to reach tumor target sites in therapeutically relevant concentrations. To assess *in vitro* effectiveness, endothelial cells were co-cultured in the various GB/DIPG treatment groups and cadherin peptide effectiveness was determined. In the presence of the BBB-GBM tumor microenvironment, we found the cadherin peptide, HAVN1, was still able to increase

paracellular permeability of FDX70,000. Taken together, this data suggests that cadherin peptides are effective at increasing endothelial cell permeability for both large and small molecular weight markers, the peptides are BBB vascular selective, and are effective in the tumor microenvironment.

4.7 Examination of Clinical Applications of the BBB-GBM Model.

The BBB-GBM microfluidic model has many uses, one of which includes examination of drugs for improved brain delivery. Historically there were few options of cancer treatment for patients which were limited to surgery, radiation therapy, chemotherapy or a combination. However, targeted therapy, personalized medicine, and new approaches such as the development of cancer biologics and immunotherapy are quickly emerging as novel cancer treatments (Debela et al., 2021). Biologics are cancer treatments that consist of a biological substance such as cells or an antibody that can be used to target specific types of cancer cells or molecules (Debela et al., 2021). Although chemotherapy remains an extremely effective strategy to target cancer cells, there is still an emerging need for the development of novel, personalized, and more effective treatments.

Case in point, Avastin is a monoclonal antibody that binds VEGF to decrease angiogenesis and limit tumor growth (Thompson et al., 2011) that is increasingly used to treat brain tumors. However, a major draw back to Avastin therapy is the restrictive nature of the BBB. Antibodies demonstrate poor brain bioavailability which can limit their therapeutic efficacy (Edavettal et al., 2022). Therefore, we sought to test endothelial cell permeability for biological agents including mAb and an antibody fragment in the presence of a cadherin peptide, HAVN1. The results of these studies showed HAVN1 can increase Avastin and a monoclonal antibody fragment permeability (Fab) across the brain endothelial cells. The antibody fragment

was included in the study to assess the role of the Fc neonatal transporter. The neonatal Fc transporter has been implicated in the removal of mAb from the brain (Ruano-Salguero & Lee, 2020). The antibody fragment cannot bind the Fc receptor, however Avastin can. When examining Avastin and Fab permeability from the blood to brain, we saw significantly less Avastin permeability in serum free conditions suggesting the neonatal Fc receptor may be actively transporting the mAb in the brain to the blood direction. However, we also wanted to determine efflux of Avastin out of the brain back into the blood and saw significantly increased Avastin permeability in comparison to Fab. This data suggests an endothelial basolateral transporter capable of internalizing IgG from the basolateral side of endothelial cells. Taken together, this data indicates the significance of cadherin peptides to be co-administered with immunotherapies to increase BBB permeability and therapeutic efficacy.

Lipid nanoparticles have attracted increased attention for their use as a chemotherapeutic drug delivery system (Kang et al., 2010). Lipid nanoparticles loaded with either doxorubicin, an anticancer agent, or SAT1 siRNA which sensitizes tumor cells to radiation, were prepared by Dr. Yathindranath in the Miller lab and their permeability was assessed in the microfluidic platform. According to the data, HAVN1 resulted in the largest increase in nanoparticle permeability. This was what was excepted for large molecular weight nanoparticles since previous findings have demonstrated HAVN1 to have the highest efficacy for increasing endothelial permeability to large molecular weight markers. Qualitatively, in the presence of HAVN1 we can see diffusion of nanoparticles out of the perfusion lane and into the gel and third compartment. This data indicates the versatility of these cadherin peptides to increase BBB permeability to an array of various sized molecules. Based on the data, cadherin peptides would be ideally suited to be co-administered with biologics as a course of treatment options. Clinically, this research provides

the steppingstone for further studies, and once validated, these peptides could have life prolonging, enhancing, or saving effects for patients suffering from GBM.

4.8 Final remarks.

The microfluidic plate provided a vast array of advantages. The BBB-GB model has the potential for personalized medicine where patients' tumors can be surgically resected, grown on the plate and screened for various drug susceptibilities. Additionally, the high throughput capability of the plate make it well suited for a variety of drug screening applications Throughout my studies the microfluidic plate was found to be best suited for functional and not molecular/expression studies. The small number of cells within each well makes it difficult to collect enough measurable cellular sample. Complications with the microfluidic model did arise throughout my research. We have found that certain lot numbers of collagen are better suited than others and the plate performs poorly in dry climates. Taken together, despite some setbacks, the microfluidic platform provided valuable data for mechanistic evaluation of the tumor microenvironment effects on BBB permeability and assessment of drug delivery approaches for improving permeability across the BBB.

4.9 Conclusions

1. The microfluidic plate provided similar permeability values to literature *in vivo* results with significantly decreased permeability compared to Transwell^{TM} inserts. This was likely due to the presence of flow within the system which could have resulted in increased expression of BBB specific genes.

2. Endothelial cell co-culturing with U87 increased BBB endothelial permeability. This was likely due to increased secretion of Il-8, triglycerides or fatty acids such as steric, palmitic, or oleic acid.
3. Co-culturing with SF8628 or by adding TCM resulted in decreased BBB endothelial permeability, this was despite increased release of proinflammatory cytokines. Investigation of sonic hedgehog revealed it is likely playing an indirect role in endothelial cell tightening. In addition to secreted factors, increased expression of tight junction proteins or decreases in vesicular transport may be leading to the increased barrier integrity.
4. When examining cadherin peptides, peptides that prevent cis or trans homodimerization are sufficient to increase paracellular permeability of small molecular weight markers. However, preventing cis binding seemed to be most effective at increasing permeability of large molecular weight molecules.
5. Cadherin peptide binding was BBB endothelial cell specific with negligible increases in permeability found in epithelial or pulmonary endothelial cells.
6. The cadherin peptide HAVN1 was equally effective at increasing permeability in tumor co-culture conditions.
7. Cadherin peptides can be co-administered with biologics such as Avastin or lipid nanoparticles to increase BBB permeability.

5.0 Bibliography

Ahlawat, J., Guillama Barroso, G., Masoudi Asil, S., Alvarado, M., Armendariz, I., Bernal, J., Carabaza, X., Chavez, S., Cruz, P., Escalante, V., Estorga, S., Fernandez, D., Lozano, C., Marrufo, M., Ahmad, N., Negrete, S., Olvera, K., Parada, X., Portillo, B., … Narayan, M. (2020). Nanocarriers as Potential Drug Delivery Candidates for Overcoming the Blood–Brain Barrier: Challenges and Possibilities. *ACS Omega*, *5*(22), 12583–12595. https://doi.org/10.1021/acsomega.0c01592

Alexandru, O., ENE, L., Purcaru, O. S., Tache, D. E., Popescu, A., Neamtu, O. M., Tatranu, L. G., Georgescu, A. M., Tudorica, V., Zaharia, C., & Dricu, A. (2014). Plasma Levels of Glucose and Insulin in Patients with Brain Tumors. *Current Health Sciences Journal*, *40*(1), 27–36. https://doi.org/10.12865/CHSJ.40.01.05

Alghamri, M. S., McClellan, B. L., Hartlage, M. S., Haase, S., Faisal, S. M., Thalla, R., Dabaja, A., Banerjee, K., Carney, S. V., Mujeeb, A. A., Olin, M. R., Moon, J. J., Schwendeman, A., Lowenstein, P. R., & Castro, M. G. (2021). Targeting Neuroinflammation in Brain Cancer: Uncovering Mechanisms, Pharmacological Targets, and Neuropharmaceutical Developments. *Frontiers in Pharmacology*, *12*. https://www.frontiersin.org/article/10.3389/fphar.2021.680021

Alphandéry, E. (2018). Glioblastoma Treatments: An Account of Recent Industrial Developments. *Frontiers in Pharmacology*, *9*. https://doi.org/10.3389/fphar.2018.00879

Andreone, B. J., Chow, B. W., Tata, A., Lacoste, B., Ben-Zvi, A., Bullock, K., Deik, A. A., Ginty, D. D., Clish, C. B., & Gu, C. (2017). Blood-brain barrier permeability is regulated by lipid transport-dependent suppression of caveolae-mediated transcytosis. *Neuron*, *94*(3), 581-594.e5. https://doi.org/10.1016/j.neuron.2017.03.043

Aryal, M., Fischer, K., Gentile, C., Gitto, S., Zhang, Y.-Z., & McDannold, N. (2017). Effects on P-Glycoprotein Expression after Blood-Brain Barrier Disruption Using Focused Ultrasound and Microbubbles. *PLoS ONE*, *12*(1), e0166061. https://doi.org/10.1371/journal.pone.0166061

Augustine, R., Aqel, A. H., Kalva, S. N., Joshy, K. S., Nayeem, A., & Hasan, A. (2021). Bioengineered microfluidic blood-brain barrier models in oncology research. *Translational Oncology*, *14*(7), 101087. https://doi.org/10.1016/j.tranon.2021.101087

Ayloo, S., & Gu, C. (2019a). Transcytosis at the Blood-Brain Barrier. *Current Opinion in Neurobiology*, *57*, 32–38. https://doi.org/10.1016/j.conb.2018.12.014

Ayloo, S., & Gu, C. (2019b). Transcytosis at the Blood-Brain Barrier. *Current Opinion in Neurobiology*, *57*, 32–38. https://doi.org/10.1016/j.conb.2018.12.014

Baeten, K. M., & Akassoglou, K. (2011). Extracellular Matrix and Matrix Receptors in Blood-Brain Barrier Formation and Stroke. *Developmental Neurobiology*, *71*(11), 1018–1039. https://doi.org/10.1002/dneu.20954

Bellettato, C. M., & Scarpa, M. (2018). Possible strategies to cross the blood–brain barrier. *Italian Journal of Pediatrics*, *44*(2), 131. https://doi.org/10.1186/s13052-018-0563-0

Belykh, E., Shaffer, K. V., Lin, C., Byvaltsev, V. A., Preul, M. C., & Chen, L. (2020). Blood-Brain Barrier, Blood-Brain Tumor Barrier, and Fluorescence-Guided Neurosurgical Oncology: Delivering Optical Labels to Brain Tumors. *Frontiers in Oncology*, *10*. https://www.frontiersin.org/articles/10.3389/fonc.2020.00739

Bergers, G., & Song, S. (2005). The role of pericytes in blood-vessel formation and maintenance. *Neuro-Oncology*, *7*(4), 452–464. https://doi.org/10.1215/S1152851705000232

Berndt, P., Winkler, L., Cording, J., Breitkreuz-Korff, O., Rex, A., Dithmer, S., Rausch, V., Blasig, R., Richter, M., Sporbert, A., Wolburg, H., Blasig, I. E., & Haseloff, R. F. (2019). Tight junction proteins at the blood-brain barrier: Far more than claudin-5. *Cellular and Molecular Life Sciences: CMLS*, *76*(10), 1987–2002. https://doi.org/10.1007/s00018-019-03030-7

Bezawork-Geleta, A., Dimou, J., & Watt, M. J. (2022). Lipid droplets and ferroptosis as new players in brain cancer glioblastoma progression and therapeutic resistance. *Frontiers in Oncology*, *12*. https://www.frontiersin.org/articles/10.3389/fonc.2022.1085034

Białkowska, K., Komorowski, P., Bryszewska, M., & Miłowska, K. (2020). Spheroids as a Type of Three-Dimensional Cell Cultures—Examples of Methods of Preparation and the Most Important Application. *International Journal of Molecular Sciences*, *21*(17), 6225. https://doi.org/10.3390/ijms21176225

Brown, L. S., Foster, C. G., Courtney, J.-M., King, N. E., Howells, D. W., & Sutherland, B. A. (2019). Pericytes and Neurovascular Function in the Healthy and Diseased Brain. *Frontiers in Cellular Neuroscience*, *13*, 282. https://doi.org/10.3389/fncel.2019.00282

Cabezas, R., Ávila, M., Gonzalez, J., El-Bachá, R. S., Báez, E., García-Segura, L. M., Jurado Coronel, J. C., Capani, F., Cardona-Gomez, G. P., & Barreto, G. E. (2014). Astrocytic modulation of blood brain barrier: Perspectives on Parkinson's disease. *Frontiers in Cellular Neuroscience*, *8*, 211. https://doi.org/10.3389/fncel.2014.00211

Canfield, S. G., Stebbins, M. J., Morales, B. S., Asai, S. W., Vatine, G. D., Svendsen, C. N., Palecek, S. P., & Shusta, E. V. (2017). An isogenic blood–brain barrier model comprising brain endothelial cells, astrocytes, and neurons derived from human induced pluripotent

stem cells. *Journal of Neurochemistry*, *140*(6), 874–888. https://doi.org/10.1111/jnc.13923

Carpenter, T. S., Kirshner, D. A., Lau, E. Y., Wong, S. E., Nilmeier, J. P., & Lightstone, F. C. (2014). A Method to Predict Blood-Brain Barrier Permeability of Drug-Like Compounds Using Molecular Dynamics Simulations. *Biophysical Journal*, *107*(3), 630–641. https://doi.org/10.1016/j.bpj.2014.06.024

Chamberlain, M. C. (2011). Bevacizumab for the treatment of recurrent glioblastoma. *Clinical Medicine Insights. Oncology*, *5*, 117–129. https://doi.org/10.4137/CMO.S7232

Chaves, C., Declèves, X., Taghi, M., Menet, M.-C., Lacombe, J., Varlet, P., Olaciregui, N. G., Carcaboso, A. M., & Cisternino, S. (2020). Characterization of the Blood-Brain Barrier Integrity and the Brain Transport of SN-38 in an Orthotopic Xenograft Rat Model of Diffuse Intrinsic Pontine Glioma. *Pharmaceutics*, *12*(5), E399. https://doi.org/10.3390/pharmaceutics12050399

Chen, X., Liu, C., Muok, L., Zeng, C., & Li, Y. (2021). Dynamic 3D On-Chip BBB Model Design, Development, and Applications in Neurological Diseases. *Cells*, *10*(11), 3183. https://doi.org/10.3390/cells10113183

Choi, Y., Lee, S., Kim, K., Kim, S.-H., Chung, Y.-J., & Lee, C. (2018). Studying cancer immunotherapy using patient-derived xenografts (PDXs) in humanized mice. *Experimental & Molecular Medicine*, *50*(8), Article 8. https://doi.org/10.1038/s12276-018-0115-0

Chow, B. W., & Gu, C. (2015). The molecular constituents of the blood-brain barrier. *Trends in Neurosciences*, *38*(10), 598–608. https://doi.org/10.1016/j.tins.2015.08.003

Cooper, P. R., Ciambrone, G. J., Kliwinski, C. M., Maze, E., Johnson, L., Li, Q., Feng, Y., & Hornby, P. J. (2013). Efflux of monoclonal antibodies from rat brain by neonatal Fc receptor, FcRn. *Brain Research, 1534*, 13–21. https://doi.org/10.1016/j.brainres.2013.08.035

Couto, M., Coelho-Santos, V., Santos, L., Fontes-Ribeiro, C., Silva, A. P., & Gomes, C. M. F. (2019). The interplay between glioblastoma and microglia cells leads to endothelial cell monolayer dysfunction via the interleukin-6-induced JAK2/STAT3 pathway. *Journal of Cellular Physiology*, *234*(11), 19750–19760. https://doi.org/10.1002/jcp.28575

Daina, A., & Zoete, V. (2016). A BOILED-Egg To Predict Gastrointestinal Absorption and Brain Penetration of Small Molecules. *Chemmedchem*, *11*(11), 1117–1121. https://doi.org/10.1002/cmdc.201600182

De Vleeschouwer, S., & Bergers, G. (2017). Glioblastoma: To Target the Tumor Cell or the Microenvironment? In S. De Vleeschouwer (Ed.), *Glioblastoma*. Codon Publications. http://www.ncbi.nlm.nih.gov/books/NBK469984/

Debela, D. T., Muzazu, S. G., Heraro, K. D., Ndalama, M. T., Mesele, B. W., Haile, D. C., Kitui, S. K., & Manyazewal, T. (2021). New approaches and procedures for cancer treatment: Current perspectives. *SAGE Open Medicine*, *9*, 20503121211034370. https://doi.org/10.1177/20503121211034366

Deng, Z., Zhou, L., Wang, Y., Liao, S., Huang, Y., Shan, Y., Tan, S., Zeng, Q., Peng, L., Huang, H., & Lu, Z. (2020). Astrocyte-derived VEGF increases cerebral microvascular permeability under high salt conditions. *Aging (Albany NY)*, *12*(12), 11781–11793. https://doi.org/10.18632/aging.103348

Duinen, V. van, Heuvel, A. van den, Trietsch, S. J., Lanz, H. L., Gils, J. M. van, Zonneveld, A. J. van, Vulto, P., & Hankemeier, T. (2017). 96 perfusable blood vessels to study vascular permeability in vitro. *Scientific Reports*, *7*(1), 1–11. https://doi.org/10.1038/s41598-017-14716-y

Dwyer, J., Hebda, J. K., Le Guelte, A., Galan-Moya, E.-M., Smith, S. S., Azzi, S., Bidere, N., & Gavard, J. (2012). Glioblastoma Cell-Secreted Interleukin-8 Induces Brain Endothelial Cell Permeability via CXCR2. *PLoS ONE*, *7*(9). https://doi.org/10.1371/journal.pone.0045562

Edavettal, S., Cejudo-Martin, P., Dasgupta, B., Yang, D., Buschman, M. D., Domingo, D., Van Kolen, K., Jaiprasat, P., Gordon, R., Schutsky, K., Geist, B., Taylor, N., Soubrane, C. H., Van Der Helm, E., LaCombe, A., Ainekulu, Z., Lacy, E., Aligo, J., Ho, J., … Singh, S. (2022). Enhanced delivery of antibodies across the blood-brain barrier via TEMs with inherent receptor-mediated phagocytosis. *Med (New York, N.Y.)*, *3*(12), 860-882.e15. https://doi.org/10.1016/j.medj.2022.09.007

Edmondson, R., Broglie, J. J., Adcock, A. F., & Yang, L. (2014). Three-Dimensional Cell Culture Systems and Their Applications in Drug Discovery and Cell-Based Biosensors. *Assay and Drug Development Technologies*, *12*(4), 207–218. https://doi.org/10.1089/adt.2014.573

Eigenmann, D. E., Xue, G., Kim, K. S., Moses, A. V., Hamburger, M., & Oufir, M. (2013). Comparative study of four immortalized human brain capillary endothelial cell lines, hCMEC/D3, hBMEC, TY10, and BB19, and optimization of culture conditions, for an in vitro blood-brain barrier model for drug permeability studies. *Fluids and Barriers of the CNS*, *10*(1), 33. https://doi.org/10.1186/2045-8118-10-33

Feliciano, P. (2012). Hedgehog in the blood-brain barrier. *Nature Genetics*, *44*(1), Article 1. https://doi.org/10.1038/ng.1059

Freed, J. K., Shortreed, M. R., Kleefisch, C. J., Smith, L. M., & Greene, A. S. (2008). Revealing the Role of Phosphatidylserine in Shear Stress –Mediated Protection in Endothelial Cells. *Endothelium : Journal of Endothelial Cell Research*, *15*(4), 225–230. https://doi.org/10.1080/10623320802228849

Guequén, A., Zamorano, P., Córdova, F., Koning, T., Torres, A., Ehrenfeld, P., Boric, M. P., Salazar-Onfray, F., Gavard, J., Durán, W. N., Quezada, C., Sarmiento, J., & Sánchez, F. A. (2019). Interleukin-8 Secreted by Glioblastoma Cells Induces Microvascular Hyperpermeability Through NO Signaling Involving S-Nitrosylation of VE-Cadherin and p120 in Endothelial Cells. *Frontiers in Physiology*, *10*, 988. https://doi.org/10.3389/fphys.2019.00988

Guo, L., Zhang, H., Hou, Y., Wei, T., & Liu, J. (2016). Plasmalemma vesicle-associated protein: A crucial component of vascular homeostasis. *Experimental and Therapeutic Medicine*, *12*(3), 1639–1644. https://doi.org/10.3892/etm.2016.3557

Halldorsson, S., Lucumi, E., Gómez-Sjöberg, R., & Fleming, R. M. T. (2015). Advantages and challenges of microfluidic cell culture in polydimethylsiloxane devices. *Biosensors and Bioelectronics*, *63*, 218–231. https://doi.org/10.1016/j.bios.2014.07.029

Harder, B. G., Blomquist, M. R., Wang, J., Kim, A. J., Woodworth, G. F., Winkles, J. A., Loftus, J. C., & Tran, N. L. (2018). Developments in Blood-Brain Barrier Penetrance and Drug Repurposing for Improved Treatment of Glioblastoma. *Frontiers in Oncology*, *8*. https://www.frontiersin.org/article/10.3389/fonc.2018.00462

Hellström, M., Gerhardt, H., Kalén, M., Li, X., Eriksson, U., Wolburg, H., & Betsholtz, C. (2001). Lack of Pericytes Leads to Endothelial Hyperplasia and Abnormal Vascular Morphogenesis. *Journal of Cell Biology*, *153*(3), 543–554. https://doi.org/10.1083/jcb.153.3.543

Hu, C., Tao, L., Cao, X., & Chen, L. (2020). The solute carrier transporters and the brain: Physiological and pharmacological implications. *Asian Journal of Pharmaceutical Sciences*, *15*(2), 131–144. https://doi.org/10.1016/j.ajps.2019.09.002

Jia, W., Martin, T. A., Zhang, G., & Jiang, W. G. (2013). Junctional Adhesion Molecules in Cerebral Endothelial Tight Junction and Brain Metastasis. *Anticancer Research*, *33*(6), 2353–2359.

Kadry, H., Noorani, B., & Cucullo, L. (2020). A blood–brain barrier overview on structure, function, impairment, and biomarkers of integrity. *Fluids and Barriers of the CNS*, *17*(1), Article 1. https://doi.org/10.1186/s12987-020-00230-3

Kang, K. W., Chun, M.-K., Kim, O., Subedi, R. K., Ahn, S.-G., Yoon, J.-H., & Choi, H.-K. (2010). Doxorubicin-loaded solid lipid nanoparticles to overcome multidrug resistance in cancer therapy. *Nanomedicine: Nanotechnology, Biology and Medicine*, *6*(2), 210–213. https://doi.org/10.1016/j.nano.2009.12.006

Kapałczyńska, M., Kolenda, T., Przybyła, W., Zajączkowska, M., Teresiak, A., Filas, V., Ibbs, M., Bliźniak, R., Łuczewski, Ł., & Lamperska, K. (2018). 2D and 3D cell cultures – a comparison of different types of cancer cell cultures. *Archives of Medical Science : AMS*, *14*(4), 910–919. https://doi.org/10.5114/aoms.2016.63743

Kusuhara, H., & Sugiyama, Y. (2005). Active efflux across the blood-brain barrier: Role of the solute carrier family. *NeuroRx: The Journal of the American Society for Experimental NeuroTherapeutics*, *2*(1), 73–85. https://doi.org/10.1602/neurorx.2.1.73

Lee, L. L., Aung, H. H., Wilson, D. W., Anderson, S. E., Rutledge, J. C., & Rutkowsky, J. M. (2017). Triglyceride-rich lipoprotein lipolysis products increase blood-brain barrier transfer coefficient and induce astrocyte lipid droplets and cell stress. *American Journal of Physiology - Cell Physiology*, *312*(4), C500–C516. https://doi.org/10.1152/ajpcell.00120.2016

Leventis, P. A., & Grinstein, S. (2010). The distribution and function of phosphatidylserine in cellular membranes. *Annual Review of Biophysics*, *39*, 407–427. https://doi.org/10.1146/annurev.biophys.093008.131234

Li, W., Chen, Z., Chin, I., Chen, Z., & Dai, H. (2018). The Role of VE-cadherin in Blood-brain Barrier Integrity under Central Nervous System Pathological Conditions. *Current Neuropharmacology*, *16*(9), 1375–1384. https://doi.org/10.2174/1570159X16666180222164809

Liu, C.-Y., Yang, Y., Ju, W.-N., Wang, X., & Zhang, H.-L. (2018). Emerging Roles of Astrocytes in Neuro-Vascular Unit and the Tripartite Synapse With Emphasis on Reactive Gliosis in the Context of Alzheimer's Disease. *Frontiers in Cellular Neuroscience*, *12*. https://www.frontiersin.org/articles/10.3389/fncel.2018.00193

Löscher, W., & Potschka, H. (2005). Blood-Brain Barrier Active Efflux Transporters: ATP-Binding Cassette Gene Family. *NeuroRx*, *2*(1), 86–98.

Luissint, A.-C., Artus, C., Glacial, F., Ganeshamoorthy, K., & Couraud, P.-O. (2012). Tight junctions at the blood brain barrier: Physiological architecture and disease-associated

dysregulation. *Fluids and Barriers of the CNS*, *9*(1), Article 1. https://doi.org/10.1186/2045-8118-9-23

Luo, H., & Shusta, E. V. (2020). Blood–Brain Barrier Modulation to Improve Glioma Drug Delivery. *Pharmaceutics*, *12*(11), 1085. https://doi.org/10.3390/pharmaceutics12111085

MacDonald, T. J. (2012). Hedgehog Pathway in Pediatric Cancers: They're Not Just for Brain Tumors Anymore. *American Society of Clinical Oncology Educational Book*, *32*, 605–609. https://doi.org/10.14694/EdBook_AM.2012.32.61

Michinaga, S., & Koyama, Y. (2019). Dual Roles of Astrocyte-Derived Factors in Regulation of Blood-Brain Barrier Function after Brain Damage. *International Journal of Molecular Sciences*, *20*(3), 571. https://doi.org/10.3390/ijms20030571

Miller, D. S., Bauer, B., & Hartz, A. M. S. (2008). Modulation of P-glycoprotein at the Blood-Brain Barrier: Opportunities to Improve CNS Pharmacotherapy. *Pharmacological Reviews*, *60*(2), 196–209. https://doi.org/10.1124/pr.107.07109

Miller, D. W., Line, S., Safa, N. A., & Zhang, Y. (2021). Blood–Brain Barrier Transporters and Central Nervous System Drug Response and Toxicity. In *Transporters and Drug-Metabolizing Enzymes in Drug Toxicity* (pp. 377–412). John Wiley & Sons, Ltd. https://doi.org/10.1002/9781119171003.ch12

Miranda-Azpiazu, P., Panagiotou, S., Jose, G., & Saha, S. (2018). A novel dynamic multicellular co-culture system for studying individual blood-brain barrier cell types in brain diseases and cytotoxicity testing. *Scientific Reports*, *8*(1), Article 1. https://doi.org/10.1038/s41598-018-26480-8

Mo, F., Pellerino, A., Soffietti, R., & Rudà, R. (2021). Blood–Brain Barrier in Brain Tumors: Biology and Clinical Relevance. *International Journal of Molecular Sciences*, *22*(23), 12654. https://doi.org/10.3390/ijms222312654

Nachtigal, P., Gojová, A., & Semecký, V. (2001). The role of epithelial and vascular-endothelial cadherin in the differentiation and maintenance of tissue integrity. *Acta Medica (Hradec Kralove)*, *44*(3), 83–87.

Nagpal, S., Harsh, G., & Recht, L. (2011). Bevacizumab Improves Quality of Life in Patients with Recurrent Glioblastoma. *Chemotherapy Research and Practice*, *2011*, 602812. https://doi.org/10.1155/2011/602812

Nilsen, J., Bern, M., Sand, K. M. K., Grevys, A., Dalhus, B., Sandlie, I., & Andersen, J. T. (2018). Human and mouse albumin bind their respective neonatal Fc receptors differently. *Scientific Reports*, *8*(1), Article 1. https://doi.org/10.1038/s41598-018-32817-0

Okada, S., Vaeteewoottacharn, K., & Kariya, R. (2019). Application of Highly Immunocompromised Mice for the Establishment of Patient-Derived Xenograft (PDX) Models. *Cells*, *8*(8), 889. https://doi.org/10.3390/cells8080889

OrganoPlate® 2-lane 96. (n.d.). Www.Mimetas.Com. Retrieved February 20, 2022, from https://www.mimetas.com/en/organoplate-2-lane-96/

OrganoPlate® 3-lane 40. (n.d.). Www.Mimetas.Com. Retrieved February 20, 2022, from https://www.mimetas.com/en/organoplate-3-lane-40/

Our Technology. (n.d.). Www.Mimetas.Com. Retrieved February 19, 2022, from https://www.mimetas.com/en/our-technology/

Pan, Y., Yu, Y., Wang, X., & Zhang, T. (2020). Tumor-Associated Macrophages in Tumor Immunity. *Frontiers in Immunology*, *11*, 583084. https://doi.org/10.3389/fimmu.2020.583084

Patching, S. G. (2017). Glucose Transporters at the Blood-Brain Barrier: Function, Regulation and Gateways for Drug Delivery. *Molecular Neurobiology*, *54*(2), 1046–1077. https://doi.org/10.1007/s12035-015-9672-6

Pompili, L., Porru, M., Caruso, C., Biroccio, A., & Leonetti, C. (2016). Patient-derived xenografts: A relevant preclinical model for drug development. *Journal of Experimental & Clinical Cancer Research : CR*, *35*, 189. https://doi.org/10.1186/s13046-016-0462-4

Prados, J., Melguizo, C., Ortiz, R., Vélez, C., Alvarez, P. J., Arias, J. L., Ruíz, M. A., Gallardo, V., & Aranega, A. (2012). Doxorubicin-loaded nanoparticles: New advances in breast cancer therapy. *Anti-Cancer Agents in Medicinal Chemistry*, *12*(9), 1058–1070. https://doi.org/10.2174/187152012803529646

Pulgar, V. M. (2019). Transcytosis to Cross the Blood Brain Barrier, New Advancements and Challenges. *Frontiers in Neuroscience*, *12*. https://www.frontiersin.org/article/10.3389/fnins.2018.01019

Pyzik, M., Kozicky, L. K., Gandhi, A. K., & Blumberg, R. S. (2023). The therapeutic age of the neonatal Fc receptor. *Nature Reviews Immunology*, 1–18. https://doi.org/10.1038/s41577-022-00821-1

Quaegebeur, A., Segura, I., & Carmeliet, P. (2010). Pericytes: Blood-Brain Barrier Safeguards against Neurodegeneration? *Neuron*, *68*(3), 321–323. https://doi.org/10.1016/j.neuron.2010.10.024

Reddan, J. M., White, D. J., Macpherson, H., Scholey, A., & Pipingas, A. (2018). Glycerophospholipid Supplementation as a Potential Intervention for Supporting Cerebral Structure in Older Adults. *Frontiers in Aging Neuroscience*, *10*, 49. https://doi.org/10.3389/fnagi.2018.00049

Rhea, E. M., & Banks, W. A. (2021). Interactions of Lipids, Lipoproteins, and Apolipoproteins with the Blood-brain Barrier. *Pharmaceutical Research*, *38*(9), 1469–1475. https://doi.org/10.1007/s11095-021-03098-6

Ruano-Salguero, J. S., & Lee, K. H. (2020). Antibody transcytosis across brain endothelial-like cells occurs nonspecifically and independent of FcRn. *Scientific Reports*, *10*, 3685. https://doi.org/10.1038/s41598-020-60438-z

Sengillo, J. D., Winkler, E. A., Walker, C. T., Sullivan, J. S., Johnson, M., & Zlokovic, B. V. (2013). Deficiency in Mural Vascular Cells Coincides with Blood–Brain Barrier Disruption in Alzheimer's Disease. *Brain Pathology*, *23*(3), 303–310. https://doi.org/10.1111/bpa.12004

Shi, L., Zeng, M., Sun, Y., & Fu, B. M. (2014). Quantification of Blood-Brain Barrier Solute Permeability and Brain Transport by Multiphoton Microscopy. *Journal of Biomechanical Engineering*, *136*(3). https://doi.org/10.1115/1.4025892

Siegal, T., Rubinstein, R., Bokstein, F., Schwartz, A., Lossos, A., Shalom, E., Chisin, R., & Gomori, J. M. (2000). In vivo assessment of the window of barrier opening after osmotic blood—Brain barrier disruption in humans. *Journal of Neurosurgery*, *92*(4), 599–605. https://doi.org/10.3171/jns.2000.92.4.0599

Sinaga, E., Jois, S., Avery, M., Makagiansar, I., Tambunan, U. S. F., Audus, K., & Siahaan, T. (2002). Increasing Paracellular Porosity by E-Cadherin Peptides: Discovery of Bulge and

Groove Regions in the EC1-Domain of E-Cadherin. *Pharmaceutical Research*, *19*, 1170–1179. https://doi.org/10.1023/A:1019850226631

Smith, M. W., & Gumbleton, M. (2006). Endocytosis at the blood–brain barrier: From basic understanding to drug delivery strategies. *Journal of Drug Targeting*, *14*(4), 191–214. https://doi.org/10.1080/10611860600650086

Sun, H., Dai, H., Shaik, N., & Elmquist, W. F. (2003). Drug efflux transporters in the CNS. *Advanced Drug Delivery Reviews*, *55*(1), 83–105. https://doi.org/10.1016/S0169-409X(02)00172-2

Sundborger, A. C., & Hinshaw, J. E. (2014). Regulating dynamin dynamics during endocytosis. *F1000Prime Reports*, *6*, 85. https://doi.org/10.12703/P6-85

Taïb, B., Aboussalah, A. M., Moniruzzaman, M., Chen, S., Haughey, N. J., Kim, S. F., & Ahima, R. S. (2019). Lipid accumulation and oxidation in glioblastoma multiforme. *Scientific Reports*, *9*(1), Article 1. https://doi.org/10.1038/s41598-019-55985-z

The different types of cell junctions | Learn Science at Scitable. (n.d.). Retrieved March 18, 2022, from https://www-nature-com.uml.idm.oclc.org/scitable/content/the-different-types-of-cell-junctions-14714296/

Thompson, E. M., Frenkel, E. P., & Neuwelt, E. A. (2011). The paradoxical effect of bevacizumab in the therapy of malignant gliomas. *Neurology*, *76*(1), 87–93. https://doi.org/10.1212/WNL.0b013e318204a3af

Ulapane, K. R., Kopec, B. M., & Siahaan, T. J. (2019). Improving In Vivo Brain Delivery of Monoclonal Antibody Using Novel Cyclic Peptides. *Pharmaceutics*, *11*(11), 568. https://doi.org/10.3390/pharmaceutics11110568

Vlachos, N., Lampros, M., Voulgaris, S., & Alexiou, G. A. (2021). Repurposing Antipsychotics for Cancer Treatment. *Biomedicines, 9*(12), 1785. https://doi.org/10.3390/biomedicines9121785

Vogel, S. M., Minshall, R. D., Pilipović, M., Tiruppathi, C., & Malik, A. B. (2001). Albumin uptake and transcytosis in endothelial cells in vivo induced by albumin-binding protein. *American Journal of Physiology-Lung Cellular and Molecular Physiology, 281*(6), L1512–L1522. https://doi.org/10.1152/ajplung.2001.281.6.L1512

Wang, Y., Peng, F., Xie, G., Chen, Z.-Q., Li, H.-G., Tang, T., & Luo, J.-K. (2016). Rhubarb attenuates blood-brain barrier disruption via increased zonula occludens-1 expression in a rat model of intracerebral hemorrhage. *Experimental and Therapeutic Medicine, 12*(1), 250–256. https://doi.org/10.3892/etm.2016.3330

Warren, K. E. (2018). Beyond the Blood:Brain Barrier: The Importance of Central Nervous System (CNS) Pharmacokinetics for the Treatment of CNS Tumors, Including Diffuse Intrinsic Pontine Glioma. *Frontiers in Oncology, 8*. https://doi.org/10.3389/fonc.2018.00239

Weksler, B., Romero, I. A., & Couraud, P.-O. (2013). The hCMEC/D3 cell line as a model of the human blood brain barrier. *Fluids and Barriers of the CNS, 10*(1), 1–10. https://doi.org/10.1186/2045-8118-10-16

Xing, G., Zhao, T., Zhang, X., Li, H., Li, X., Cui, P., Li, M., Li, D., Zhang, N., & Jiang, W. (2020). Astrocytic Sonic Hedgehog Alleviates Intracerebral Hemorrhagic Brain Injury via Modulation of Blood-Brain Barrier Integrity. *Frontiers in Cellular Neuroscience, 14*. https://www.frontiersin.org/articles/10.3389/fncel.2020.575690

Xu, C., Wu, X., & Zhu, J. (2013). VEGF promotes proliferation of human glioblastoma multiforme stem-like cells through VEGF receptor 2. *TheScientificWorldJournal*, *2013*, 417413. https://doi.org/10.1155/2013/417413

Xu, L., Nirwane, A., & Yao, Y. (2018). Basement membrane and blood–brain barrier. *Stroke and Vascular Neurology*, *4*(2), 78–82. https://doi.org/10.1136/svn-2018-000198

Yeung, Y., McDonald, K., Grewal, T., & Munoz, L. (2013). Interleukins in glioblastoma pathophysiology: Implications for therapy. *British Journal of Pharmacology*, *168*(3), 591–606. https://doi.org/10.1111/bph.12008

Yu, F., Hunziker, W., & Choudhury, D. (2019). Micromachines Engineering Microfluidic Organoid-on-a-Chip Platforms. *Micromachines*, *10*, 165.

Yu, H., Huang, X., Ma, Y., Gao, M., Wang, O., Gao, T., Shen, Y., & Liu, X. (2013). Interleukin-8 Regulates Endothelial Permeability by Down-regulation of Tight Junction but not Dependent on Integrins Induced Focal Adhesions. *International Journal of Biological Sciences*, *9*(9), 966–979. https://doi.org/10.7150/ijbs.6996

Yu, X., Ji, C., & Shao, A. (2020). Neurovascular Unit Dysfunction and Neurodegenerative Disorders. *Frontiers in Neuroscience*, *14*. https://www.frontiersin.org/article/10.3389/fnins.2020.00334

Zardini Buzatto, A., Tatlay, J., Bajwa, B., Mung, D., Camicioli, R., Dixon, R. A., & Li, L. (2021). Comprehensive Serum Lipidomics for Detecting Incipient Dementia in Parkinson's Disease. *Journal of Proteome Research*, *20*(8), 4053–4067. https://doi.org/10.1021/acs.jproteome.1c00374

Zhao, Y.-L., Song, J.-N., & Zhang, M. (2014). Role of caveolin-1 in the biology of the blood-brain barrier. *Reviews in the Neurosciences*, *25*(2), 247–254. https://doi.org/10.1515/revneuro-2013-0039

Zhou, M., Shi, S. X., Liu, N., Jiang, Y., Karim, M. S., Vodovoz, S. J., Wang, X., Zhang, B., & Dumont, A. S. (2021). Caveolae-Mediated Endothelial Transcytosis across the Blood-Brain Barrier in Acute Ischemic Stroke. *Journal of Clinical Medicine*, *10*(17), 3795. https://doi.org/10.3390/jcm10173795